Technische Universität München
TUM School of Natural Sciences

Peroxide-Based Chemical Oxygen Generation for Aviation Purposes – from Basic Chemistry to Prototype Design

Alexander M. Imhof

Vollständiger Abdruck der von der TUM School of Natural Sciences der

Technischen Universität München zur Erlangung eines

Doktors der Naturwissenschaften (Dr. rer. nat.)

genehmigten Dissertation.

Vorsitz: Prof. Dr. Ulrich K. Heiz

Prüfer*innen der Dissertation:

1. Prof. Dr. Fritz E. Kühn
2. Prof. Dr. Kai-Olaf M. Hinrichsen

Die Dissertation wurde am 17.02.2023 bei der Technischen Universität München eingereicht und durch die TUM School of Natural Sciences am 16.03.2023 angenommen.

„Wenn du einmal den Geschmack des Fliegens erlebt hast, wirst du für immer auf der Erde wandeln und deine Augen zum Himmel richten, denn dort warst du und dorthin wirst du immer zurückkehren wollen“

Leonardo da Vinci

Die vorliegende Arbeit wurde im Zeitraum von Januar 2020 bis Dezember 2022 an der Professur für Molekulare Katalyse der Technischen Universität München angefertigt.

Mein ganz besonderer Dank gilt meinem Doktorvater

Herrn Prof. Dr. Fritz E. Kühn

für die Aufnahme in den Arbeitskreis, das mir entgegengebrachte Vertrauen und die Möglichkeit meine Doktorarbeit zu diesem vielfältigen Thema anfertigen zu dürfen. Vielen Dank für die hervorragenden Forschungs- und Arbeitsbedingungen, das Vertrauen in fordernden Zeiten und die Freiheiten, die Sie mir in den letzten Jahren gegeben haben. Besonders über Ihren Rückhalt in allen Angelegenheiten rund um eine nicht nur wirtschaftlich schwer gezeichnete Branche bin ich Ihnen sehr dankbar.

Danksagung

Besonders bedanken möchte ich mich bei einer ganzen Reihe von Personen, die auf verschiedenste Art und Weise am Gelingen dieser Arbeit beteiligt sind.

Zuallererst möchte ich mich bei **Dr. Christoph Kallfaß** für all seine Mühen und die Unterstützung in den letzten Jahren bedanken. Vielen Dank für deine unendlich langen Zugfahrten nach Garching und deine Bereitschaft auch mal außerhalb der klassischen Bürozeiten ein Problem zu erörtern. Und ganz besonders dafür, die Probleme eines stark gebeutelten Unternehmens so gut es eben geht ebendort zu belassen.

Ein ganz besonderer Dank geht an **Dr. Andreas Hinterberger**, meinem Vorgänger auf diesem Projekt. Vielen Dank noch einmal für die hervorragende Betreuung meiner Masterarbeit und die freundschaftliche Zusammenarbeit!

Frau Hifinger und **Dr. Robert Reich** danke ich für jegliche Unterstützung in allen Belangen der Hochschulbürokratie. Vielen Dank für Ihre Unterstützung bei der Bearbeitung von Dienstreisen und Rechnungen, sowie bei der Vorbereitung der zahlreichen Firmentreffen!

Ebenfalls ein herzliches Dankeschön an **Olaf Ackermann** und **Jürgen Kudermann** für die analytische Hilfe rund um Titrationen, Hochdruckpressen und UV/Vis-Messungen.

Besonders bedanken möchte ich mich bei **Dr. Gabriele Raudaschl-Sieber** für die perfekt organisierten Praktika und die lukullischen Genüsse danach.

Ein herzliches Dankeschön auch an **Leon** der, abgesehen davon, dass er ein großartiger Mensch im Allgemeinen ist, auch äußerst elektronisierend inspiriert. Vielen Dank **Alex** für das angenehme Katalysepraktikum als gemeinsamer Start in dieser Gruppe und Dankeschön **Michi** für die Motivation, nicht nur bei Rückenwind und Sonnenschein in die Pedale zu treten!

Besonderer Dank gebührt natürlich auch allen Studenten, die mir im Laufe der letzten Jahre einiges an Arbeit abgenommen haben. **Jennifer Keller** mit ihrer Masterarbeit über die Zersetzung von anorganischen Peroxiden und **Van Son Nguyen** mit seiner Studie zu einem Generatorkonzept. Auch unsere verlorenen Söhne **Thomas Brunn** und **Maximilian Schick** haben unter schwierigen Bedingungen Bestes geleistet.

Ich danke außerdem allen KollegInnen des AK Kühn dafür, dass die letzten drei Jahre zu einer wirklich schönen Zeit geworden sind! Besonderer Dank gilt dabei meinen direkten LaborkollegInnen **Carla**, **Tim**, **Jens**, **Jonas**, **Eva**, **Lilli**, **Nadine**, **Christian**, **Yogi** und **Nici** für die angenehme Zeit und das unkomplizierte Zusammenarbeiten. Auch meine KollegenInnen im unteren Labor **Marco**, **Flo**, **Dani**, **Greta** und **Johannes** haben stets für eine lockere Stimmung und eine super Atmosphäre gesorgt. Herzlichen Dank für den großartigen Zusammenhalt in der Gruppe, die zahlreichen Feierabendbierchen, Grillabende und Hüttenausflüge! Ihr alle macht diese fabelhafte Arbeitsgruppe zu dem, was sie ist!

Abstract

In pursuit of a next generation of low temperature chemical oxygen generators for civil aviation purposes, the decomposition of lithium peroxide, sodium peroxide and calcium peroxide in mixtures of acidic and basic aqueous solutions and ionic liquids applying MnO_2, $Mn(AcO)_2 \times 4\ H_2O$ and [BMIM][$FeCl_4$] was examined. Due to the strong dependence between the ambient temperature and die decomposition activity, the decomposition behavior in the temperature range from -20 °C up to +25 °C was investigated. Especially at low temperatures the weak solubility of the oxygen sources in ionic liquids adversely affects the decomposition reaction. Therefore, multiple ionic liquids mixed with various acidic and basic aqueous solutions of different acids and bases were studied by means of decomposition activity, melting point and oxygen source solubility. With the main decomposition reaction components optimized, it was possible to run a decomposition reaction with 90 g lithium peroxide in a mixture of 270 mL HCl (15%) and 180 mL [EMIM][SO4Me] as well as 480 mg $Mn(OAc)_2 \times 4\ H_2O$ evolving 17 L gaseous oxygen corresponding to approximately 20% scale of the finale target size of a chemical oxygen generator. As the combination of these components is completely new, a patent application was filed for the composition and method of generating oxygen (EP 4 071 107 A1).

The formation of disruptive foam occurring during the decomposition of inorganic peroxides was successfully suppressed by detailed investigations and the addition of various antifoaming agents, resulting in an increased oxygen yield and smoother oxygen flow rate profile. As the use of antifoaming agents in the process of oxygen evolution is completely new, a patent application was filed (pending).

A feasible chemical oxygen generator concept containing five major technical compartments was conceived and made with the aid of 3d-printing. To realize a printable, thermal stable and airworthy generator housing materials like chlorinated polyethylene and polycarbonate need to be used. For space-saving storage of all chemical components and reliable functionality within the required temperature range and all spatial alignments a novel concept of a radially symmetric generator layout was developed, whereby the reaction medium is released with a torque mechanism. Teflon-based membranes with a pore size of 1.7 µm were particularly suitable for separating the evolving gaseous oxygen from the liquid reaction mixture, as demonstrated by decomposition experiments in a specially designed test rig.

Zusammenfassung

Im Rahmen der Entwicklung eines Niedertemperatur-Sauerstoffgenerators der nächsten Generation für die zivile Luftfahrt wurde die Zersetztung von Lithium-, Natrium- und Calciumperoxid in Mischungen aus sauren und basischen wässrigen Lösungen und ionischen Flüssigkeiten katalysiert durch MnO_2, $Mn(AcO)_2 \times 4\ H_2O$ und [BMIM][$FeCl_4$] untersucht. Durch die starke Abhängigkeit der Zersetzungsaktivität von der Umgebungstemperatur wurde das Zersetzungsverhalten im Temperaturbereich von -20 °C bis +25 °C untersucht. Besonders bei niedrigen Temperaturen wirkt sich die schwache Löslichkeit der Sauerstoffquellen in ionischen Flüssigkeiten negativ auf die Zersetzungsaktivität aus. Mit optimierten Komponenten konnten 90 g Lithiumperoxid in einer Mischung aus 270 ml HCl (15 %) und 180 ml [EMIM][SO_4Me] mit 480 mg $Mn(AcO)_2 \times 4\ H_2O$ zersetzt werden. Dabei enstanden circa 17 L reines Sauerstoffgas was ungefähr 20% der späteren Zielgröße des Sauerstoffgenerators entspricht. Da die Kombination dieser Komponeten neuartig ist, wurde die Zusammensetzung und das Verfahren zur kontrollierten Sauerstofferzeugung zum Patent angemeldet (EP 4 071 107 A1).

Die bei der Zersetzung von anorganischen Peroxiden auftretende störende Schaumbildung konnte durch eingehende Untersuchungen und die Zugabe verschiedener Entschäumer erfolgreich unterdrückt werden, was zu einer erhöhten Sauerstoffausbeute und einem günstigeren Flussprofil führte. Da der Einsatz von Antischaummitteln im Prozess der Sauerstoffentwicklung ebenfalls neuartig ist, wurde auch hierzu eine Patentanmeldung eingereicht (pending).

Außerdem wurde ein neuartiges Konzept für einen chemischen Sauerstoffgenerator bestehend aus fünf Komponetnen konzipiert und additive gefertigt. Um ein thermisch stabiles und flugtaugliches Generatorgehäuse zu fertigen, wurde chloriertes Polyethylen und Polyarbonat verwendet. Zur platzsparenden Lagerung aller chemischen Komponenten und zuverlässiger Funktionalität im erforderlichen Temperaturbereich und allen räumlichen Ausrichtungen wurde ein neuartiges radialsymmetrisches Generatorlayouts entwickelt, wobei das Reaktionsmedium mit einem Drehmechanismus freigesetzt wird. Teflonmembranen mit einer Porengröße von 1,7 µm eignen sich besonders, um den entstehenden Sauerstoff aus dem Reaktionsgemisch abzutrennen, wie Zersetzungsexperimente in einem eigens konstruierten Versuchsstand zeigten.

Table of Contents

1 Introduction

Is flying still morally acceptable in this day and age? The impact on the environment is enormous. Around three percent of the world's annual CO_2 emissions are caused by civil aviation. A small but wealthy part of the world thus cause serious consequences for the entire planet. Tragically, poorer parts of the world are particularly harder hit by climate change.[1] In addition, it is not only the carbon dioxide emitted or other gases produced during the combustion of kerosene, such as various nitrogen oxides or particulate matter, that are problematic, but also simply the height of their emissions. Due to the fine dispersion in such cold parts of the atmosphere, the greenhouse gases have a particularly long and intensive effect. Even the water vapor produced during combustion has a warming effect in the form of cirrus clouds. These cirrus clouds allow ultraviolet radiation from the sun to pass through, but reflect infrared radiation from the earth.[2] Summing up all these side effects civil aviation accounts for around five percent of global warming.[1]

As well as being driven by environmental concerns, the aerospace- and aviation industries have always been known for their groundbreaking inventions and technical masterpieces. In addition to aircraft’s building materials which are increasingly lightweight materials such as carbon fiber composite materials, from a chemical point of view weight can be saved inside the passenger cabin too. As both air pressure and oxygen partial pressure steadily decrease with increasing altitude, exchange of CO_2 and O_2 in the lungs becomes more and more difficult. Depending on the degree of deficiency fatigue and nausea up to unconsciousness as well as lasting damage to the brain can occur, with all its fatal consequences.[3]

This is why passenger cabins are pressurized with so-called bleed air from the overpressure area of the turbines or auxiliary power unit.[4] Later breathing air from the combustion chamber is filtered and passed through a decomposition unit using ozone and noble metal catalysts. In order to prevent fatal consequences for pilots and passengers in case of faults or errors within the oxygen supply technology or overpressure hull an emergency oxygen system has to be provided.

The most commonly used method are chemical oxygen generators, which, as **Scheme 1** illustrates, release oxygen from metal chlorates by thermal decomposition.

$$2\ NaClO_3 \longrightarrow 2\ NaCl + 3\ O_2$$

Scheme 1: Thermal decomposition of sodium chlorate.

Since they were invented and adapted 80 years ago, these so-called chlorate candles have undergone extensive research. Nevertheless, there have been no major improvements till today, nor have other products been able to establish themselves. The cross section of a commonly used chlorate candle is shown in **Figure 1**.[5]

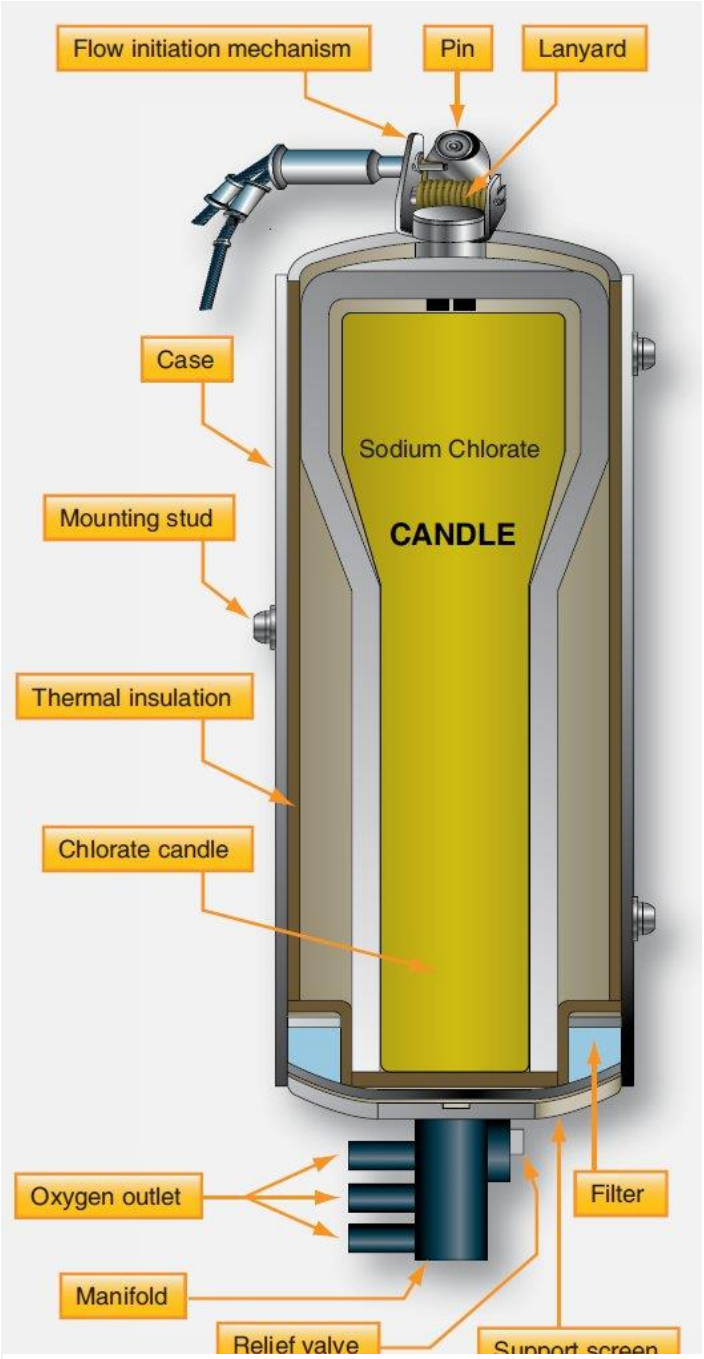

Figure 1: Cross section of a common chlorate candle.[5]

The oxygen supply unit OSU, shown in **Figure 2**, comprises all associated and necessary components like heat shielding, oxygen masks, tubing and the chlorate candle itself.[6]

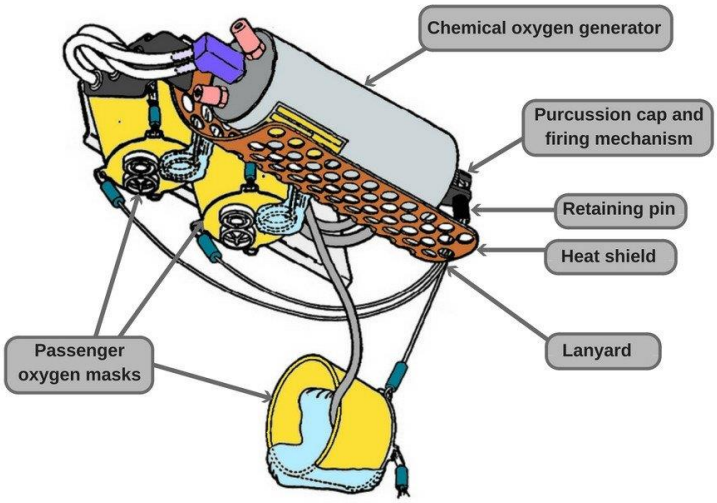

Figure 2: Schematic outline of an oxygen supply unit.[6]

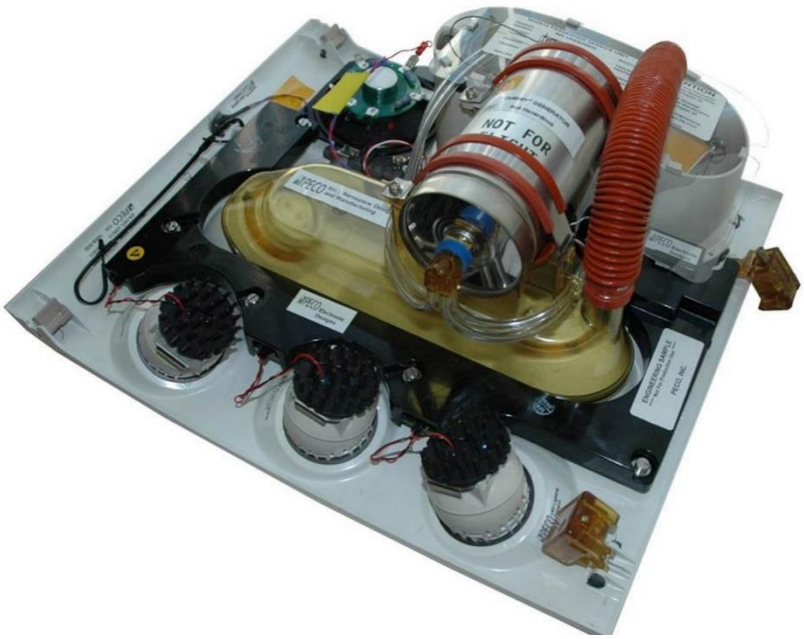

Figure 3: Passenger supply unit.[3]

The oxygen supply unit, shown in **Figure 2**, thereby is included within the passenger supply unit PSU, illustrated in **Figure 3**. The latter comprises all crucial components for passengers like service buttons, reading lamps, air ventilation and loudspeakers.

2 Scope of Work

Chemical oxygen generators for emergency use in aircrafts are mainly based on the thermal decomposition of sodium chlorate. A major drawback of these systems is their high reaction temperature. At least 300 °C are required to initiate the reaction, and temperatures as high as 650 °C are necessary during the exothermic decomposition to maintain it. Therefore, extensive insulation in order to prevent damage to the surrounding devices, is required. Additionally, the choice of housing materials is restricted and most commonly metals have to be used. This all adds up to a significant handicap in terms of weight and size.

Low-temperature systems could enable the use of lightweight materials like plastic and could potentially eliminate the need for heavy and space-consuming insulation. For this purpose, a more activated oxygen source, such as peroxide compounds would be beneficial. In spite of the fact that the reaction enthalpy for the decomposition of H_2O_2 is greater than that of sodium chlorate, peroxides might be a good choice since they can already initiate the reaction at room temperature.

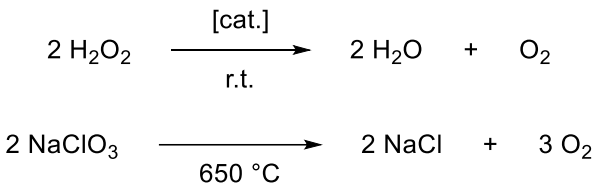

Scheme 2: Catalytic decomposition of hydrogen peroxide H_2O_2 and thermal decomposition of sodium chlorate $NaClO_3$.

In patent literature chemical oxygen generators which are based on the decomposition of peroxide compounds are already described. Nevertheless, these systems are mainly based on water as solvent what is viable since oxygen generators for commercial aircrafts have to work properly at freezing temperatures. In addition, mainly diluted hydrogen peroxide solutions are used, which are also not suitable since the occasionally high temperatures within an air- and spacecrafts as well as their high weight makes their utilization inappropriate.

Previous work within the group has laid the foundation for the use of urea hydrogen peroxide UHP, an adduct made of urea and H_2O_2 as an oxygen source.[3, 36, 37] It is decomposed by transition metal catalysts based on manganese or iron in ionic liquids as reaction medium.

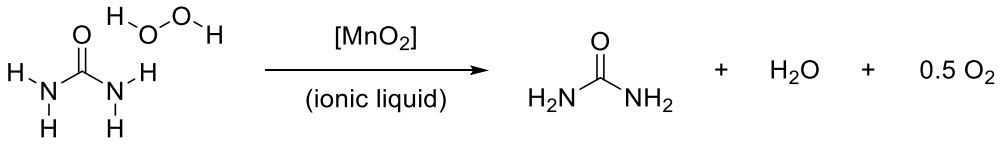

Scheme 3: Decomposition of urea hydrogen peroxide UHP with MnO_2 in an ionic liquid yielding urea, water and oxygen.

Based on the hitherto derived results, the present work will focus on a further improvement of the chemical components in terms of kind, appearance and composition.

As is known from previous studies, up to now investigated oxygen sources like urea hydrogen peroxide UHP, sodium perborate SPB or sodium percarbonate SPC suffer from their insufficient thermal stability and bear inadequate shelf life. Therefore, within this thesis inorganic peroxides like lithium peroxide LPO, sodium peroxide SPO and calcium peroxide CPO will be examined as new and suitable oxygen sources for chemical oxygen generators. As for their decomposition at lower temperatures protons are required, a new reaction medium has to be in compiled. Due to that, a variety of acidic and basic aqueous solvents will be investigated towards their feasibility, as well as the influence of ionic liquids in terms of manner, concentration and acidity.

As a second large activity, a mock-up of an airworthy generator housing is designed developed. For this purpose, all central technical compartments inside the housing, such as a membrane, a filter unit, a starter mechanism and a reaction chamber will be constructed and additively manufactured.

3 Technical and Theoretical Background

3.1 Ionic liquids

In spite of the fact that Ionic Liquids are frequently referred to as brand new inventions, low melting salts have existed since the 19th century. In those days, salts with melting points below 100 °C were considered to be ionic liquids. In 1914, Walden published the synthesis of [EHHHN][NO_3] that gave rise to room temperature ionic liquids, salts that are liquid at room temperature.[7] Due to the water sensitivity no further research was attempted at this time. It was in 1940 that the use of aluminum chloride based Ionic Liquids for electroplating proved to be highly erratic.[8] Ionic liquids based on alkylimidazolium did not become widely popular until the early 1980s. The discovery of [EMIM][$AlCl_4$] in 1982 led to propulsion of new developments in both academia and industry.[9]

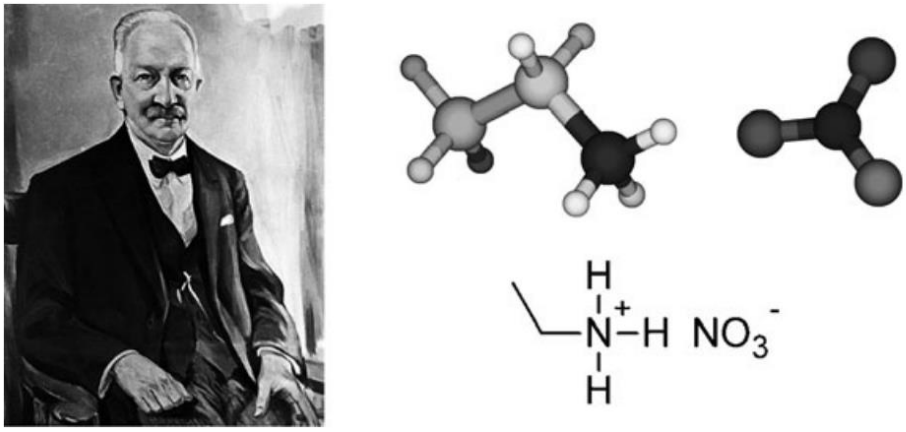

Figure 4: Paul Walden and the chemical structure of [EHHHN][NO_3].[10]

A salt with a melting point below 373 K is considered an Ionic Liquid. These generally have low vapor pressure, excellent solubility properties, high chemical and thermal stability, and a wide liquid range. This makes them a potential alternative to solvents that is both more environmentally friendly and safer. Chemically, Ionic Liquids are characterized by their unique physicochemical properties, such as melting point, polarity, viscosity, solubility, and density. he described properties can be specifically adjusted in a targeted manner via the manifold modifiable molecular structure of anion and cation. In addition to their ability to be used in classical fields like inorganic,

organic, and electrochemical, ionic liquids are also suitable for new applications such as engineering and analytics.[10]

One purpose of this thesis is to investigate the suitability of ionic liquids as solvents in a wide temperature range under harsh reaction conditions. In contrast to conventional organic solvents, the liquid range is defined not by melting and boiling point but by melting point and thermal decomposition temperature. Ionic Liquids have negligible vapor pressure.

3.2 *Brønsted* acidic ionic liquid

A *Brønsted* acidic ionic liquid (BAIL) is an ionic liquid that is formed by the transfer of a proton from a *Brønsted* acid to a *Brønsted* base, as illustrate in **Scheme 4**. In contrast to aprotic ionic liquids, BAILs have at least one exchangeable proton and, therefore, exhibit *Brønsted* acidity.[11, 12]

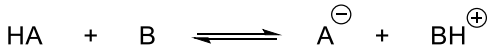

Scheme 4: Neutralization reaction of acid and base.

There are different functional groups that can hold exchangeable protons. Common locations within a molecule include oxygen and nitrogen atoms. They can reside within the cation, the anion, or both. **Figure 5** illustrates typical protic cations and anions which can be found in commonly used BAILs.[13]

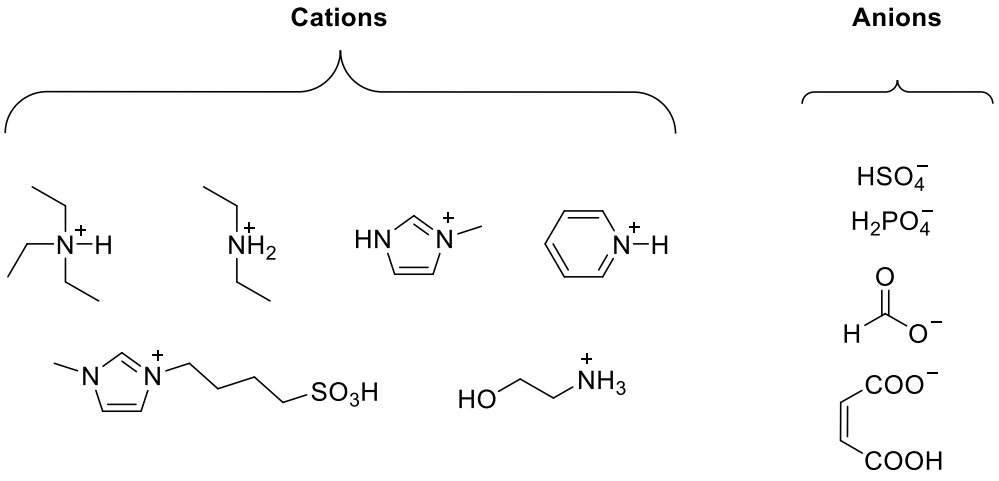

Figure 5: Protic cations and anions that commonly occur within BAILs.[11, 13]

Physiochemical properties of ionic liquids are affected by different functional groups within them. For example, ionic liquids bearing a -SO_3H group are likely to exhibit a stronger *Brønsted* acidity than ammonium derivatives. BAILs have been evaluated for their suitability for a variety of applications. On a multikilogram scale, molten pyridinium hydrochloride has been used for demethylation of 4-methoxyphenylbutyric acid.[14] It has also been demonstrated that BAILs containing -SO_3H groups can be used in reactions such as the *Fischer esterification* or *Ritter* chemistry to synthesize amides.[15, 16]

It is important to consider the degree of proton transfer and hydrogen bonding when attempting to understand the properties of BAILs. **Figure 6** illustrates the four possible outcomes of BAILs which have been reported in literature before.[12]

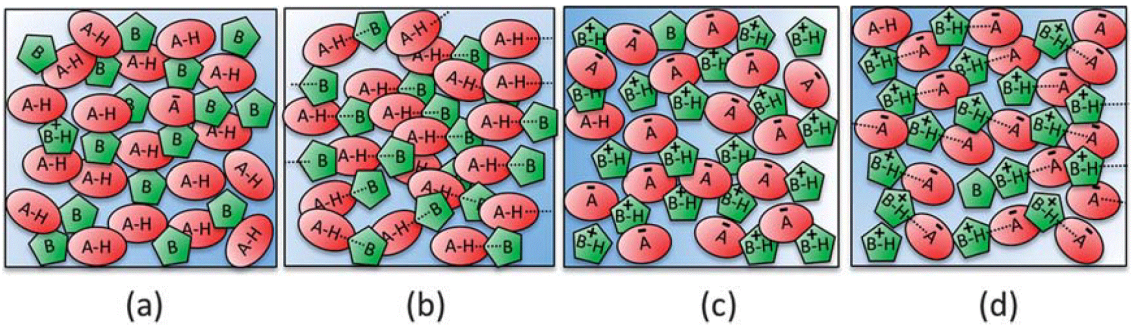

Figure 6: Four possible types of BAILs: (a) mostly unionised acid and base; (b) hydrogen bonded acid-base pairs (no proton transfer); (c) mostly ionised BAIL (proton transfer occurred, independent ions); (d) associated BAIL (proton transfer occurred but ions associate through hydrogen bonding).[11, 12]

To be considered "pure", the equilibrium of the reaction in **Scheme 4** must lie at least 99% along the ionic species to not be a complex mixture of acids, bases and salts. For case (c) *Angell et al.* suggest that the difference in the aqueous pKa values between acid and base should be > 10.[17]

3.3 Ionic liquids in aviation and space technology

Traveling away from Earth places us in a very extreme environment. There is a lack of oxygen, very low pressures, extreme variations in temperature, ionizing radiation, highly reactive species, dust, etc., which requires sophisticated equipment to protect us from these threats and to facilitate research. This is all following a safe launch from Earth. Several space technologies have been developed using ionic liquids, so let's take a closer look at what is possible.[18]

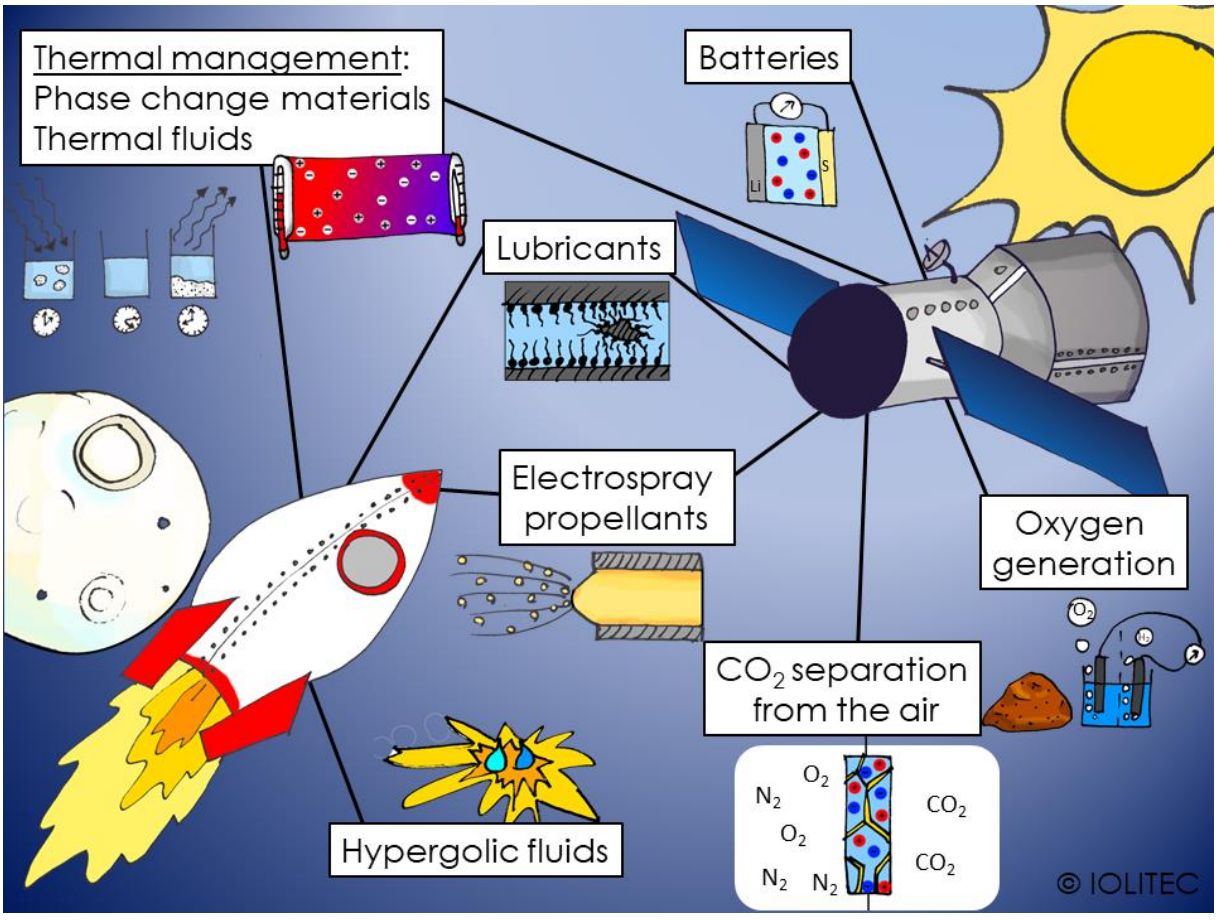

Figure 7: Applications or ionic liquids in space technology.[18]

3.3.1 Propellants

Getting into space is the first challenge, wherefore fuel is needed. Typically, hypergolic fluids are used as propellants for spacecrafts. They are highly energetic and ignite spontaneously when mixed with any oxidant. Ionic liquids can be used as hypergolic fluids an offer several benefits. Firstly, because of their low vapor pressure, they enable easier handling and safer storage and decreased loss due to no evaporation. Secondly, they are relatively stable, which means that they do not need to be stored in complex and heavy tanks, for example cryogenic containers like hydrazine or liquified hydrogen and oxygen. Additionally, ionic liquids are designable, enabling optimization towards high energy output, high energy density and wide liquidus range. In particular, ionic liquids containing dicyanamide as an anion have demonstrated their utility as hypergolic fluids.[18, 19]

The high solubilizing power of ionic liquids allows them to be used in combination with other, sometimes solid propellants. Boranes, for example, have been used in a mixture of [BMIM][BF_4], [BMIM][DCA] and [BMPyrr][DCA] as illustrated in **Figure 8** in order to increase their performance as propellants and outperform current hydrazine-based systems.[20]

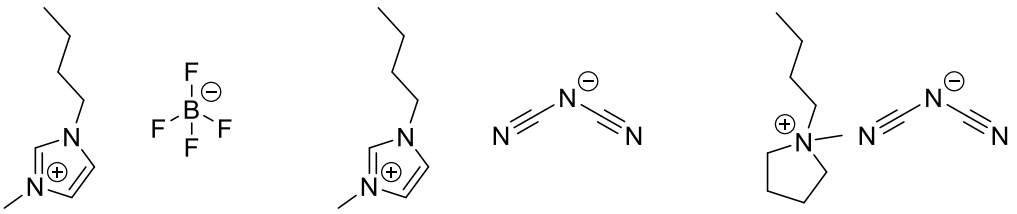

Figure 8: Structural formula of [BMIM][BF_4], [BMIM][DCA] and [BMPyrr][DCA].[20]

3.3.2 Life-support systems

In order to provide an atmosphere which is suitable to humans, carbon dioxide must be removed and consumed oxygen replaced constantly. Especially for sensitive technology on board of a spacecraft dust, water vapor, microorganisms and fats have to be removed too. In addition to being extensively investigated for removing CO_2 from gas mixtures, ionic liquids are also promising for this propose of managing air quality.

3.3.2.1 SILM technology

The low vapor pressure makes them ideal for use as part of supported ionic liquid membranes, since it allows the waste CO_2 to be emitted directly into space without losses of ionic liquids. The ultra-low vapor pressure also prevents air contamination with ionic liquids inside the spacecraft.[18]

First, carbon dioxide adsorbs on the ionic liquid within the polymer matrix. Once in the membrane, carbon dioxide now diffuses trough the membrane to the other side, supported by the ionic liquids present in the membrane. There, the carbon dioxide desorbs due to concentration differences or usually applied vacuum, as illustrated in **Figure 9**.[21]

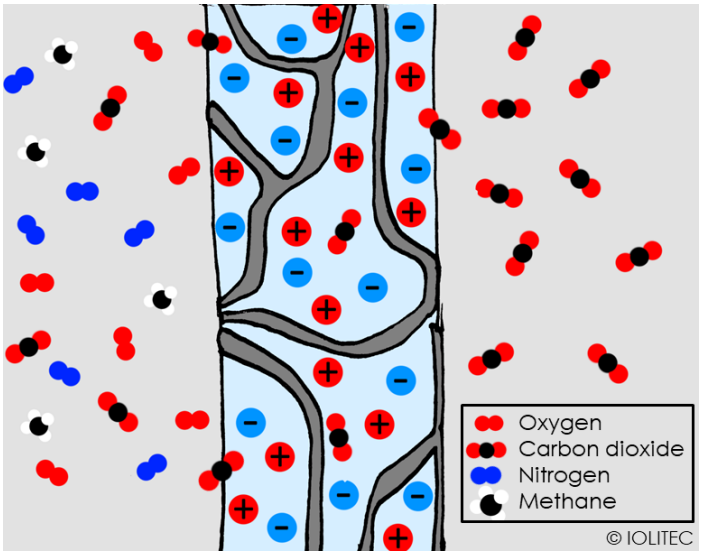

Figure 9: Carbon dioxide diffusion trough a supported ionic liquid membrane (SILM).[21]

3.3.2.2 Absorption and stripper technology

An absorption process for carbon dioxide typically involves a feed gas, an absorption column, a stripper column and two output gas streams of carbon dioxide rich and poor gases. In the case of ionic liquids, the process could be similar to that of amine gas treatment, where the carbon dioxide is regenerated in the stripper at higher temperatures. Alternatively, ionic liquids can also be stripped inert gases, reducing the process energy requirement.[21] In order to increase the capacity of the ionic liquids, task-specific ionic liquids employing chemisorption and physisorption are being developed. Promising results are obtained with the ionic liquid 1-butyl-3-propylamineimidazolium tetrafluoroborate [NH_2PBIM][PF_6]. As shown in **Figure 10** the ionic liquid is capturing carbon dioxide with its amine functionality by the formation of a carbamate.[22, 23]

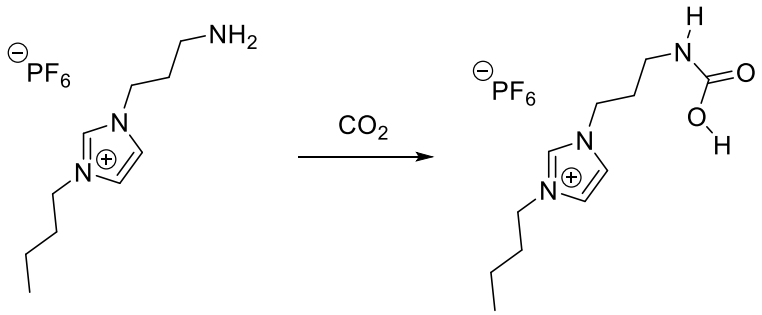

Figure 10: Carbamate formation with the ionic liquid [NH_2PBIM][PF_6] and CO_2.

3.3.3 Lubricants

As the universe bears both, very high and very low temperatures, free-radical environments containing H•, cosmic dust and space debris, high wear and abrasion of surfaces and moveable parts occurs during all kinds of operation. On the other hand, maintenance in space is costly and difficile.

High-performance lubricants can prevent these problems. For applications in space, ionic liquids seem ideal lubricants, as they possess ultra-low vapor pressure avoiding evaporation into space, high heat capacity and thermal stability avoiding overheating and welding, electrical conductivity inhibits surface charging as well as their intrinsic resistance to oxidation and radiation.

Ionic liquids based on the Bistriflimide anoin showed effective lubricating properties during application in space, especially [HexMIM][TFSI].[24]

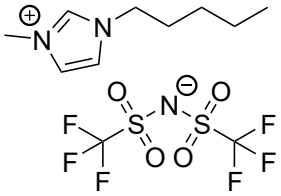

Figure 11: Structural formula of [HexMIM][BTA].

3.3.4 Energy management

The equipment on board the spacecraft is powered by a variety of energy sources. Currently, lithium-sulfur batteries are mainly used for space applications due to their light weight and high energy density. These can be combined very well with solar panels, allowing them to be charged slowly in the sunlight and discharged when it's dark. Nowadays mainly ionic liquids like [HexMPyrr][TFSI] and [OctMPip][DCA] are in common use.[25] Also hybrid-ionic liquid-based electrolytes are known and promising due to the merits of acceptable ion conductivity, moderate polysulfide solubility and good lithium compatibility.

One example of such an electrolyte is a mixture of [MMOEPyrr][TFSI], 1,3-dioxolane (DOL) and 1,1,2,2-tetrafluoroethyl-2,2,2-trifluoroethyl ether (TFTFE).[26]

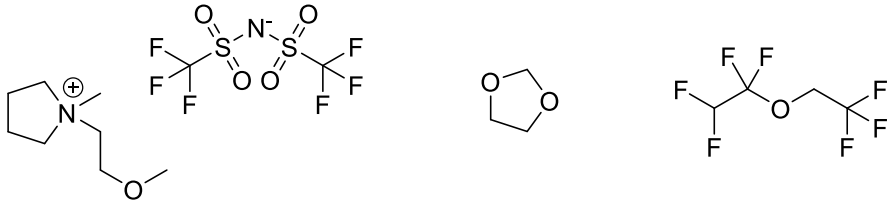

Figure 12: Structural formula of [MMOEPyrr][TFSI], 1,3-dioxolane (DOL) and 1,1,2,2-tetrafluoroethyl-2,2,2-trifluoroethyl ether (TFTFE).

Beside power supply of a spacecraft, thermal regulation is crucial too, as temperature can vary easily from -100 °C up to +50 °C between day and night. The human body is unable to survive in these conditions, and even unmanned spacecraft require temperature regulation for correct functionality.

Using thermal fluids, excess heat can be transferred from one location to another. In addition to their high thermal stability, wide liquidus range and high heat capacity, ionic liquids are eminently suitable for the use as thermal and heat transfer fluids. The application of phase change materials is another option for heat management. Phase change materials can absorb energy and turn from solid to liquid, storing energy in the liquid state and releasing it upon solidification.[18] [HexdMIM][Br] has proven to be an adequate candidate for this application.[27]

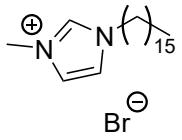

Figure 13: Structural formula of [HexdMIM][Br].

3.4 Oxygen liberation from inorganic peroxides in ionic liquids

In the process of oxygen liberation from peroxide-based oxygen sources like hydrogen peroxide adducts or inorganic peroxides, after dissolution in water one mole of hydrogen peroxide is decomposed into one mole of water and one-half mole of oxygen as shown in **Scheme 5** below. According to the ideal gas law one mole of hydrogen peroxide therefore liberates 12 L of gaseous oxygen under standard conditions.

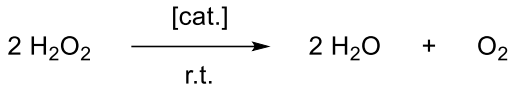

Scheme 5: Catalytic decomposition of hydrogen peroxide.

In contrast, chlorates and perchlorates of alkali metals such as lithium, sodium and potassium decompose directly to oxygen and the corresponding chloride salts as it is depicted in **Scheme 6**.

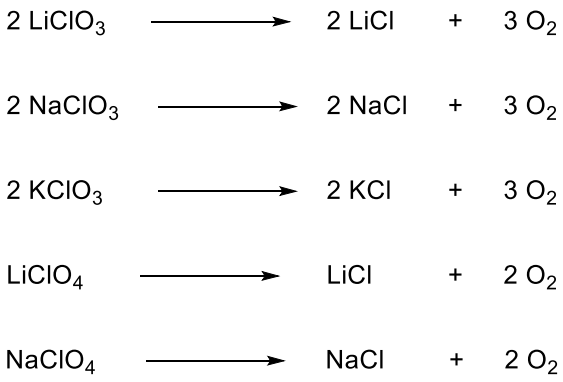

Scheme 6: Liberation of oxygen from lithium, sodium and potassium chlorate as well as from lithium and sodium perchlorate.

Using the above-mentioned model and taking into account the individual AOCs of the compounds, **Table 1** provides a general overview of the required mass of various peroxide compounds and sodium chlorate for a four-person oxygen generator.

Table 1: Required mass of different potential oxygen sources to liberate a total of 120 L oxygen and the respective active oxygen content.

compound	mass [g]	AOC [%]
lithium peroxide Li_2O_2	459	35
sodium peroxide Na_2O_2	780	21
calcium peroxide CaO_2	720	29
urea hydrogen peroxide $CO(NH_2)_2 \times H_2O_2$	940	17
lithium chlorate $LiClO_3$	306	53
sodium chlorate $NaClO_3$	360	45
potassium chlorate $KClO_3$	415	39
lithium perchlorate $LiClO_4$	280	60
sodium perchlorate $NaClO_4$	312	52

Hydrogen peroxide adduct compounds require a greater amount of mass than conventional sodium chlorate compounds, however, this class of compounds is highly promising due to their previously mentioned beneficial properties as well as their potential for use in oxygen generators at low temperatures. It is also important to note that the stated value for sodium chlorate does not account for the fact that an important portion of oxygen is reacted with a metal fuel in the chlorate candle and is therefore unavailable to the passenger. Thus, the actual amount of sodium chlorate is much higher.

3.5 Requirements for emergency chemical oxygen generators

There are strict regulations governing emergency oxygen generators used in aviation which are defined in the Aerospace Standards by *SAE International*. Performance characteristics like total oxygen volume, gas purity, oxygen flow rate as well as temperature strains are part of the detailed demand profile. As a first guide, one can use the data from commercial chlorate candles to determine the oxygen flow rate and the total oxygen volume. **Figure 14** illustrates the flow rate profile of a state-of-the-art oxygen generator manufactured by *Avox Systems*.[28] This system, designed for four passengers, releases 60 L of pure oxygen over the course of 12 min. In order to maintain the desired flow rate profile, the aircraft's current cruising altitude is taken into consideration. After the chlorate candle starts generating oxygen, the pilots start a step and fast descend, so-called emergency descend, from the current cruising altitude down to a safe heigh with adequate breathing air at approximately 3000 , to 4000 m depending on the ground level. At high altitudes, it requires a relatively high initial oxygen flow rate to sustain a sufficient level of hemoglobin oxygen saturation and to flush the tubing and masks. As altitude decreases, less oxygen is required to be administered to the passenger to prevent oxygen intoxication and symptoms of the *Paul Bert* effect.

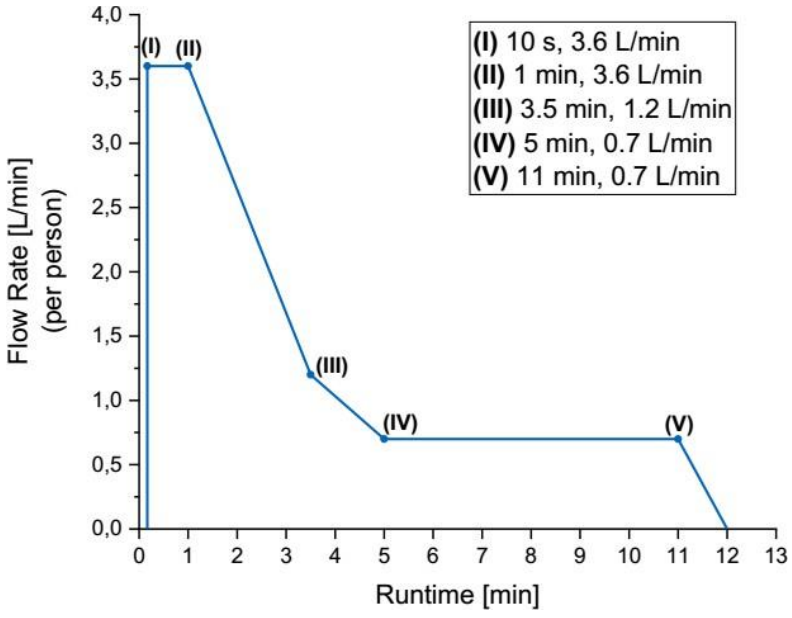

Figure 14: Typical oxygen flow rate profile per person for an oxygen generator by *Avox Systems* designed for four passengers.[28]

According to *SAE AS8010C*, requirements concerning the gas purity of chemical oxygen generators used in emergency situations are specified.[29] It is necessary to have an oxygen content of at least 99.5 % in the liberated gas stream, to be free of objectionable odors and to have no water content exceeding 20 mg/L (21.1 °C, 1.013 bar). The maximum permitted impurity concentrations are listed in **Table 2** below.

Table 2: Constituent maximum concentrations for a chemical oxygen generator for emergency use. The stated values are the time weighted average concentrations for periods not exceeding 5 min over the duration of operation.[29]

compound	max. concentration [ppm]
CO_2	5000
CO	50
Cl_2 & chlorine derivates	0.2
solvents (e.g. CCl_3)	0.2

Emergency oxygen systems must function under a variety of environmental conditions. Over a wide range of ambient temperatures, adequate oxygen liberation must be ensured. The oxygen generator by *Avox Systems* mentioned above has a specified temperature range for operation of -20 °C to +45 °C.[28] For the current work, this range is extended to -20 °C up to +60 °C as a first guideline to ensure proper shelf life.

The chemical oxygen generator must be fully functional aligned in all spatial directions and meet the demanded flow rate profile. In a sometimes highly tumultuous emergency descent, the airplane can get in a variety of positions whereby not only gravity but also g-forces stress the generator housing and other emergency oxygen supply equipment.

4 Results and discussion

4.1 General considerations

Choosing the oxygen liberation agent is one of the most crucial decisions when developing a novel oxygen generation system. It should be easily accessible, stable at the right temperature and pressure, and, of course, provide steady oxygen liberation during its decomposition. It is further recommended that the weight of the material be as low as possible, i.e. the active oxygen content should be as high as possible, in order to ensure the portability of the oxygen generator.

Peroxides provide a reliable and available oxygen source. The oxygen source mainly used is lithium peroxide Li_2O_2 and calcium peroxide CaO_2. Several studies have examined the oxygen evolution activity of calcium peroxide in particular.[30] Li_2O_2 and CaO_2 are thermally stable at a range of temperatures from -20 °C to +60 °C, what is a legal requirement for the use in chemical oxygen generators.[31]

Scheme 7 shows the reaction equations for the decomposition of Li_2O_2 and CaO_2 under wet conditions.

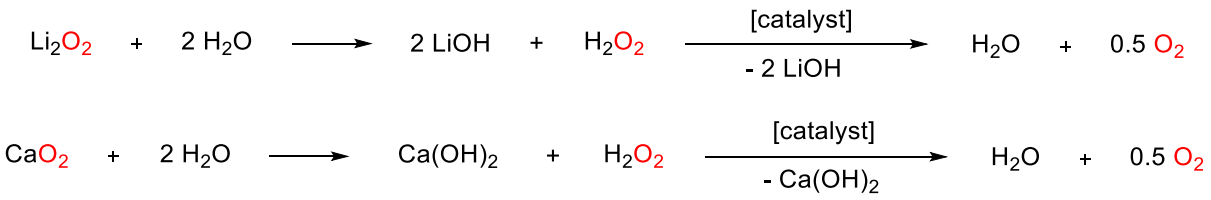

Scheme 7: Reaction equations for the decomposition of Li_2O_2 and CaO_2 under wet conditions.[31]

The utilized reaction medium must also meet the legal requirements for stability and availability and therefore must ha a liquidus range from -20 °C to +60 °C. As a result, pure water cannot be used as a reaction medium because it would freeze at 0 °C. Thus, different acidic and basic aqueous solutions with melting points below 20 °C are tested as reaction media. Ionic liquids are another class of chemicals that meet these requirements. Due to their wide liquidus range, they may also be appropriate as solvent in this reaction.

We attempt to define the conversion of the oxygen source utilized in each of the investigated systems in order to establish a comparison between them. The maximum theoretical oxygen volume is calculated by determining the amount of substance of oxygen that can be evolved if all the active oxygen in the oxygen source is converted into oxygen gas. The volume is calculated using the molar volume of an ideal gas at 25 °C and 101.3 kPa. As the utilized inorganic peroxides do not have a purity of 100%, their individual purity has to be taken into account. Therefore, is necessary to multiply the theoretical oxygen volume by 0.9 in the case of lithium peroxide, which has a purity of 90%, and with 0.75 in the case of calcium peroxide since its purity is 75%. It is important to note that this definition of conversion is only an estimate. In Chapter 4.3 and 4.4, this topic is further discussed as well as other issues related to the measurement of evolved gas volumes.

4.2 Ionic Liquids

Several ionic liquids are synthesized and applied over the course of this thesis. The syntheses are conducted according to procedures known in literature. **Figure 15** provides an overview of the utilized compounds.

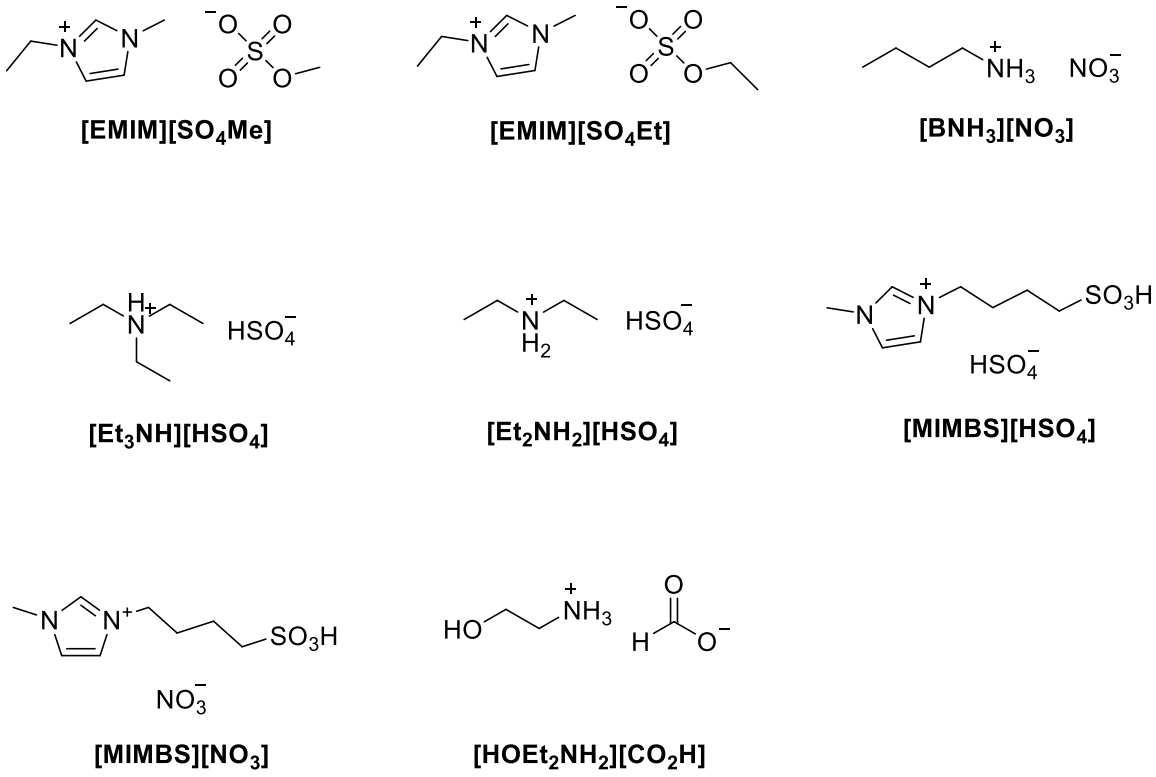

Figure 15: Valence structural formula of applied Ionic Liquids.[11]

4.3 Catalytic oxygen liberation from lithium peroxide

To develop a next generation chemical oxygen generation based on a novel oxygen liberation compound, lithium peroxide is the first material to be tested, as it provides the highest Active Oxygen Content (34.8 wt-%) of all metal peroxides.[32] Small-scale experiments have shown that lithium peroxide exhibits promising oxygen liberation activities when combined with $Mn(OAc)_2 \times 4\ H_2O$ as a catalyst in aqueous solvents. In order to meet the requirements for COG for aviation purposes, it is attempted to improve the reaction conditions upon complete conversion as well as a steady decomposition reaction. The first step is to conduct small-scale experiments to determine how various parameters affect the oxygen evolving reaction.

4.3.1 Lithium peroxide decomposition experiments – 1% of target size

At room temperature, small-scale experiments are conducted to determine whether lithium peroxide can liberate oxygen in a constant fashion. In order to facilitate this process, 5 g of lithium peroxide is decomposed in different solvents under ambient conditions. $Mn(OAc)_2 \times 4\ H_2O$ has been shown to be effective as a catalyst for promoting the release of gaseous oxygen from other peroxides in a constant manner. Additionally, the lithium peroxide powder is pressed into cylindrical compacts (CCs), which is discussed in greater detail in chapter 4.3.2.1 on page 38. Unless otherwise stated, all 1% scale experiments use 5 g of lithium peroxide in the form of one cylindrical compact, compressed under 500 kPa pressure for one minute.

4.3.1.1 Variation of the aqueous solvent

As a first parameter, the aqueous solvent is varied in the gas evolving system of lithium peroxide. The presence of water facilitates the reaction from lithium peroxide to H_2O_2 and subsequently to oxygen, as shown in **Scheme 7** on page 19. Since water has a melting point of 0 °C, it cannot be used as a solvent. A chemical oxygen generator based on pure water would not meet the requirements for a chemical oxygen generator for aviation purposes, since it has to function at a temperature of -20 °C.[31] To this end,

different acidic and basic aqueous solvents with melting points lower than 20 °C have been tested.

The evolving volume and gas flow rates for the decomposition of 5 g lithium peroxide with 0.25 mol-% of $Mn(OAc)_2 \times 4\ H_2O$ in 25 ml of the basic aqueous solvents NaOH (25%) and KOH (25%) at room temperature are shown in **Figure 16**.

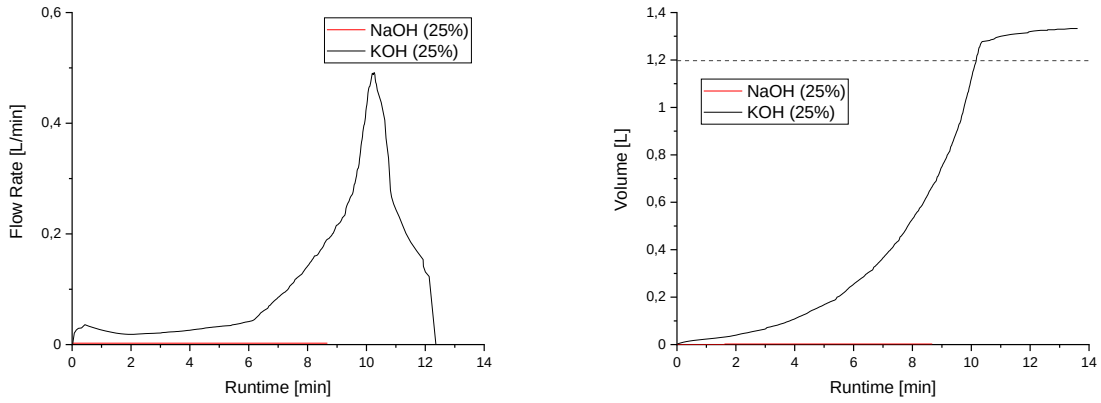

Figure 16: Evolving gas volume and gas flow rates for the reaction of 5 g lithium peroxide and 0.25 mol-% $Mn(OAc)_2 \times 4\ H_2O$ in 25 ml of NaOH (25%) and KOH (25%) at room temperature. The dashed line marks 100% of theoretical lithium peroxide conversion.

According to the diagram, both the flow rate and the volume evolved are zero for the system with NaOH (25%). In the case of KOH (25%), gas evolution proceeds slowly at the beginning, at a rate of 0.02 L/min, but eventually reaches a maximum flow rate of 0.49 L/min towards the end of the reaction after ten minutes. For the reaction in KOH (25%) the liberated gas volume increases linearly for the first six minutes and then almost exponentially towards the end of the reaction until it reaches a plateau after ten minutes.

As can be seen, the choice of solvent significantly influences the evolution of a gas. There is no measurable gas evolution in NaOH (25%). The reason for this may be the insolubility of lithium peroxide in NaOH (25%), which prevents the formation of H_2O_2 and, consequently, the release of oxygen. Consequently, NaOH (25%) is not suitable as a solvent for chemical oxygen generators based on lithium peroxide. By contrast, KOH (25%) results in measurable gas evolution due to the fact, that lithium peroxide dissolves in that reaction medium properly. KOH (25%) is therefore better suited for use in a chemical oxygen generator based on lithium peroxide than NaOH (25%). The actual gas volume, however, is greater than the theoretical

maximum oxygen volume that can be produced from 5 g of lithium peroxide. There is a complete lithium peroxide conversion, which is desirable, but there may be other reasons for the higher gas volume than expected. In the following paragraph, this issue is further discussed. It should be noted that the maximum flow rate is reached at the end of the reaction, which is contrary to what is desired for a chemical oxygen generator designed for aircraft applications.

In some cases, a gas volume that exceeds the theoretically calculated value can be attributed to a variety of reasons. In order to simplify the calculation, the theoretical amount of oxygen is calculated using the molar volume of ideal gases. It should be noted that this is only an estimate based upon the actual gases examined. Furthermore, the temperature of the evolved gas is unknown. Gases released during the reaction are not immediately transported to gas meters, but rather are transported via tubes, which correspond to a distance of one meter in transportation. During the transportation process, the gas is potentially cooling down, as the tubes are not insulated. It is also possible that other gases may be released during the decomposition process in addition to oxygen. Gases generated during the reaction vary depending on the reaction medium, including water vapor, HCl, CO, CO_2, O_3, acetic acid, NH_3 and NO_x. This could be due to evaporation caused by elevated reaction temperatures, or due to decomposition caused by utilized reaction compounds under harsh reaction conditions, or even to a combination of both. Additionally, it is important to note that the used lithium peroxide and other used oxygen sources in general do not possess 100% purity. Throughout this thesis, lithium peroxide with a purity of 90% is primarily used. Although this value represents a minimum, it is possible for the material to contain more than 90% lithium peroxide. In addition, it is unknown what the additional 10% of compounds in the sample are and they also may contribute to the evolution of gas during their composition. Furthermore, the drum-type gas meter utilized is calibrated for a flow rate ranging from 900 L/h up to 900 L/h. Flow rates that are above or below that range may lead to inaccurate measurements.

Next, the acidic aqueous solvents H_2SO_4 (30%) and HCl (15%) are examined, as according to **Scheme 7** acidic reaction conditions are favorable. The flow rate of the liberated gas as well as the gas volume for the reaction of 5 g lithium peroxide and 0.25 mol-% of $Mn(OAc)_2 \times 4\ H_2O$ in the acidic aqueous solvents H_2SO_4 (25%) and HCl (15%) are depicted in **Figure 17**.

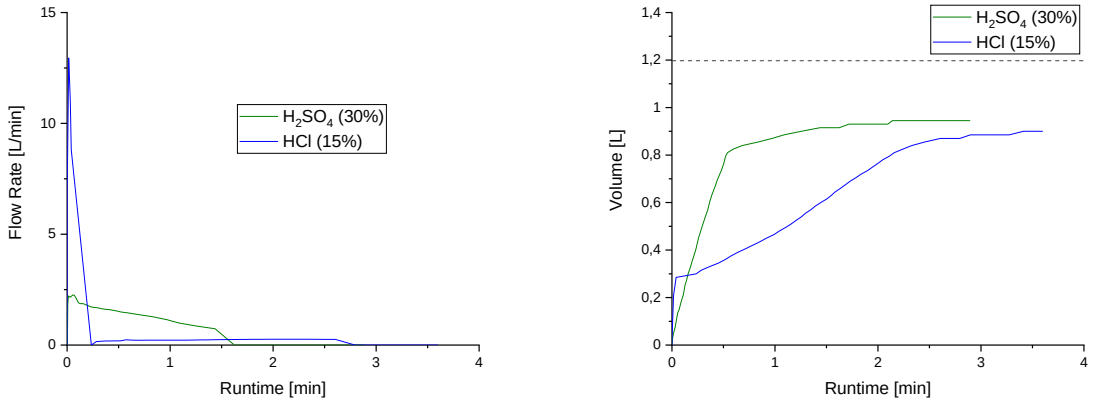

Figure 17: Liberated gas volume and gas flow rate for the reaction of 5 g LPO and 0.25 mol-% $Mn(OAc)_2 \cdot 4\ H_2O$ in 25 ml of H_2SO_4 (30%) and HCl (15%) at room temperature. The dashed line represents 100% of theoretical LPO conversion.

The flow rate plot for the reaction in HCl (15%) exhibits a peak of 13.0 L/min at the beginning of the reaction, before the flow rate drops over a period of 15 s and the reaction proceeds for another 150 s with a gas flow rate of around 0.2 L/min. It stops after a total of 2.75 min. The gas volume of the reaction rises accordingly in the beginning to 0.3 L after a few seconds, and then continues to increase steadily until a volume of 0.8 L is reached after 2.5 min. The flow rate of the reaction in H_2SO_4 (30%) is also highest at the beginning of the reaction. However, it does not exhibit a sharp peak, but decreases slowly over a period of 1.5 min, after which the flow rate subsequently drops to zero.

There is generally a higher maximum flow rate and a shorter reaction time in systems that contain acidic aqueous solutions as compared to systems that use the basic solvent KOH (25%). **Table 3** summarizes the values for the reaction time, the maximum flow rate, and the conversion. The maximum flow rates for both reactions with H_2SO_4 (30%) and HCl (15%) are observed at the beginning of each reaction. For the reaction in H_2SO_4, the flow rate decreases steadily over 1.5 min, whereas for the lithium peroxide decomposition in HCl (15%), the flow rate reaches a rapid peak in the beginning of the reaction and rapidly drops from 13 L/h down to 0.2 L/h over the course of 15 s. In contrast to the reaction in KOH (25%), the maximum flow rate occurs at the beginning of the reaction, which corresponds to the requirements for chemical oxygen generators in aviation. Despite this, the maximum flow rate of 13 L/min exceeds the required initial flow rate of 3.6 L/min by more than three times.

In addition, the incompleteness of the decomposition reactions at the chosen reaction conditions must be mentioned. A possible explanation is the evaporation of water during the reaction as a result of the high level of reactivity and the subsequent rise in temperature. In this case, water is no longer available for lithium peroxide dissolution and reaction (**Scheme 7**), resulting in a lower yield of H_2O_2 and a lower amount of oxygen being released. In **Table 3**, the durations, maximum flow rates, and conversions of oxygen liberation reactions in different aqueous solvents are summarized.

Table 3: Duration, maximum flow rate and conversion for the reaction of 5 g of lithium peroxide and 0.25 mol-% of $Mn(OAc)_2 \times 4\ H_2O$ in different aqueous solvents.

solvent	duration [min]	max. flow rate [L/min]	conversion [%]
NaOH (25%)	-	-	-
KOH (25%)	12	0.49	111
H_2SO_4 (30%)	1.4	2.26	78.9
HCl (15%)	2.6	13.0	75.2

There is evidence in the literature that decomposition of H_2O_2 with soluble manganese catalysts occurs at a slower rate in acidic media than in basic media.[33] The experiments above, however, demonstrate opposite reactivity. Among the reasons for this may be that *Watts et al.* examined hydrogen peroxide decomposition, while the reactions presented in this chapter use lithium peroxide as starting material. Even without the presence of a catalyst, lithium peroxide is known to strongly react with inorganic acids, under some circumstances resulting in its decomposition. Accordingly, the gas evolution rate is mainly determined by the first partial reaction shown in **Scheme 7**, namely the protonation reaction of lithium peroxide with the solvent, rather than the decomposition of H_2O_2 with the aid of the catalyst.[34]

4.3.1.2 Addition of room temperature ionic liquids

For the decomposition of lithium peroxide, aqueous acidic solvents provide the highest reactivity. The decomposition reactions, however, proceed very rapidly. In order to increase the reaction duration and to smoothen the flow rate profile, ionic liquids are added to the reaction mixture. The melting point and viscosity of various ionic liquids have been measured in previous work within the group to determine their potential for use in chemical oxygen generators.[3] A promising candidate was identified in these studies as 1-ethyl-3-methylimidazolium methyl sulphate [EMIM][SO_4Me] with a dynamic viscosity of 1.07 Pas at -20 °C. It has a relatively low viscosity in comparison with other imidazolium-based ionic liquids.

The following experiments examine the effect of the quantity of ionic liquid on the decomposition reaction. For this purpose, 5 g of lithium peroxide are decomposed with 0.25 mol-% of $Mn(OAc)_2 \times 4\ H_2O$ in 15 ml of H_2SO_4 (30%) with different amounts of the ionic liquid [EMIM][SO_4Me]. Two diagrams depicting the results in terms of gas volume and flow rate can be found in **Figure 18**.

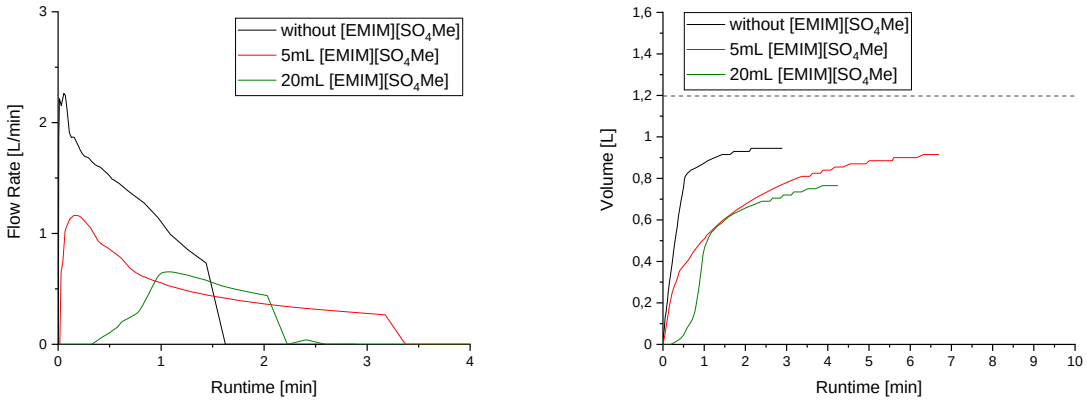

Figure 18: Flow rate and volume development for the reaction of 5 g lithium peroxide and 0.25 mol-% $Mn(OAc)_2 \times 4\ H_2O$ in 15 ml of H_2SO_4 (30%) and different amounts of [EMIM][SO_4Me] at room temperature. The dashed line marks 100% of theoretical lithium peroxide conversion.

In **Table 4**, the duration, maximum flow rate, and conversion of the respective reactions are summarized.

Table 4: Results for the duration, maximum flow rate and conversion for the reaction of 5 g LPO and 0.25 mol-% of $Mn(OAc)_2 \times 4\ H_2O$ in 15 mL of H_2SO_4 and varying amounts of [EMIM][SO_4Me].

solvent	duration [min]	max. flow rate [L/min]	conversion [%]
without [EMIM][SO_4Me]	1.4	2.2	79
5 mL [EMIM][SO_4Me]	3.2	1.2	76
20 mL [EMIM][SO_4Me]	2.0	0.65	64

The flow rate plot indicates the maximum flow rate at the beginning of each decomposition reaction. The maximum flow rate obtained is therefore highest in the experiment without any ionic liquid and lowest in the experiment with the greatest amount of ionic liquid. In addition, the reaction with 20 mL [EMIM][SO_4Me] shows an onset time, i.e., the decomposition does not start immediately, but after 20 s. It is important to note that whereas the catalyst loading relative to lithium peroxide remains the same in all of the experiments, the concentration of the catalyst decreases with an increase of the amount of ionic liquid added. In addition, the heat capacity of RTIL differs from that of aqueous solution. If more heat is required to increase the reaction temperature, the reaction could begin later and reach a lower temperature overall. The addition of 5 mL of [EMIM][SO_4Me] increased the duration of the reaction by 1.5 min compared to the reaction without any ionic liquid. In addition, the maximum flow rate decreased by almost half, indicating that the reaction proceeds at a slower pace.

The amount of evolved gas is also affected by the addition of [EMIM][SO_4Me]. Considering the chosen conditions, the highest gas volume is observed when no [EMIM][SO_4Me] is present during the decomposition reaction, and the volume of evolved oxygen decreases with increasing amounts of [EMIM][SO_4Me]. Therefore, a decrease in gas evolution is associated with a slowdown of the reaction. It appears that there is an optimal amount of ionic liquid that, when added to the reaction mixture, leads to a milder reaction without significantly reducing the amount of gas liberated.

4.3.1.3 Mixtures of different Aqueous Acidic Solvents

H_2SO_4 (30%) and HCl (15%) are both promising solvents for the oxygen liberation reaction from lithium peroxide in a constant fashion. The use of HCl (15%) comes with the risk of evaporating HCl and Cl_2 gas, while the use of H_2SO_4 (30%) should not result in any volatile compounds besides water. It has been found that the reaction proceeds more smoothly when HCl (15%) is used as a solvent than with H_2SO_4 (30%). It is recommended that the amount of utilized HCl (15%) is reduced so as to minimize the production of volatile HCl und Cl_2 gas and yet benefit from the beneficial influence on the decomposition reaction. It is therefore investigated whether the properties of both aqueous solvents can be combined by mixing HCl (15%) and H_2SO_4 (30%) in different ratios. **Figure 19** shows the flow rate and volume developments for the decomposition of 5 g lithium peroxide and 0.25 mol-% $Mn(OAc)_2 \times 4\ H_2O$ in 10 mL [EMIM][SO_4Me] and 15 mL of a mixture of different volume ratios of H_2SO_4 (30%) and HCl (15%).

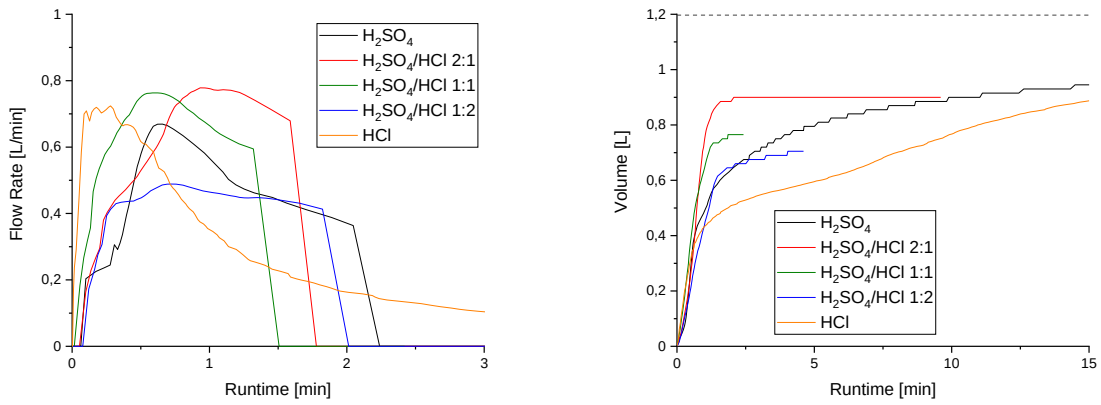

Figure 19: Flow rate and volume developments for the decomposition of 5 g lithium peroxide in 10 mL [EMIM][SO_4Me] and 0.25 mol-% $Mn(OAc)_2 \times 4\ H_2O$ and 15 mL of a mixture of H_2SO_4 (30%) and HCl (15%) consisting of different volume ratios.

The results of the experiments are summarized in **Table 5**, which shows the reaction times, maximum flow rates, and conversion rates for each experiment.

Table 5: Results for the duration, maximum flow rate and conversion for the decomposition of 5 g lithium peroxide in 10 mL [EMIM][SO_4Me] and 0.25 mol-% $Mn(OAc)_2 \times 4\ H_2O$ and 15 mL of a mixture of H_2SO_4 (30%) and HCl (15%) consisting of different volume ratios.

solvent	duration [min]	max. flow rate [L/min]	conversion [%]
H_2SO_4	2.2	0.67	79
H_2SO_4/HCl 2:1	1.7	0.78	75
H_2SO_4/HCl 1:1	1.5	0.76	64
H_2SO_4/HCl 1:2	2.0	0.49	59
HCl	17.3	0.72	77

In general, the flows and conversions of the reactions are similar, except for the 1:2 mixture of H_2SO_4 (30%) and HCl (15%), where both values are lower than those of the other decompositions under different conditions. It should be noted that the reaction in pure HCl (15%) stands out in terms of its reaction duration, which exceeds the values of the other conditions by around 15 min. Overall, the flow rate peaks at the beginning of the reaction and then smoothly continues for another 15 min, thereby maintaining a nearly constant flow rate throughout. As compared to all other conditions chosen so far, this reaction comes closest to the requirements for chemical oxygen generators used in civil aviation. It has been found that mixing H_2SO_4 (30%) with HCl (15%) does not result in the desired flow rate.

The duration of the 1:2 mixture decomposition reaction would therefore be expected to be similar to the HCl (15%) reaction, however, interestingly, this is not the case. Adding even small amounts of H_2SO_4 (30%) drastically reduces the reaction time from around 17 min down to two minutes.

4.3.1.4 Variation of the amount of aqueous solvent

According to **Scheme 7** on page 19, decomposing inorganic peroxides requires their solvation and subsequent transformation to H_2O_2. This equation enables us to calculate the theoretically required amount of H_2O for a complete conversion of the inorganic peroxide, while also taking into account the purity of the oxygen source. It has been determined that 3 mL of solvent is required for the stochiometric solvation and subsequent decomposition of 5 g lithium peroxide in a 30% (H_2SO_4) aqueous solution. In all the experiments described previously, this requirement has been exceeded. In spite of this, the gas evolution from LPO appears to be incomplete at the chosen reaction conditions.

Additionally, the amount of aqueous solvent is examined to see if it affects the conversion and flow rate of the reaction. As shown in **Figure 20**, the volume and flow rate developments for the decomposition of 5 g lithium peroxide with 0.25 mol-% $Mn(OAc)_2 \times 4\ H_2O$ and 10 mL of [EMIM][SO_4Me] with various amounts of H_2SO_4 (30%) are depicted.

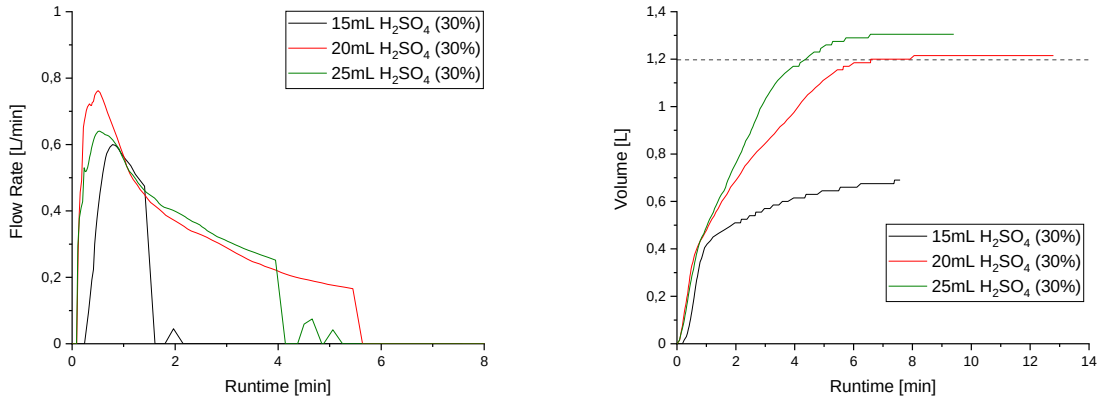

Figure 20: Flow rate and volume developments for the decomposition of 5 g lithium peroxide with 0.25 mol-% $Mn(OAc)_2 \times 4\ H_2O$ in 10 ml of [EMIM][SO_4Me] and different amounts of H_2SO_4 (30%) at room temperature. The dashed line marks 100% of theoretical lithium peroxide conversion.

In **Table 6**, the findings are summarized in terms of reaction duration, maximum flow rate and conversion rate.

Table 6: Duration, maximum flow rate and conversion for the reaction of 5 g lithium peroxide, 0.25 mol-% of $Mn(OAc)_2 \times 4\ H_2O$ and 10 mL of [EMIM][SO_4Me] in varying amounts of H_2SO_4 (30%).

solvent	duration [min]	max. flow rate [L/min]	conversion [%]
15 mL H_2SO_4 (30%)	1.9	0.60	58
20 mL H_2SO_4 (30%)	5.4	0.76	100
25 mL H_2SO_4 (30%)	4.1	0.64	109

While the amount of acid should theoretically be sufficient to convert LPO fully to oxygen in each experiment, the conversions differed significantly. The evolution of gas is almost doubled for experiments with 15 mL of H_2SO_4 (30%) and 20 mL of H_2SO_4 (30%). The evaporation of water within the reaction mixture may be caused by the increase in temperature during the reaction. Furthermore, less liquid may disturb the diffusion of reaction components within the system. In the case of 20 mL H_2SO_4 (30%), 100% conversion was achieved. In these conditions, there is also a smoother development of the flow rate. It has been observed that adding more H_2SO_4 (30%) results in conversions higher than 100%, which may indicate that the ionic liquid is decomposing due to very harsh reaction conditions and the evaporation of water. Experimental results indicate that utilizing the minimal amount of water necessary for the full conversion of oxygen is not sufficient. When excessive quantities of aqueous solvents are used, this may even be the case. In order to achieve complete peroxide decomposition, the amount of aqueous solvent required must be carefully determined for each individual system.

4.3.1.5 Variation of the catalyst

The previously described experiments are performed with $Mn(OAc)_2 \times 4\ H_2O$ as a H_2O_2 decomposition catalyst. Compared to other catalysts described in literature, $Mn(OAc)_2 \times 4\ H_2O$ is a homogeneous catalyst that is soluble in the applied reaction medium. As a consequence of the oxidation of aqueous Mn(II) to $Mn(IV)O_2$ during the decomposition reaction, macroscopically the formation of a precipitate indicates that the catalysis does not proceed entirely homogeneously.[35] We are now attempting to compare soluble manganese catalysts to heterogeneous manganese catalysts MnO_2 to determine whether the solubility of the catalysts influences the gas evolution. There are also other transition metal catalysts that are known to catalyze this reaction, including iron. To examine the advantages of adding the transition metal via the anion of an ionic liquid to the decomposition process, the room temperature ionic liquid and catalyst 1-butyl-3-methylimidazolium tetrachloroferrate [BMIM][$FeCl_4$] is tested.

As shown in **Figure 21**, the gas flow rate and gas volume were determined for the reaction of 5 g lithium peroxide in 10 mL of [EMIM][SO_4Me] and 15 mL of H_2SO_4 (30%) containing 0.25 mol % of different catalysts.

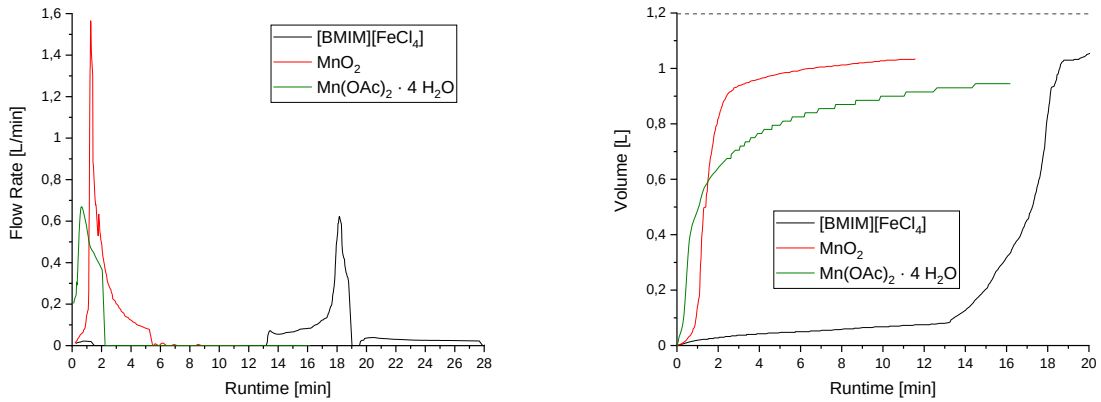

Figure 21: Gas flow rate and gas volume for the reaction of 5 g lithium peroxide in 10 mL [EMIM][SO_4Me] and 15 mL H_2SO_4 (30%) with 0.25 mol-% of different catalysts. The dashed line represents the theoretical conversion of 100% lithium peroxide.

Reaction time, maximum flow rate and conversion for the described decompositions reactions are listed in **Table 7**.

Table 7: Results for the duration, the maximum flow rate and the conversion for the decomposition of 5 g lithium peroxide in 10 mL [EMIM][SO_4Me] and 15 mL H_2SO_4 (30%) with 0.25 mol-% of different catalysts.

catalyst	duration [min]	max. flow rate [L/min]	conversion [%]
[BMIM][$FeCl_4$]	28	0.62	89
MnO_2	6.4	1.56	86
$Mn(OAc)_2 \times 4\ H_2O$	2.2	0.67	79

The flow rate for the reaction with MnO_2 as a catalyst exhibits its maximum after 2 min. After 5.5 min it decreases and the reaction ceases. For the reaction of lithium peroxide with [BMIM][$FeCl_4$], a measurable flow rate is obtained after 13 min. The flow rate increases steadily over the course of 4 min. After 1 minute, it reaches its maximum, followed by a sharp drop after another minute. When mixing $Mn(OAc)_2 \times 4\ H_2O$, the reaction reaches its maximum flow rate. The flow rate then decreases until the reaction is completed after two minutes.

There is no doubt that the choice of catalyst has a major impact on the flow rate and volume profiles. A 13 min onset time is observed for the decomposition with [BMIM][$FeCl_4$], whereas other examined catalysts do not exhibit this characteristic under the chosen conditions. It is not preferred to have an onset time, since the start of gas evolution should directly controllable and the reaction should begin immediately after the reaction components are mixed. In the case of the reaction with MnO_2, the gas evolution reaches its maximum after 1.5 min. With MnO_2, the maximum flow rate was more than twice as high as with $Mn(OAc)_2 \times 4\ H_2O$. Thus, MnO_2 appears to be a more effective catalyst. Although this could be beneficial for lithium peroxide decomposition, it could also result in excessive flow rates, especially when considering upscaling.

As considered in more detail later in chapter 4.8 on page 71, the use of a soluble catalyst is preferred in terms of housing and generator design. Since the advantages of higher decomposition activity of MnO_2 does not account for the constructional more demanding housing concept, focus will be in particular on the utilization of soluble catalysts like $Mn(OAc)_2 \times 4\ H_2O$. However, over the course of the decomposition reaction with $Mn(OAc)_2 \times 4\ H_2O$, a precipitate mainly consisting of MnO_2 is formed *in*

situ and its particle size distribution and morphology are not controlled.[35] As especially these characteristics influence the decomposition activity of a precipitated catalyst, the uncontrolled formation of different Mn species may lead to a ambiguous decomposition behaviour. Since the morphology of the compound used is known beforehand, adding purchased MnO_2 directly to the reaction can be considered a better approach from a chemical point of view.

4.3.1.6 Variation of the catalyst loading

So far, the experiments are performed with a catalyst loading of 0.25 mol-%. Next, it is examined whether the catalyst loading influences the course of the reaction. **Figure 22** and **Table 8** summarize the results for the reaction of 5 g LPO in 10 mL [EMIM][SO_4Me] and 15 mL H_2SO_4 (30%) with different catalyst loadings of $Mn(OAc)_2 \cdot 4\ H_2O$.

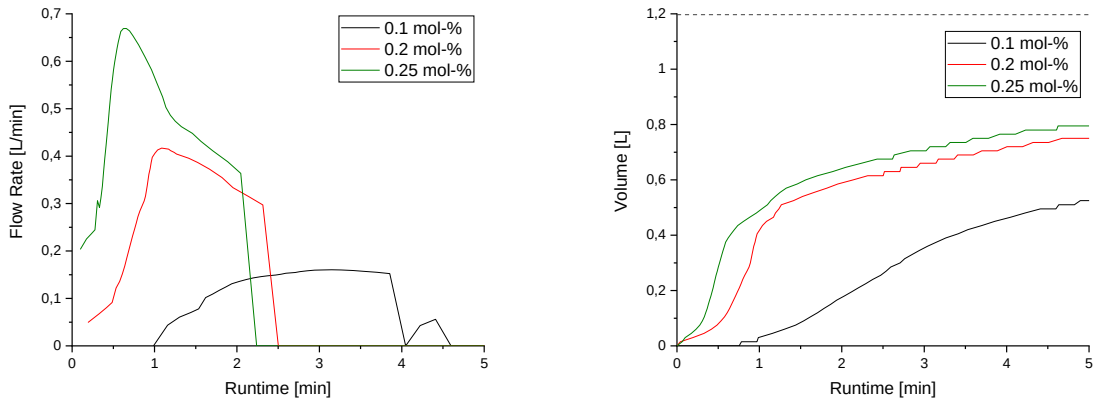

Figure 22: Results for the flow rate and evolving gas volume for the decomposition of 5 g lithium peroxide in 10 mL [EMIM][SO_4Me] in 15 mL H_2SO_4 (30%) with different catalyst loadings of $Mn(OAc)_2 \times 4\ H_2O$. The dashed line represents 100% lithium peroxide conversion.

Table 8: Duration, maximum flow rate and conversion for the decomposition of 5 g lithium peroxide in 10 mL [EMIM][SO_4Me] and 15 mL H_2SO_4 (30%) with different catalyst loadings of $Mn(OAc)_2 \times 4\ H_2O$.

[catalyst]	duration [min]	max. flow rate [L/min]	conversion [%]
0.1 mol-%	3.5	0.16	44
0.2 mol-%	2.5	0.42	65
0.25 mol-%	2.0	0.67	66

As expected, the flow rate plot indicates that the maximum flow rate increases with increasing catalyst loading, and the reaction time is shortest for the highest catalyst loading. As the catalyst loading increases, the decomposition of H_2O_2 to O_2 proceeds more rapidly and the total volume of evolved gas increases too, supporting the findings already discussed.

4.3.1.7 Decomposition reactions -20 °C

As required by law, the liberation of oxygen must occur at temperatures as low as -20 °C for civil aviation purposes.[31] For this reason, some of the most promising reactions from previous experiments are tested at -20 °C using a climate chamber. The objective of this study is to determine how ambient temperature affects parameters of the decomposition reaction such as starting behavior, reaction time and maximum flow rate. A description of the climate chamber setup can be found in chapter 7.4 on page 91.

Figure 23 shows the flow rate and volume developments for the decomposition of 5 g lithium peroxide with 0.25 mol-% of $Mn(OAc)_2 \times 4\ H_2O$ in different solvents and solvent combinations at -20 °C. **Table 9** summarizes the findings in terms of duration, maximum flow rate and conversion.

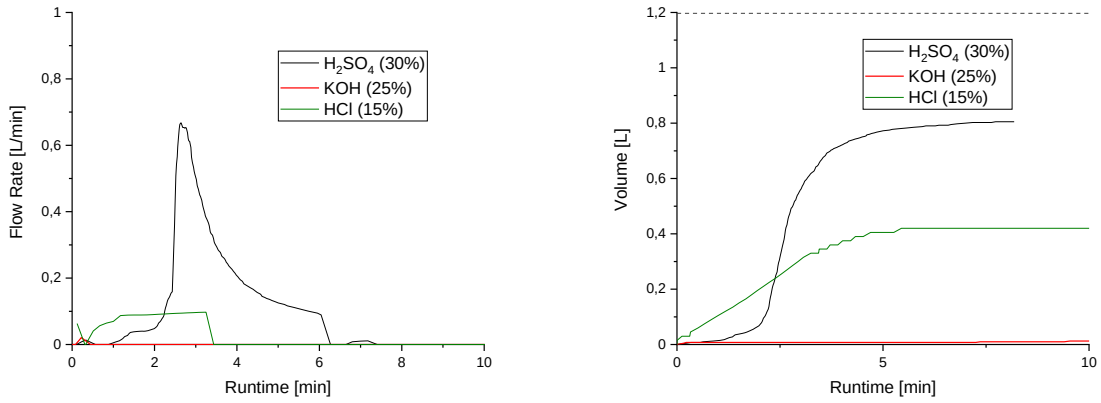

Figure 23: Flow rate and volume developments for the decomposition of 5 g lithium peroxide with 0.25 mol-% of $Mn(OAc)_2 \times 4\ H_2O$ in 25 mL of KOH (25%) in a mixture of 10 mL [EMIM][SO_4Me] and 15 mL H_2SO_4 (30%) or in a mixture of 10 mL [EMIM][SO_4Me] and 15 mL HCl (15%) at -20 °C. The dashed line marks 100% of lithium peroxide decomposition.

Table 9: Summary of the duration, maximum flow rate and conversion of the decomposition of 5 g lithium peroxide with 0.25 mol-% of $Mn(OAc)_2 \times 4\ H_2O$ in 25 mL KOH (25%) or 10 mL [EMIM][SO_4Me] and 15 mL H_2SO_4 (30%).

solvent	duration [min]	max. flow rate [L/min]	conversion [%]
KOH (25%)	-	0.02	1.9
H_2SO_4 (30%)	7.4	0.67	67
HCl (15%)	3.4	0.10	31

As opposed to the experiments conducted at room temperature, oxygen is not evolved in KOH (25%) at -20 °C at sufficient rates. Only 1.9% of the lithium peroxide is converted to oxygen after 30 min. Thus, pure KOH (25%) is not suitable for oxygen evolution reactions under these conditions.

The reaction proceeds at -20 °C in a mixture of [EMIM][SO_4Me] and H_2SO_4 (30%). In the experiments conducted at -20 °C, the maximum flow rate was similar to that observed at room temperature, however, the duration increased from around three minutes to over seven minutes, which is more than double. Consequently, the reaction takes longer to complete at lower temperatures. Furthermore, an onset of the decomposition can be observed at -20 °C, i.e. the reaction does not begin immediately, but rather after a period of time, as opposed to experiments at room temperature.

4.3.2 Upscaling lithium peroxide decomposition experiments – 7% to 10% of target size

Small-scale experiments conducted so far have shown that lithium peroxide exhibits promising oxygen liberation activities. Consequently, these experiments have been scaled up. Thus, experiments are conducted with 30 g lithium peroxide or 40 g lithium peroxide mixed with 10 g sodium peroxide, which correspond to 7% and 10% of a full-sized chemical oxygen generator, respectively. The experiments are conducted at ambient conditions as well as at -20 °C in order to develop a system that is operable in the legally required temperature range from -20 °C to +60 °C.[31]

4.3.2.1 Variation of the compression force

First, based on the results of the small-scale experiments, it was attempted to increase the amount of lithium peroxide utilized while maintaining the ratio of other compounds. The first parameter to be varied is the size of the lithium peroxide cylindrical compacts. Two press dies with diameters of 5 cm and 3.2 cm are used for compaction of lithium peroxide cylindrical compacts. The 3.2 cm press die is used for cylindrical compacts containing 5 g lithium peroxide while the 5 cm press die is used for all larger cylindrical compacts. A summary of the geometrical properties of the used lithium peroxide cylindrical compacts is given in **Table 10**.

Table 10: Geometric properties of the lithium peroxide cylindrical compacts.

mass [g]	diameter [cm]	height [cm]	surface area [cm^2]	density [g/cm^3]	pressing force [Pa]	pressing time [min]
5	3.2	1.0	26.1	0.62	500	1
15	5.0	1.3	59.7	0.58	500	1
30	5.0	2.3	75.4	0.66	500	1
40	5.0	3.5	94.2	0.58	500	1

First, the influence of the applied pressure of the lithium peroxide cylindrical compacts on the gas evolution reaction is examined. For this purpose, 40 g lithium peroxide in form of a cylindrical compact and 10 g sodium peroxide are decomposed with 0.25 mol-% of $Mn(OAc)_2 \times 4\ H_2O$ in 200 mL KOH (25%). As the decomposition reaction proceeds slower in KOH (25%), the effect of the pressing power is more significant when conducted in that medium. As a result of omitting the prior used ionic liquid [EMIM][SO_4Me] the system is further simplified. Without compaction of the lithium peroxide powder prior to pressing the cylindrical compact 40 g of lithium peroxide powder can fit into the 5 cm press die.

Figure 24 shows the evolving gas volume and gas flow rates of the decomposition of 40 g lithium peroxide and 10 g sodium peroxide with 0.25 mol-% of $Mn(OAc)_2 \times 4\ H_2O$ in 200 mL KOH (25%) at room temperature with different compressive strength applied during the production of the lithium peroxide cylindrical compacts.

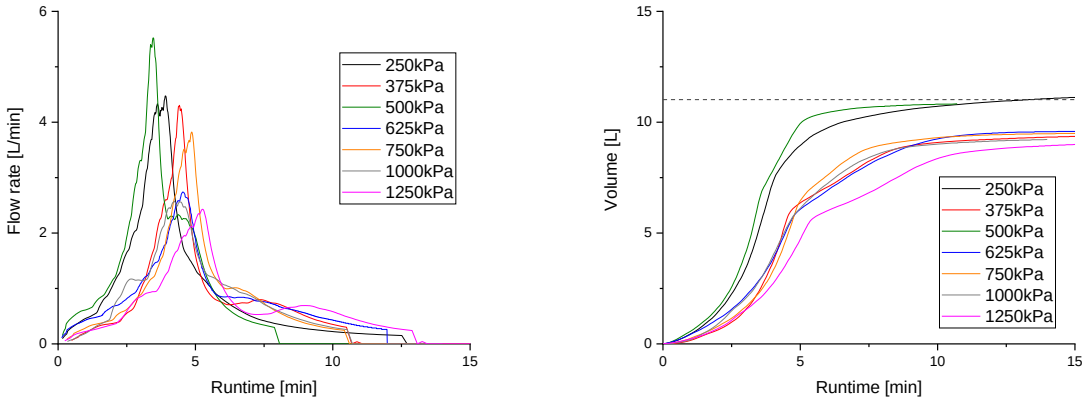

Figure 24: Evolving gas volume and gas flow rate for the decomposition of 40 g lithium peroxide and 10 g sodium peroxide with 0.25 mol-% of $Mn(OAc)_2 \times 4\ H_2O$ in 200 mL KOH (25%) at room temperature with different compressive strength applied to the lithium peroxide cylindrical compacts. The dashed line represents 100% theoretical gas evolution of lithium peroxide and sodium peroxide.

Table 11 displays the maximum flow rate, reaction time and conversion.

Table 11: Duration, maximum flow rate and conversion for the decomposition of 40 g lithium peroxide and 10 g sodium peroxide with 0.25 mol-% of $Mn(OAc)_2 \times 4\ H_2O$ in 200 mL KOH (25%) at room temperature with different compressive strength applied to the lithium peroxide cylindrical compacts.

pressing force [Pa]	duration [min]	max. flow rate [L/min]	conversion [%]
250	12.7	4.47	100
375	11.1	4.30	85
500	8.06	5.52	98
625	12.0	2.74	87
750	10.4	3.82	86
1000	10.7	2.57	84
1250	13.3	2.43	82

As the reaction progresses, the flow rates gradually increase, reaching their maximum after about 3 min to 5 min. Afterwards, the flow rate decreases again, and after 8 min to 15 min depending on the plot no more flow rate is observed. In the early stages of the reaction, the gas volume rises reaching a plateau around 10 min later.

The duration of the decomposition is longer at the highest and lowest applied compressive strengths and shows a minimum of 8 min at 500 kPa applied compressive strength. In other words, the reaction proceeds most rapidly when the lithium peroxide cylindrical compact is pressed at a medium pressure. This behavior may be explained by the porosity of the compact, which should be higher when the material is weakly compressed. As a result, the pellet becomes more reactive, since the liquid is able to enter the pellet's pores more easily, increasing the surface area on which the reaction can occur. In contrast, a densely pressed compact exhibits smaller pores, leading to a smaller reaction surface and a slower reaction. In case the compression force is high enough, visible cracks traverse the compact resulting in a larger surface.

Both *Groche* and *Hinterberger* examined the morphology of urea hydrogen peroxide compacts with the aid of micro X-ray computer tomography. Both confirm that an increase in the applied compression strength leads to a decrease in the porosity of the pellet but also can lead to cracks within the compact's structure.[36, 37]

4.3.2.2 Variation of the lithium peroxide cylindrical compact size

Then, when pressure and pressing time are kept constant, cylindrical compacts with different sizes are evaluated for their reactivity. It can be seen from **Table 11** that diameter and height of the cylindrical compacts vary. As a result, the surface area exposed to the reaction medium differs too. When the surface area of peroxide compact is greater, reactions are expected to proceed faster and more intensely. As a result, using more but smaller compacts should increase the reactivity of the system compared to using fewer but bigger compacts when the total mass of lithium peroxide is equal in both cases. The following experiments are conducted to test this hypothesis. Following the findings from the variation of the compression force, see chapter 4.3.2.1 on page 38, the following experiments are conducted with compacts pressed for 1 min at 500 kPa.

Figure 23 displays the flow rate and volume developments for the decomposition of 30 g lithium peroxide with 0.25 mol% $Mn(OAc)_2 \times 4\ H_2O$ in 60 mL [EMIM][SO_4Me] and 90 mL H_2SO_4 (30%), while size and quantity of the compacts are varied. Experiments are conducted in a climate chamber at a temperature of -20 °C.

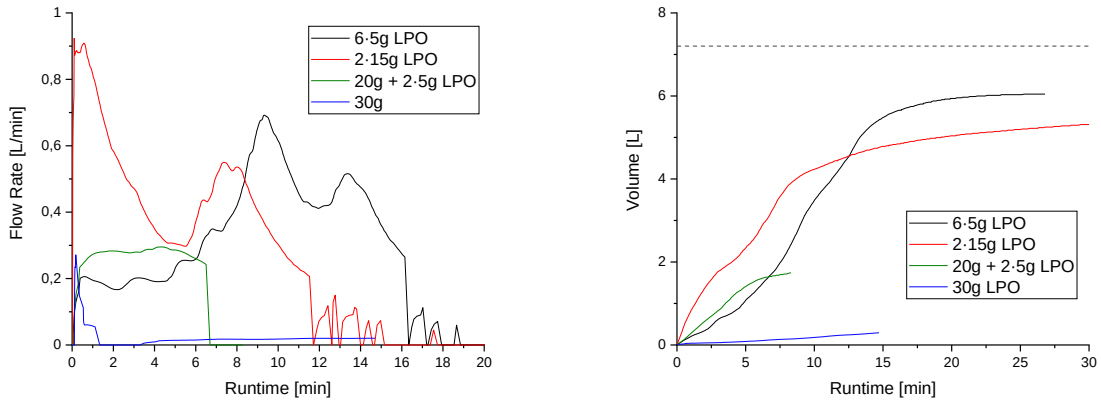

Figure 25: Flow rate and volume developments for the decomposition of 30 g lithium peroxide with 0.25 mol-% $Mn(OAc)_2 \times 4\ H_2O$ in a mixture consisting of 60 mL [EMIM][SO_4Me] and 90 mL H_2SO_4 (30%) at -20 °C, thereby varying the size of the cylindrical compact. The dashed line represents 100% theoretical conversion of lithium peroxide.

A summary of the duration, maximum flow rate and conversion of the decomposition reactions is presented in **Table 12**.

Table 12: Results for the duration, maximum flow rate and conversion of the decomposition of 30 g lithium peroxide with 0.25 mol-% $Mn(OAc)_2 \times 4\ H_2O$ in a mixture consisting of 60 mL [EMIM][SO_4Me] and 90 mL H_2SO_4 (30%) at -20 °C with different sizes of the cylindrical compact.

oxygen source	duration [min]	max. flow rate [L/h]	conversion [%]
6 × 5 g LPO	17	41.5	84
2 × 15 g LPO	15	54.5	74
20 g + 2 × 5 g LPO	6.6	17.7	24
30 g LPO	-	1.23	4.0

In the experiments, it was shown that the size of the cylindrical compact has a significant impact on its solvation and subsequent oxygen liberation. The smallest compact size of 5 g lithium peroxide leads to the longest duration and the highest conversion. On the other hand, a larger compact size reduces the reaction duration, but results in a lower conversion of lithium peroxide to oxygen. Especially for the reaction with one compact of 30 g lithium peroxide, gas evolution does only occur with a negligible rate and a conversion of only 4% after almost 15 min. It is clear from this finding that not only the composition of the compounds used, but also their appearance, is important. This finding may be due to the decrease in surface area caused by using larger but fewer cylindrical compacts. By having a smaller surface area, less lithium peroxide is exposed to the aqueous solvent and is therefore less likely to react to H_2O_2. At low temperatures, this effect may be enhanced because it is assumed that the reaction time is affected by the ambient temperature, and as a result, the reaction proceeds at a slower pace.

The shape of the flow rate developments must be noted. Under the chosen conditions, the flow rate does not exhibit the desired behavior, i.e., it does not peak at the beginning of the reaction and it does not react consistently over the course of several minutes. The maximum flow rate is reached somewhere in the middle of the decomposition, except the experiments with 1 • 20 g lithium peroxide and 2 •10 g lithium peroxide. During the reaction, the pellet may have broken or the peroxide powder is inhomogeneously compressed within the compact, what may have caused this issue.

As the decomposition of one 30 g lithium peroxide compact did not proceed at -20 °C, it was attempted to add lithium peroxide powder to the reaction mixture. The increase of the surface area should lead to increased reactivity of the system.

Figure 26 illustrates the volume development and flow rate for a decomposition of 30 g lithium peroxide compact (500 kPa, 1 min) with 0.25-mol% $Mn(OAc)2 \times 4\ H_2O$ in 60 mL [EMIM][SO_4Me] and 90 mL H_2SO_4 (30%) at -20 °C.

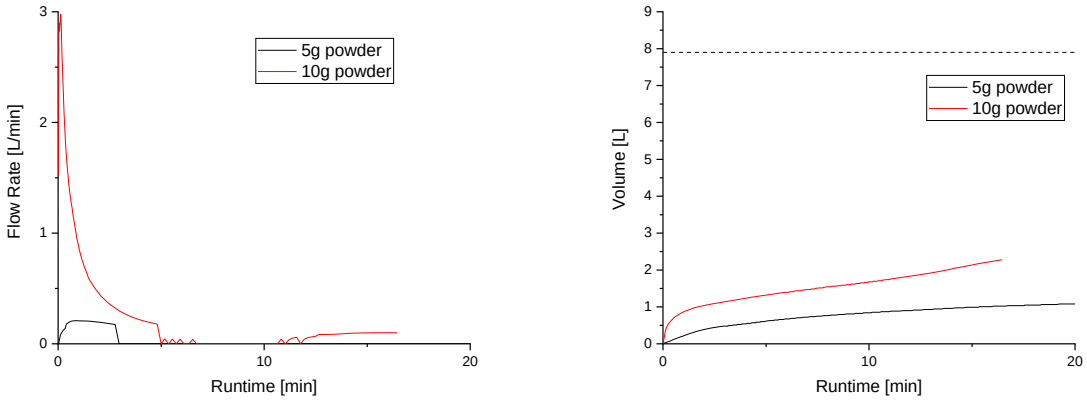

Figure 26: Flow rate and volume developments for the decomposition of 30 g lithium peroxide in form a cylindrical compact and different amounts of lithium peroxide powder with 0.25 mol-% $Mn(OAc)_2 \times 4\ H_2O$ in 60 mL [EMIM][SO_4Me] and 90 mL H_2SO_4 (30%) at -20 °C. The dashed line represents 100% conversion of LPO.

Table 13 illustrates the measured volumes as well as the theoretical volumes for the decomposition of the entire amount of lithium peroxide used.

Table 13: Results for the volume generated from the decomposition of one 30 g lithium peroxide cylindrical compact and different amounts of lithium peroxide powder with 0.25 mol-% $Mn(OAc)_2 \times 4\ H_2O$ in 60 mL [EMIM][SO_4Me] and 90 mL H_2SO_4 (30%) at -20 °C, as well as the theoretical conversions of the entire lithium peroxide and the used lithium peroxide powder.

oxygen source	volume [L]	total theoretical volume [L]	total conversion [%]	theoretical volume powder [L]	conversion of powder [%]
5 g powder, 30 g LPO CC	1.11	8.40	13.2	1.20	92.5
10 g powder, 30 g LPO CC	2.28	8.61	26.5	2.40	95.0

Based on **Table 13**, the obtained conversions resemble the theoretical conversions of the applied LPO powder at 92.5% and 95.0%, respectively. In contrast, when taking into account the total amount of lithium peroxide utilized, the conversion is far from complete with 13.2% and 26.5%, respectively. At -20 °C, the addition of lithium peroxide powder does not increase the reactivity of the applied 30 g lithium peroxide cylindrical compact. This indicates that the heat generated during the decomposition of the powder is not sufficient to activate the lithium peroxide within the compact, hence no solvation or subsequent reaction with H_2O_2 occurs.

4.3.2.3 Influence of the ambient temperature

Based on the experiments performed with 5 g LPO, it can be determined that ambient temperature has an impact on the system's reactivity. In order to investigate the extent of this influence, two decomposition reactions were performed on a 30 g scale, one at room temperature and one at -20 °C with the same components and reaction conditions. **Figure 27** shows the evolved gas volume and gas flow rate for the decomposition of 6 × 5 g lithium peroxide in 60 mL [EMIM][SO_4Me] and 90 mL HCl (15%) with a catalyst loading of 0.25 mol-% $Mn(OAc)_2 \times 4\ H_2O$ at room temperature (r.t.) as well as at -20 °C. The duration, maximum flow rate and conversion are listed in **Table 14**.

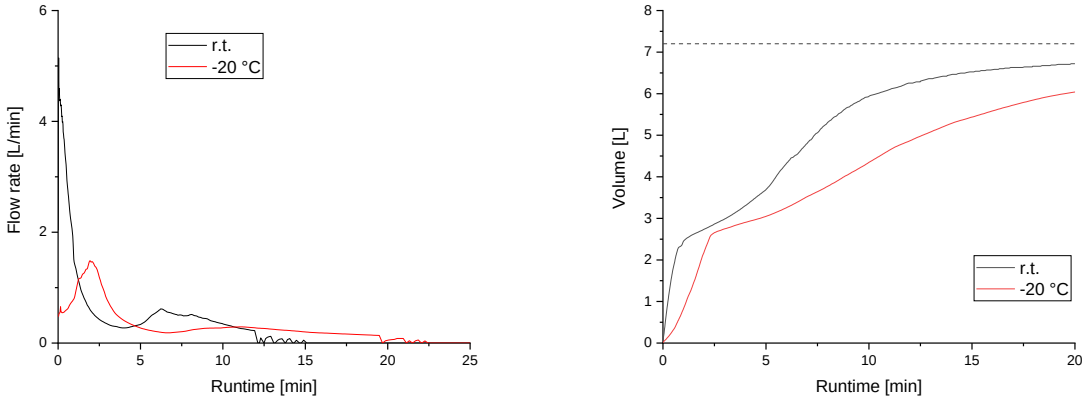

Figure 27: Evolved gas flow rate and volume for the decomposition of 6 × 5 g lithium peroxide in 60 mL [EMIM][SO_4Me] and 90 mL HCl (15%) with 0.25 mol-% $Mn(OAc)_2 \times 4\ H_2O$ at r.t. as well as at -20°C. The dashed line represents 100% of theoretical lithium peroxide conversion.

Table 14: Duration, maximum flow rate and conversion for the decomposition of 6 × 5 g lithium peroxide in 60 mL [EMIM][SO_4Me] and 90 mL HCl (15%) with 0.25 mol-% $Mn(OAc)_2 \times 4\ H_2O$ at r.t. and at -20°C.

temperature	duration [min]	max. flow rate [L/min]	conversion [%]
r.t.	14.5	4.7	90
-20 °C	22.3	1.5	86

When the decomposition is conducted at room temperature, the maximum flow rate is observed immediately at the beginning of the reaction, while when the reaction is conducted at -20 °C, the maximum flow rate is observed after 2.3 min of decomposition reaction. Accordingly, the maximum flow rate for the experiment conducted at room temperature is more than three times greater than that for the experiment conducted at -20 °C. Despite differences of 4%, both experiments demonstrate similar reaction volumes and similar conversions.

At lower temperatures, the gas evolution occurs slower and smoother. From 14.5 min to 22.3 min, the reaction time increases by 53%, and the maximum flow rate is reached later in the decomposition reaction. For the development of a chemical oxygen generator that must operate properly in the temperature range between -20 °C and +60 °C, this finding must be considered. Thermal insulation of the reactor is one possibility for increasing the reactivity of the system at -20 °C. Consequently, the exothermic reaction would emit less heat to the environment and heat itself more efficiently, leading to the evolution of gas more rapidly.

An attempt is made to compare the reaction temperature development inside the reactor for two systems that differ only in ambient temperature to better understand the

impact of the ambient temperature. **Figure 28** shows the temperature development in the reaction medium for the decomposition of 6 × 5 g lithium peroxide in 60 mL [EMIM][SO_4Me] and 120 mL H_2SO_4 (30%) with a catalyst loading of 0.25 mol-% $Mn(OAc)_2 \times 4\ H_2O$ at room temperature (r.t.) and at -20 °C.

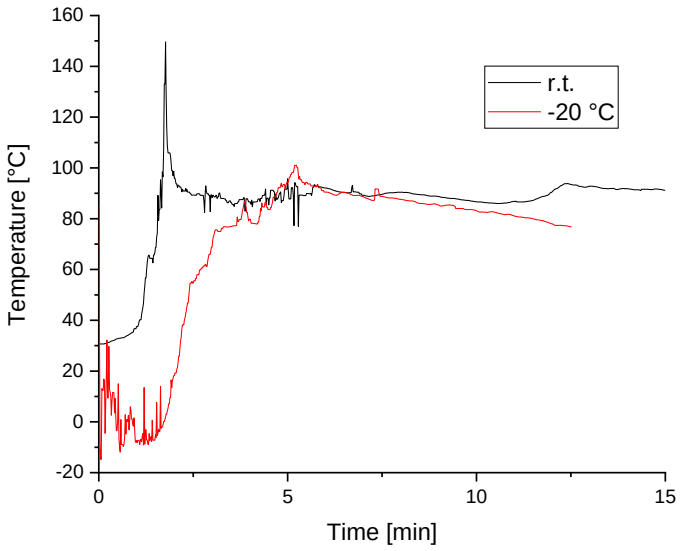

Figure 28: Temperature development for the decomposition of 6 × 5 g lithium peroxide in 60 mL [EMIM][SO_4Me] and 120 mL H_2SO_4 (30%) with a catalyst loading of 0.25 mol % $Mn(OAc)_2 \times 4\ H_2O$ at room temperature and at -20 °C.

At the beginning of the decomposition, the reaction temperatures are equal to the ambient temperatures, indicating sufficient precooling of all components and the reaction vessel. Within the first five minutes of gas evolution, the reaction temperatures differ the most. After 1.8 min, the decomposition at room temperature reaches its maximum of 150 °C. The reaction temperature then decreases over the course of 20 s to approximately 90 °C and remains at this level until the reaction ends. During the first two minutes of the reaction at 20 °C, the reaction temperature remains below 0 °C. After two minutes, it reaches a temperature of around 90 °C.

There is a significant difference in the reaction temperatures at the beginning of the respective decomposition reactions, as shown in the plots. It takes approximately two minutes longer for the decomposition reaction to reach the same reaction temperature within the reaction medium at a temperature of -20 °C as it does at a temperature of 25 °C. After five minutes, however, the reaction temperatures of both decompositions are almost equal and remain so until the reactions end. In other words, the system can

release enough heat at a temperature of -20 °C to achieve the same reaction temperature as if it were started at room temperature. Due to the fact that the system is self-sufficient, it should be investigated whether thermal insulation of the reactor at -20 °C would result in a more similar flow rate for both decompositions.

4.3.3 Upscaling lithium peroxide decomposition experiments – 13% to 20% of target size

4.3.3.1 Variation of the solvent and other parameters

The lithium peroxide decomposition experiments are being upscaled. In order to test some of the reaction conditions, 90 g of lithium peroxide are used along with the upscaled amounts of the other reactants. Detailed descriptions of the two decomposition systems that led to measurable gas flow rates and volume plots are provided in the following sections.

Figure 29 illustrates the development of flow rate and volume for the decomposition of 3 × 30 g lithium peroxide compacts with different amounts of aqueous solvent, [EMIM][SO_4Me] and $Mn(OAc)_2 \times 4\ H_2O$.

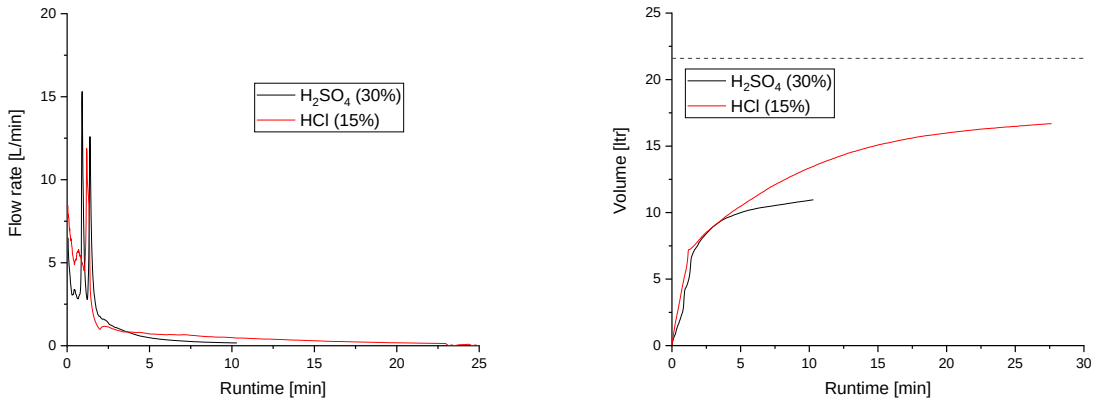

Figure 29: Flow rate and volume developments for the decomposition of 3 × 30 g lithium peroxide with 120 mL [EMIM][SO_4Me], 240 mL H_2SO_4 (30%) and 0.167 mol-% $Mn(OAc)_2 \times 4\ H_2O$ and the decomposition of 3 × 30 g lithium peroxide with 180 mL [EMIM][SO_4Me], 270 mL HCl (15%) and 0.1 mol-% of $Mn(OAc)_2 \times 4\ H_2O$.

Table 15 summarizes the durations, maximum flow rates and conversions of the respective decomposition reactions.

Table 15: Duration, maximum flow rate, maximum reaction temperature and conversion of the decomposition of 3 × 30 g lithium peroxide with 120 mL [EMIM][SO_4Me], 240 mL H_2SO_4 (30%) and 0.167 mol-% $Mn(OAc)_2 \times 4\ H_2O$, and the decomposition of 3 × 30 g lithium peroxide with 180 mL [EMIM][SO_4Me], 270 mL HCl (15%) and 0.1 mol-% of $Mn(OAc)_2 \times 4\ H_2O$.

solvent	duration [min]	max. flow rate [L/min]	max. temperature [°C]	conversion [%]
H_2SO_4 (30%)	10	15.3	109.9	51
HCl (15%)	23	11.9	137.5	76

In the presented decompositions, the flow rate exhibits a sharp peak at the beginning and then steadily decreases until the reaction is completed. Thus, the maximum flow rate of the H_2SO_4 (30%) reaction is higher than that of the HCl (15%) reaction, whereas the latter exhibits a longer duration and a higher conversion rate. It is possible that the higher maximum flow rate in that experiment is due to the higher catalyst loading. These curve shapes are similar to those observed in the 30 g lithium peroxide reactions with similar reactant ratios. It is important to note, however, that the catalyst loading has been reduced in comparison to the 30 g lithium peroxide experiments. Due to their high reactivity, experiments with 0.25 mol-% $Mn(OAc)_2\ 4\ H_2O$ and 90 g lithium peroxide resulted in a rupture of the reaction vessel. The decomposition with H_2SO_4 (30%) is also performed with a lower catalyst loading than 0.25 mol-% used in most smaller experiments. Also, it should be noted that the amount of solvent is reduced relative to the amount of lithium peroxide, compared to the experiments described in chapter 4.3.2. Consequently, the reduction in solvent amount results in a less aggressive reaction in a similar manner to the reduction in catalyst loading. Nevertheless, a conversion of 51% for the H_2SO_4 (30%) system is far from complete. It is necessary to conduct more decomposition experiments in order to improve the reaction conditions of the applied systems with 90 g lithium peroxide in such a way that the conversion increases without causing the reactor to burst.

4.3.3.2 Comparison of differently sized systems

A comparison of gas evolution reactions with different amounts of lithium peroxide is conducted to examine how upscaling impacts the reaction system, while maintaining constant the ratios of the components utilized in the decomposition reaction.

The evolved gas volumes and gas flow rates for the decomposition of 5 g lithium peroxide in 10 mL [EMIM][SO_4Me] and 15 mL HCl (15%), the decomposition of 2 × 30 g lithium peroxide compacts in 120 mL [EMIM][SO_4Me] and 180 mL HCl (15%) and the decomposition of 3 × 30 g lithium peroxide compacts in 180 mL [EMIM][SO_4Me] and 270 mL HCl (15%) with a catalyst loading of 0.25 mol-% $Mn(OAc)_2 \times 4\ H_2O$ are shown in **Figure 30**.

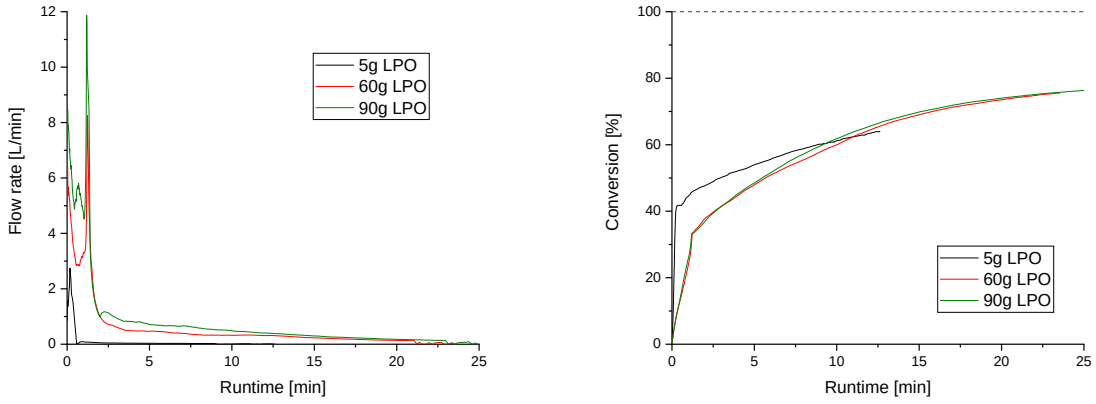

Figure 30: Gas flow rate and conversion for the decomposition of 5 g lithium peroxide in 10 mL [EMIM][SO_4Me] and 15 mL HCl (15%), the decomposition of 2 × 30 g lithium peroxide compacts in 120 mL [EMIM][SO_4Me] and 180 mL HCl (15%) and the decomposition of 3 × 30 g lithium peroxide compacts in 180 mL [EMIM][SO_4Me] and 270 mL HCl (15%) with a catalyst loading of 0.25 mol-% $Mn(OAc)_2 \times 4\ H_2O$, respectively. The dashed line represents 100% theoretical lithium peroxide conversion.

Table 16 summarizes the durations, maximum flow rates, evolved gas volumes and conversions of the respective decomposition reactions.

Table 16: Summary of the duration, maximum flow rate, evolved gas volume and conversion for the decomposition of 5 g lithium peroxide in 10 mL [EMIM][SO_4Me] and 15 mL HCl (15%), the decomposition of 2 × 30 g lithium peroxide comapcts in 120 mL [EMIM][SO_4Me] and 180 mL HCl (15%) and the decomposition of 3 × 30 g lithium peroxide compacts in 180 mL [EMIM][SO_4Me] and 270 mL HCl (15%) with a catalyst loading of 0.25 mol-% $Mn(OAc)_2 \times 4\ H_2O$, respectively.

oxygen source	duration [min]	max. flow rate [L/min]	volume [L]	conversion [%]
5 g LPO	12.3	2.74	0.765	63.9
60 g LPO	21.2	8.25	10.8	75.5
90 g LPO	26.8	11.9	24.3	77.0

The maximum flow rate is observed for all three decompositions at the beginning of the reaction. Thus, the flow rate plot for the decomposition of 5 g lithium peroxide shows one maximum, while the flow rate plots for the systems with 60 g and 90 g lithium peroxide compacts show two maxima within the first two minutes. This effect may be caused by the use of cylindrical compacts with higher mass. According to *Groche*, cracks within densely pressed urea hydrogen peroxide pellets improved access to the oxygen source and reduced the onset time its decomposition, which led to more rapid gas evolution.[37] The observed flow rate spikes may be the result of cracks and inhomogeneous densities within the pellet when using larger lithium peroxide compacts. All three decomposition reactions result in similar conversion. Due to this, direct upscaling has no major effect on the conversion of the oxygen source. A greater amount of oxygen source will result in a longer reaction time. By increasing the amount of lithium peroxide from five grams to 90 g the duration more than doubles. This can be explained by the decrease in surface area that occurs when larger cylindrical compacts are utilized. Based on **Table 10** on page 38, the surface area of a five grams pellet is larger than that of a 30 g compact. Thus, it can be assumed that the gas evolution proceeds faster when smaller CCs are used.

4.3.3.3 Temperature considerations

A temperature curve is plotted for the 90 g lithium peroxide decompositions experiments in order to gain a better understanding of the reaction system and its temperature dependency. An overview of the reactions medium's temperature development for the decomposition reactions described above is shown in **Figure 31**.

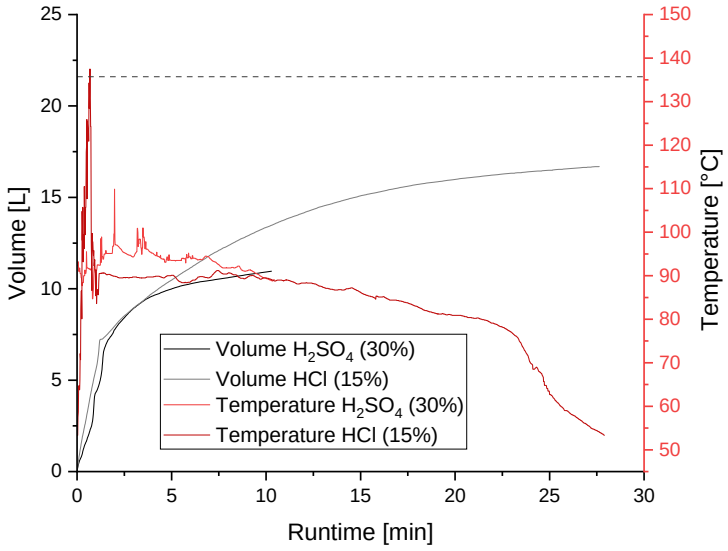

Figure 31: Temperature development of the decomposition of 3 × 30 g lithium peroxide compacts with 120 mL [EMIM][SO_4Me], 240 mL H_2SO_4 (30%) and 0.167 mol-% $Mn(OAc)_2 \times 4\ H_2O$ and the decomposition of 3 × 30 g lithium peroxide compacts with 180 mL [EMIM][SO_4Me], 270 mL HCl (15%) and 0.1 mol-% of $Mn(OAc)_2 \times 4\ H_2O$.

Both decompositions reach their maximum temperatures at the beginning of the reaction, as shown in **Figure 31**. After its maximum the reaction medium's temperature decreases steadily. The decomposition with HCl (15%) reaches a maximum temperature of 138 °C, whereas the decomposition with H_2SO_4 (30%) reaches a maximum temperature of 110 °C.

The observed temperatures are much lower than those typically reached during the combustion of a chlorate candle, which can be as high as 600 °C.[38] These results suggest that lithium peroxide is a promising oxygen source for developing a next generation low-temperature chemical oxygen generator.

4.3.4 Lithium peroxide decomposition with Brønsted acidic ionic liquids

As indicted by their name, BAILs are acidic because they bear at least one acidic proton. Due to the fact that oxygen liberation from inorganic peroxides occurs through proton transition, which is responsible for the formation of H_2O_2 as shown in **Scheme 7** on page 19, the question arises whether providing additional protons to the reaction system of ionic liquid and acidic aqueous solution will benefit the decomposition reaction. This is tested by replacing the ionic liquid [EMIM][SO_4Me] with various ionic liquids that contain at least one Brønsted functionality. The structural formulas of the BAILs used can be seen in **Figure 15** on page 21. **Figure 32** summarizes the findings.

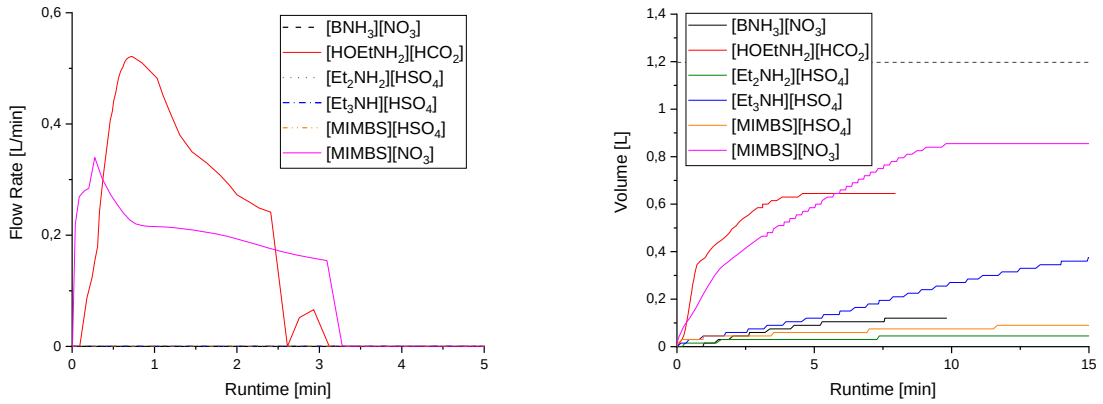

Figure 32: Volume and flow rate developments for the decomposition of 5 g lithium peroxide and 0.25 mol-% $Mn(OAc)_2 \times 4\ H_2O$ in 10 mL H_2SO_4 (30%) and various BAILs at room temperature. The dashed line represents 100% theoretical conversion of lithium peroxide.

There is no measurable flow rate in most of the conducted experiments, and less than 40% conversion is observed. The only exceptions are [$HOEt_2NH_2$][CO_2H] and [MIMBS][NO_3], where conversions exceed 60%. It appears that the choice of the ionic liquid makes a significant difference to the decomposition reaction, whereas Brønsted-acidic functionalities do not necessarily enhance the reactivity of the system.

4.4 Catalytic oxygen liberation from calcium peroxide

In a similar manner to the experiments conducted with lithium peroxide, calcium peroxide is used to investigate oxygen release reactions. The active oxygen content of calcium peroxide is 22.2 wt-%, which is lower than that of lithium peroxide. However, since calcium peroxide is used in a variety of applications, the product is more readily available.[32]

4.4.1 Calcium peroxide decomposition experiments at room temperature

As with lithium peroxide, the first experiments conducted with calcium peroxide are at room temperature. calcium peroxide experiments are performed with 10 g calcium peroxide to achieve a similar gas evolution as the 5 g lithium peroxide experiments. Cylindrical compacts of calcium peroxide are also considered in order to utilize calcium peroxide. The calcium peroxide cylindrical compacts are prone to breaking, however, which posed a problem for this attempt. The calcium peroxide powder could only be compressed with a pressing force of 82 kg for one minute in order to obtain a usable pellet. A greater pressing force or longer pressing duration did not improve the stability of the cylindrical compacts. The pressing force is adjusted for calcium peroxide so that it does not break when handled prior to a reaction. Since the compression of the tablet should ideally be optimized for flow rate development, this is not an ideal solution. The geometric data, pressing force, and time for the calcium peroxide cylindrical compact are shown in **Table 17**. This was the only type of calcium peroxide cylindrical compact to be used throughout the decomposition experiments due to its practicability.

Table 17: Geometric data, compression force and pressing time for the applied calcium peroxide cylindrical compact.

mass [g]	diameter [cm]	height [cm]	surface area [cm^2]	density [g/cm^3]	pressing force [kg]	pressing time [min]
10	3.2	1.2	28.1	1.03	82	1

4.4.1.1 Variation of the solvent

As a first step, the aqueous solvent utilized will be varied. **Figure 33** illustrates the evolved gas volume and gas flow rate for the decomposition of ten grams calcium peroxide and 0.25 mol-% $Mn(OAc)_2 \times 4\ H_2O$ in 15 mL [EMIM][SO_4Me] and 15 mL of different acidic aqueous solvents.

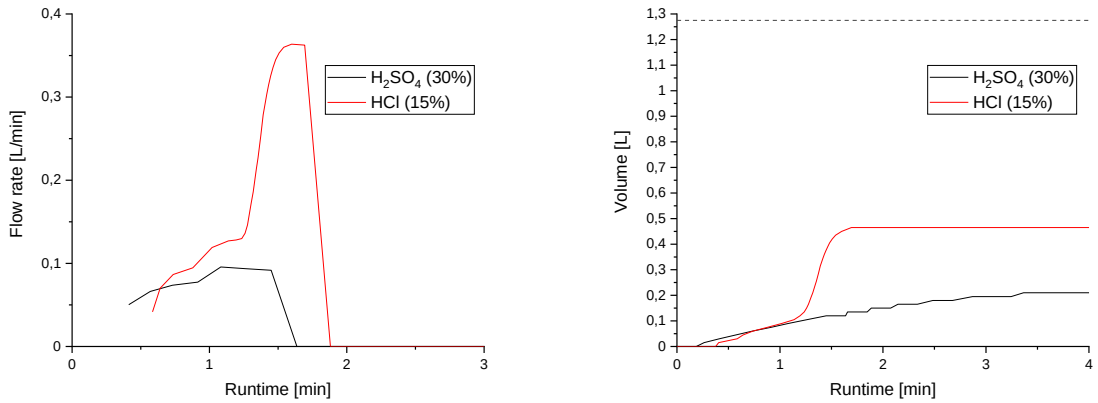

Figure 33: Evolved gas volume and gas flow rate for the decomposition of 10 g calcium peroxide and 0.25 mol-% Mn(OAc)2 × 4 H_2O in 15 mL [EMIM][SO4Me] and 15 mL of different acidic aqueous solvents. The dashed line represents the theoretical conversion of 100% calcium peroxide, assuming a purity of 75%.

Table 18 lists the duration, maximum flow rate and conversion for each decomposition reaction.

Table 18: Summary of the duration, maximum flow rate and conversion for the decomposition of 10 g calcium peroxide and 0.25 mol-% $Mn(OAc)_2 \times 4\ H_2O$ in 10 mL [EMIM][SO_4Me] and 15 mL of different acidic aqueous solvents.

solvent	duration [min]	max. flow rate [L/min]	conversion [%]
H_2SO_4 (30%)	1.6	0.10	21
HCl (15%)	1.8	0.36	36

Approximately 0.1 L/min flow rate is observed in both systems within one minute after start of the decomposition reaction. After one minute, the flow rate in H_2SO_4 (30%) increases to 0.1 L/min while in HCl (15%) it reaches a maximum flow rate of 0.36 L/min. After 1.6 min and 1.8 min the gas evolution ceases.

According to the data, the reaction with H_2SO_4 (30%) proceeds slower than the decomposition with HCl (15%). The maximum flow rate of the reaction in HCl (15%) is 3.6 times greater than the maximum flow rate in H_2SO_4 (30%), therefore, the latter

system is less reactive. The formation of $CaSO_4$ within the H_2SO_4 (30%) system may explain this coherence. It is noted that $CaSO_4$ has an extremely poor solubility in water (2.4 g/L) compared to $CaCl_2$ (740 g/L) which is generated in the HCl (15%) system.[32] As a consequence of the poor solubility, the reaction mixture becomes a slurry, which leads to a reduced mixing of the components within the system. In this regard, H_2SO_4 (30%) is unfavorable within a gas evolution system based on calcium peroxide as major oxygen source.

Despite this, the reaction in HCl (15%) does not proceed sufficiently. As the gas output is only 36% compared to the theoretically available oxygen in calcium peroxide with a purity of 75%, it appears to be insufficient. In this case, a slow reaction may be caused by the high pressing force that must be applied to press the calcium peroxide cylindrical compact. When the material is pressed densely, the surface available for its decomposition decreases, which results in a slower and sometimes incomplete decomposition reaction. It is also possible that the amounts of catalyst or solvent utilized are insufficient to promote an adequate decomposition.

4.4.1.2 Variation of the catalyst

As a next step, it is investigated whether changing the utilized catalyst contributes to a better gas evolution in the calcium peroxide system. For this purpose, the same catalysts as for lithium peroxide are used, namely $Mn(OAc)_2 \times 4\ H_2O$, MnO_2 and [BMIM][$FeCl_3$].

As shown in **Figure 34**, the evolved gas volume and gas flow rate for the decomposition of 10 g calcium peroxide in 10 mL [EMIM][SO_4Me] and 15 mL HCl (15%) with 0.25 mol-% of different transition metal catalysts are shown.

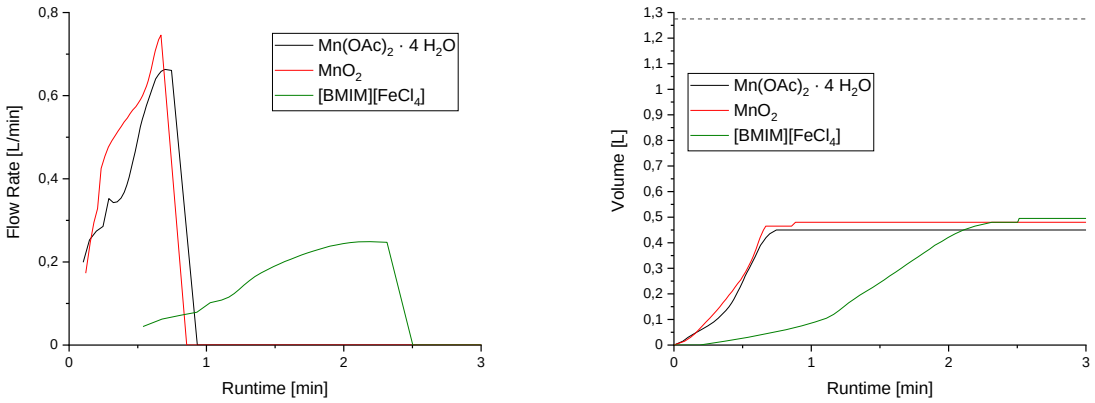

Figure 34: Evolved gas volume and gas flow rate for the decomposition of 10 g calcium peroxide in 10 mL [EMIM][SO_4Me] and 15 mL HCl (15%) with 0.25 mol-% of different transition metal catalysts. The dashed line marks 100% of theoretical calcium peroxide conversion, if a calcium peroxide purity of 75% is assumed.

In **Table 19** duration, maximum flow rate and conversion of the different decomposition reactions are summarized.

Table 19: Duration, maximum flow rate and conversion for the decomposition of 10 g calcium peroxide in 10 mL [EMIM][SO_4Me] and 15 mL HCl (15%) with 0.25 mol-% of different transition metal catalysts.

catalyst	duration [min]	max. flow rate [L/min]	conversion [%]
$Mn(OAc)_2 \times 4\ H_2O$	0.93	0.66	35
MnO_2	0.85	0.75	36
[BMIM][$FeCl_4$]	1.97	0.25	38

Following the reaction of $Mn(OAc)_2 \times 4\ H_2O$ with MnO_2, the flow rate increases almost linearly until it reaches its maximum after around 45 sec. Subsequently, the flow rate decreases rapidly, and the reaction ceases after one minute. After 2.3 minutes, the flow rate for the reaction with [BMIM][$FeCl_4$] increases, before decreasing and ceasing after 2.5 min. In both cases, the gas evolution proceeds very similarly. During the experiments, the duration and the maximum flow rate only differ by 9% and 12%. In this manner, the reaction with MnO_2 proceeds slightly faster and reaches a higher maximum flow rate, speaking for a more active catalyst than $Mn(OAc)_2 \times 4\ H_2O$. The activity of both catalysts towards the decomposition of calcium peroxide is comparable. Nevertheless, the decomposition with the aid of [BMIM][$FeCl_4$] proceeds slower, resulting in a maximum flow rate of only one third compared to that with MnO_2, which is not desirable at this time. Further experiments will be conducted with

$Mn(OAc)_2 \times 4\ H_2O$ to ensure comparability with the lithium peroxide experiments, which are also mostly conducted with $Mn(OAc)_2 \times 4\ H_2O$.

It should be noted that, similarly to the decompositions of lithium peroxide described in chapter 4.3, the decomposition of calcium peroxide is not entirely homogeneously catalyzed. The catalytic process produces MnO_2 particles resulting in a partial heterogeneous catalysis on their surface. Additionally, system's pH value plays an important role in the catalytic procedure, since it directly affects the nature of the manganese species present.[3, 36]

4.4.1.3 Variation of the catalyst loading

The previously described experiments were conducted with a catalyst loading of 0.25 mol-%. A catalyst loading of 0.1 mol-% is used to test whether lower catalyst loadings are also feasible for the decomposition of calcium peroxide.

Figure 35 shows the plots for the flow rate and volume development for the decomposition of 10 g calcium peroxide in 10 mL [EMIM][SO_4Me] and 15 mL HCl (15%) with different loadings of Mn(OAc)2 × 4 H_2O.

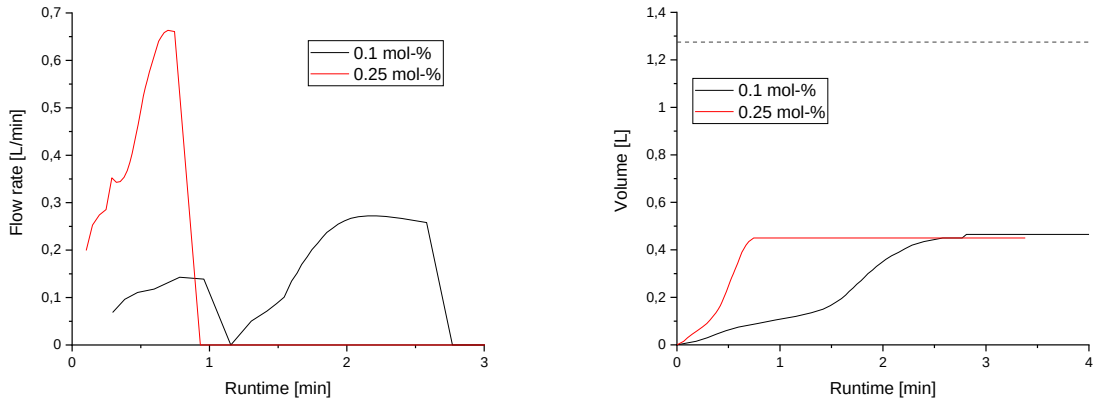

Figure 35: Flow rate and volume plots for the decomposition of 10 g calcium peroxide in 10 mL [EMIM][SO_4Me] and 15 mL HCl (15%) with different loadings of $Mn(OAc)_2 \times 4\ H_2O$. The dashed line marks 100% of theoretical calcium peroxide conversion.

Table 25 provides values for duration, maximum flow rate and conversion for each decomposition reaction.

Table 20: Duration, maximum flow rate and conversion for the reaction of 10 g calcium peroxide in 10 mL [EMIM][SO_4Me] and 15 mL HCl (15%) with different loadings of $Mn(OAc)_2 \times 4\ H_2O$.

concentration	duration [min]	max. flow rate [L/min]	conversion [%]
0.1 mol-%	2.8	0.27	36
0.25 mol-%	0.9	0.66	35

There is a lower maximum flow rate for the lower catalyst loading, as expected. The maximum flow rate responds linearly to the catalyst loading, i.e. the maximum flow rate increases by 2.4 as the catalyst loading increases by 2.4. It is interesting to note that the conversion for both reactions is almost the same. Thus, at least in this case, conversion does not increase with increasing catalyst loading, at least for small catalyst loadings.

4.4.2 Calcium peroxide decomposition experiments at -20 °C

A chemical oxygen generator for aviation purposes must operate at a temperature of -20 °C to meet the legal requirements.[31] As a result, decompositions experiments with calcium peroxide are conducted in a climate chamber at -20 °C.

Figure 36 compares the evolved gas flow rate and volume development for the decomposition of 10 g CPO in 10 mL [EMIM][SO_4Me] and 15 mL HCl (15%) with 0.25 mol-% $Mn(OAc)_2 \times 4\ H_2O$ as well as the decomposition of 10 g CPO in 10 mL [EMIM][SO_4Me] and 25 mL H_2SO_4 (30%) with 0.5 mol-% $Mn(OAc)_2 \times 4\ H_2O$.

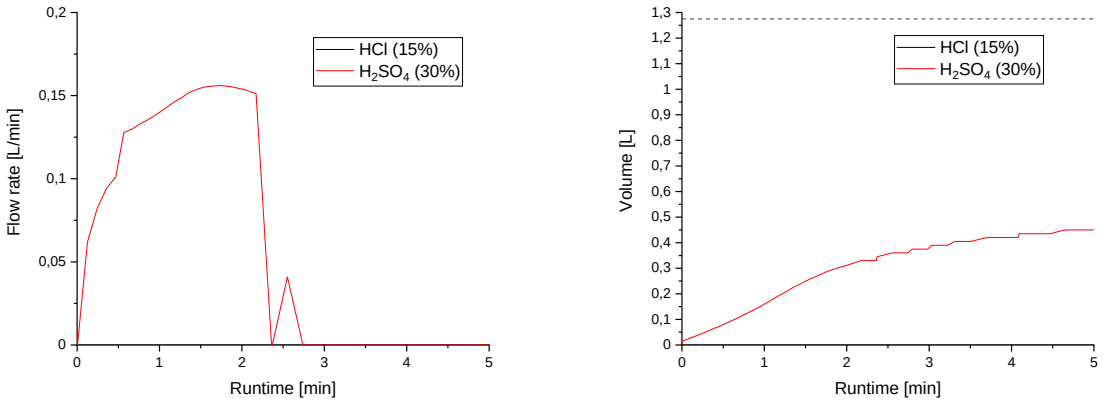

Figure 36: Evolved gas volume and flow rate for the decomposition of 10 g calcium peroxide in 10 mL [EMIM][SO_4Me] and 15 mL HCl (15%) with 0.25 mol-% $Mn(OAc)_2 \times 4\ H_2O$ and the decomposition of 10 g calcium peroxide in 10 mL [EMIM][SO_4Me] and 25 mL H_2SO_4 (30%) with 0.5 mol-% $Mn(OAc)_2 \times 4\ H_2O$. The dashed line marks 100% of theoretical calcium peroxide conversion.

Table 21 shows the values for the duration, maximum flow rate and conversion.

Table 21: Duration, maximum flow rate and conversion for the decomposition of 10 g calcium peroxide in 10 mL [EMIM][SO_4Me] and 15 mL HCl (15%) with 0.25 mol-% $Mn(OAc)_2 \times 4\ H_2O$ and the decomposition of 10 g calcium peroxide in 10 mL [EMIM][SO_4Me] and 25 mL H_2SO_4 (30%) with 0.5 mol-% $Mn(OAc)_2 \times 4\ H_2O$.

solvent	duration [min]	max. flow rate [L/min]	conversion [%]
HCl (15%)	-	-	-
H_2SO_4 (30%)	2.7	0.16	31

Under the chosen conditions the decomposition performed in HCl (15%) does not result in a measurable gas flow rate or gas volume. It is interesting to note that the decomposition reaction in H_2SO_4 (30%), a solvent that was less reactive at room temperature, succeeded in evoking gas at -20 °C, despite being a less reactive solvent at room temperature. An explanation might be the increased catalyst loading of 0.5 mol-% applied for the decomposition in H_2SO_4 (30%) compared to 0.25 mol-% for the decomposition in HCl (15%).

4.5 Mixtures of lithium peroxide and calcium peroxide

4.5.1 Decomposition reactions at room temperature

With the aim of combining the advantages of a more reactive and easier-to-prepare lithium peroxide with a cheaper but less reactive calcium peroxide, oxygen liberation experiments have been attempted using both of these inorganic peroxides as oxygen sources. In this manner, different ratios of both inorganic peroxides are tested. As opposed to the experiments with pure calcium peroxide, it was possible to compress the mixed powders of lithium peroxide and calcium peroxide under the same conditions as the pure lithium peroxide compacts. Thus, the decomposition reactions are carried out at with cylindrical compacts pressed with a compression force of 500 kPa for one minute.

Figure 37 illustrates flow rate and volume developments for the decomposition of 5 g of different compositions of lithium peroxide and calcium peroxide in 10 mL [EMIM][SO_4Me] and 15 mL H_2SO_4 (30%) with 0.25 mol-% $Mn(OAc)_2 \times 4\ H_2O$ at room temperature.

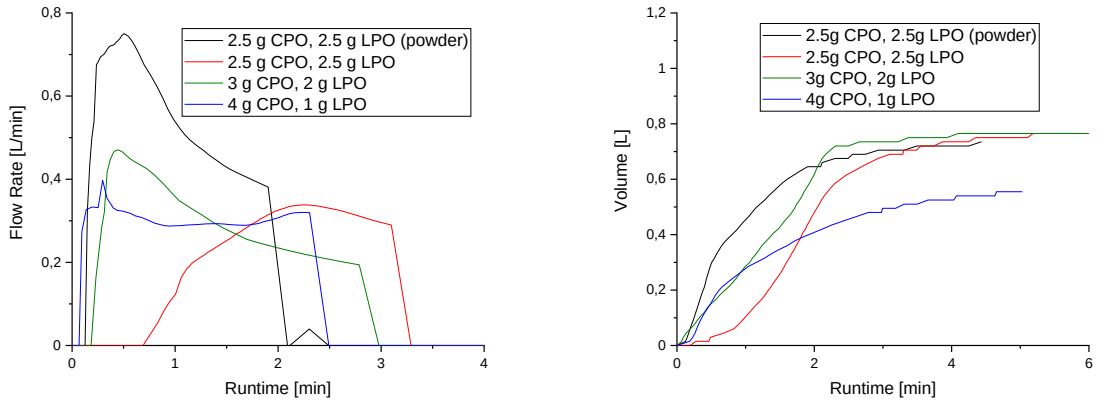

Figure 37: Flow rate and volume developments for the reaction of 5 g of different compositions of LPO and CPO and 0.25 mol % $Mn(OAc)_2 \cdot 4\ H_2O$ in 10 mL [EMIM][SO_4Me] and 15 mL H_2SO_4 (30%) at room temperature.

Table 22 shows duration, maximum flow rate and conversion of the respective reactions.

Table 22: Summary of the duration, maximum flow rate and conversion for the reaction of 5 g of different compositions of LPO and CPO and 0.25 mol % $Mn(OAc)_2 \times 4\ H_2O$ in 10 mL [EMIM][SO_4Me] and 15 mL H_2SO_4 (30%) at room temperature.

oxygen source	duration [min]	max. flow rate [L/min]	conversion [%]
2.5 g CPO, 2.5 g LPO (powder)	2.3	0.75	69
2.5 g CPO, 2.5 g LPO	3.3	0.34	70
3 g CPO, 2 g LPO	3.0	0.47	77
4 g CPO, 1 g LPO	2.3	0.40	84

As soon as the components are mixed, most reactions begin to decompose producing evolving gas. Only the reaction with a cylindrical compact of 2.5 g lithium peroxide and 2.5 g calcium peroxide shows an onset time of 45 s before its decomposition begins. The highest maximum flow rate was found for the system with 2.5 g lithium peroxide in form of powder and the highest conversion for the system with 4 g calcium peroxide and 1 g lithium peroxide.

At room temperature, all systems investigated exhibit decent oxygen evolution activity with comparatively slow and mild decompositions. In general, a higher amount of lithium peroxide increases the maximum flow rate.

4.5.2 Decomposition reactions at -20 °C

The next step is to apply mixtures of calcium peroxide and lithium peroxide at a temperature of -20 °C. Similar to chemical oxygen generators which contain only one inorganic peroxide, a chemical oxygen generator based on two inorganic peroxides must also meet legal requirements, namely, it must work between -20 °C and +60 °C.[31]

As in the room temperature experiments, the inorganic peroxide powders are mixed prior to being compressed into cylindrical compacts applying 500 kPa for one minute. **Figure 38** illustrates volume development and flow rate for the decomposition of 5 g of different compositions of lithium peroxide and calcium peroxide with 0.25 mol-% $Mn(OAc)_2 \times 4\ H_2O$ in a mixture of 10 mL [EMIM][SO_4Me] and 15 mL H_2SO_4 (30%).

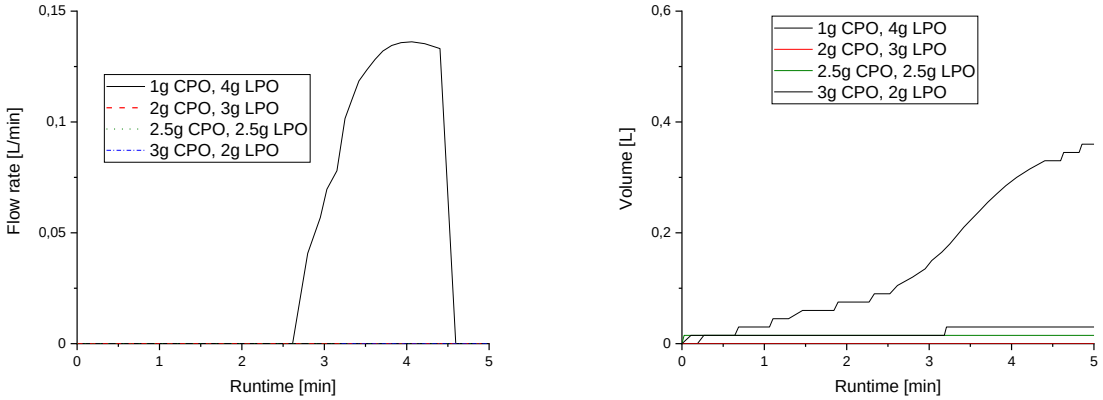

Figure 38: Evolving gas volume and flow rate for the decompositionn of 5 g of different compositions of lithium peroxide and calcium peroxide with 0.25 mol-% $Mn(OAc)_2 \times 4\ H_2O$ in 10 mL [EMIM][SO_4Me] and 15 mL H_2SO_4 (30%).

Table 23 summarizes duration, maximum flow rate and conversion of the respective decompositions.

Table 23: Duration, conversion and maximum flow rate for the decomposition 5 g of different compositions of lithium peroxide and calcium peroxide with 0.25 mol-% $Mn(OAc)_2 \times 4\ H_2O$ in 10 mL [EMIM][SO_4Me] and 15 mL H_2SO_4 (30%).

oxygen source	duration [min]	max. flow rate [L/min]	conversion [%]
1 g CPO, 4 g LPO	1.8	0.14	42
2 g CPO, 3 g LPO	-	-	-
2.5 g CPO, 2.5 g LPO	-	-	-
3 g CPO, 2 g LPO	-	-	-

Among the tested reactions, only one evolved gas at -20 °C when one gram of calcium peroxide was combined with four grams of lithium peroxide. Other peroxide compositions did not emit any measurable gas flow. It appears that even for the decomposition of 4 g lithium peroxide the conversion is lower than for the decompositions described in chapter 4.3.2.3 on page 44 where only lithium peroxide is decomposed. It is possible that calcium peroxide has an inhibitory effect on lithium peroxide, i.e., a decrease in its reactivity in the presence of calcium peroxide. In accordance with the findings from chapter 4.4.1.1 on page 54, calcium peroxide might not be an appropriate oxygen source for a chemical oxygen generator that must evolve gas at ambient temperatures of -20 °C. There is still a need to investigate whether different and improved reaction conditions result in better results when it comes to the evolution of oxygen from calcium peroxide.

4.6 Anti-foaming agents

Particularly at the end of the decomposition reactions, macroscopically conspicuous and stiff foam forms within and especially on top of the reaction medium. Foam should be avoided since it may lead to an incomplete reaction due to poor miscibility of the reaction components. The reaction medium is therefore supplemented with anti-foaming agents. In a similar manner to the experiments that investigate the compression strength, the reactions are conducted using KOH (25%) as reaction medium. In basic media and especially in KOH (25%), enhanced foaming is observed compared to media with acidic conditions.

Figure 39: Two photos on the left show solid residues of the decomposition reaction floating on top of the reaction medium at the end of the decomposition. These residues consist mainly of undecomposed peroxides. On the right side, one can see the strong foam formation during an ongoing decomposition reaction, which leads to inhomogeneous mixing.

The evolved gas volume and gas flow rate for the reaction of 40 g lithium peroxide and ten grams sodium peroxide in 200 mL KOH (25%) with 0.25 mol-% $Mn(OAc)_2 \times 4\ H_2O$ and 15 g of the respective anti-foaming agent is shown in **Figure 40**. **Table 24** summarizes the findings for duration, maximum flow rate and conversion of the decompositions.

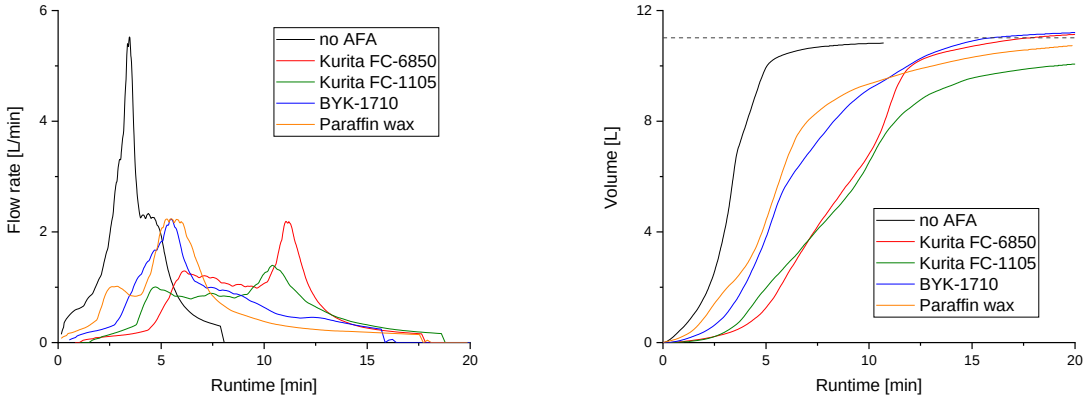

Figure 40: Evolved gas volume and gas flow rate for the decomposition of 40 g lithium peroxide and 10 g sodium peroxide in 200 mL KOH (25%) with 0.25 mol-% $Mn(OAc)_2 \times 4\ H_2O$ and 15 g of the respective anti-foaming agent. The dashed line represents 100% of theoretical inorganic peroxide conversion.

Table 24: Summary of the duration, maximum flow rate and conversion for the decomposition of 40 g lithium peroxide and 10 g sodium peroxide in 200 mL KOH (25%) with 0.25 mol-% $Mn(OAc)_2 \times 4\ H_2O$ and 15 g of the respective anti-foaming agent.

AFA	duration [min]	max. flow rate [L/min]	conversion [%]
-	8.06	5.52	97
Kurita FC-6850	17.8	2.19	101
Kurita FC-1150	18.6	1.40	92
BYK-1710	16.4	2.23	102
paraffin wax	17.7	2.24	97

Flow rates peak five to twelve minutes after the reaction begins. Thus, the maximum flow rate for *Kurita FC-6850* is obtained six minutes after the maximum flow rate for Paraffin wax and *BYK 1710*. A maximum flow rate of 1.40 L/min was observed for *Kurita FC1150*, which is 36% lower than all other tested anti-foaming agents. For all decompositions, the volumes and conversions are quite similar, only differing by 4% from the lowest to the highest conversion.

As a result of the addition of an anti-foaming agent, the flow rate plot takes on a different shape. The maximum flow rate is observed later in the decomposition with *Kurita FC-6850* and *Kurita FC-1150*, where the maximum flow rate is observed later during the decomposition reaction. In addition, the maximum flow rates are lower and the reaction time is increased by a factor of two as compared to the decomposition experiments without any anti-foaming agent. It is possible that dilution effects might be responsible for these observations, since as more compounds are added to the reaction mixture, the overall volume increases within the reaction medium.

Another important factor to consider is the chemical composition of the anti-foaming agent. Due to the unknown chemical structures of the applied anti-foaming agent no assumptions can be made towards which compound will result in a certain flow rate. Foam formation is not completely prevented by the addition of anti-foaming agents at the macroscopic level. Additionally, it is important to determine whether there are any ionic liquids that provide an anti-foaming effect.

4.7 Particle size analysis

Based on the findings of previous chapters, the morphology of the utilized peroxide cylindrical compacts plays an important role for the reactivity of the oxygen liberation system, influencing the flow rate as well as the volume developments. Compacts based on lithium peroxide are also more stable and less likely to break than compacts based on calcium peroxide. The particle size distributions of lithium peroxide and calcium peroxide powder were examined to gain a better understanding of the compacting behavior of the utilized inorganic peroxides. Accordingly, d_{10}, d_{50}, and d_{90} values for the respective particle distributions are determined, along with their spans. The d_{10} diameter is used to determine the percentage of particles with diameters equal to or smaller than the d_{10} value in a particle size or volume distribution. The d_{50} and d_{90} values are calculated in the same way.[39] According to **Scheme 8**, the span provides information about the width of the particle size distribution.[40, 41]

$$Sp = \frac{d_{90} - d_{10}}{d_{50}}$$

Scheme 8: Definition of the span as a function of d_{10}, d_{50} and d_{90}.[40]

The quantity distribution as well as the volume distribution of the particles within the lithium peroxide sample are shown in **Figure 41**. **Table 25** summarizes the characteristic diameters d_{10}, d_{50} and d_{90} and the respective spans.

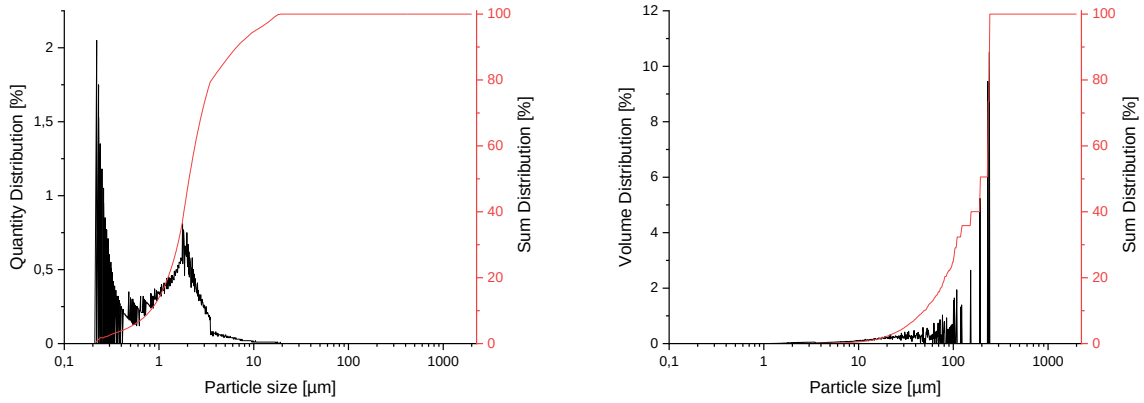

Figure 41: Quantity distribution (left) and volume distribution (right) as well as sum distributions of lithium peroxide particles.

Table 25: Results for the d_{10}, d_{50} and d_{90} values and the spans of the quantity distribution and volume distribution of lithium peroxide powder.

$d_{n,10}$ [µm]	$d_{n,50}$ [µm]	$d_{n,90}$ [µm]	$d_{n,sp}$ [µm]	$d_{v,10}$ [µm]	$d_{v,50}$ [µm]	$d_{v,90}$ [µm]	$d_{v,sp}$ [µm]
0.81	2.08	6.6	2.78	49	193	240	0.99

According to the data, the average diameters of the size distribution (2.08 µm) and the volume distribution (193 µm) of lithium peroxide differ by two orders of magnitude. That means, that there are many small particles in the powder sample that contribute only to a very small volume fraction of the respective lithium peroxide sample, while few particles with a large diameter account for a significant portion of the powder volume. Because the smaller particles fill the gaps between the larger ones, the big differences in particle size allow sufficient compressibility. The quantity distribution, the volume distribution and the sum distributions of calcium peroxide powder are depicted in **Figure 42**.

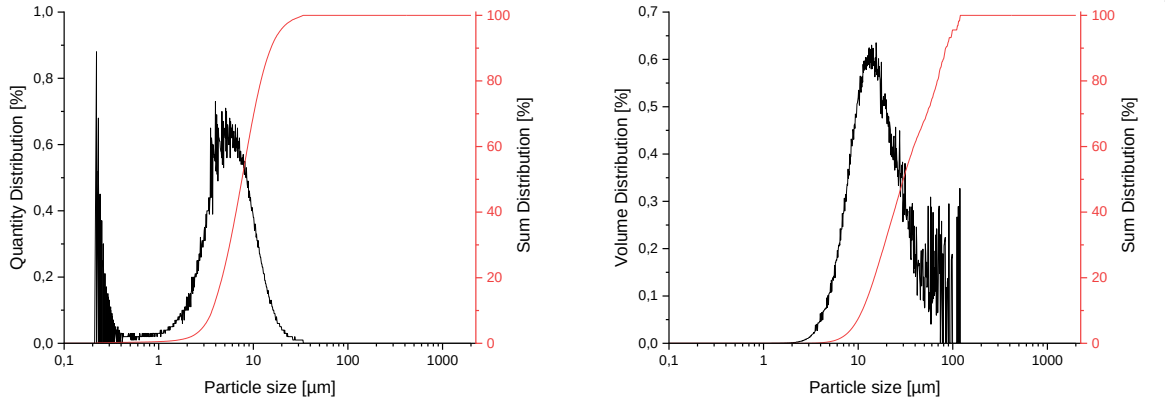

Figure 42: Quantity distribution (left) and volume distribution (right) as well as sum distributions of calcium peroxide particles.

Table 26 summarizes the characteristic diameters d_{10}, d_{50} and d_{90} and the respective spans.

Table 26: Results for the d_{10}, d_{50} and d_{90} values and the spans of the quantity distribution and volume distribution of calcium peroxide powder.

$d_{n,10}$ [µm]	$d_{n,50}$ [µm]	$d_{n,90}$ [µm]	$d_{n,sp}$ [µm]	$d_{v,10}$ [µm]	$d_{v,50}$ [µm]	$d_{v,90}$ [µm]	$d_{v,sp}$ [µm]
3.68	7.58	15.5	1.56	11.0	30.0	84.1	2.44

Both the quantity distribution curve and the volume distribution curve of calcium peroxide powder exhibit Gaussian characteristics. The particles are generally of similar size with an average particle diameter of dn_{50} = 7.58 µm, which is larger than the dn_{50} value of lithium peroxide powder. Sodium peroxide powder, however, has a higher dv_{50} value. Contrary to lithium peroxide, the average diameters of the size distribution (7.58 µm) and volume distribution (30 µm) of sodium peroxide differ by only one order of magnitude. In general, this means that sodium peroxide powder has larger particles with similar diameters than lithium peroxide, which makes it harder to compress into pellets when compared with lithium peroxide, as there are no small particle fillings the gaps. By grinding, sieving, and combining powder fractions with suitable average diameters, the particle size distribution of sodium peroxide could be optimized to improve its compressibility.

4.8 Generator design and concept

The demands and technical requirements for the generator housing and its compartments are described in detail in chapter 3.5 on page 17.

A full concept development and design process is based on morphological analysis. This technique can help solve a complex, non-quantified and multidimensional problem. For morphological analysis a table is created with different parameters listed vertically and its associated features listed horizontally. A matrix can be created by collecting different combinations of parameters from different features to determine the best solution. Similarly, the concept in this study will be based upon the same methodology, with each section discussing a parameter of the chemical oxygen generator and suggesting a feature for that parameter.

Table 27: Morphological analysis for novel generator layout and concept.

parameter		feature				
exterior	form	cylinder	cube	complex		
	material	PTFE	CPE+	PC	PEEK	metal
chemistry	O_2-source	Li_2O_2	Na_2O_2	CaO_2	$NaClO_3$	$NaClO_4$
	form of O_2-source	cylinder	granules	pellets	hollow cylinder	
	reaction medium	water with antifreeze admixture	ionic liquid	ionic liquid, water and acid/base		
	activator	protons H^+	catalyst			
interieur	separation	PTFE-membrane	PVDF-membrane			
	starting mechanism	blade on carriage	rotary closure	injection syringe		
	impurities	filter	suitable educts			

4.8.1 Starting mechanism

The starting mechanism starting the decomposition reaction by its activation for example by bringing the oxygen source in contact with the reaction medium. Throughout this section, we will examine different concepts for starting mechanisms that have potential to be implemented within a future chemical oxygen generator.

4.8.1.1 Injection syringe

Already *Hinterberger* suggested using an injection syringe to deliver the reaction medium and the catalyst to the oxygen source, as shown in **Figure 43**.[36] The concept of Hinterberger is based on the utilization of a medium-viscosity ionic liquid like [EMIM][PO_4Et_2], suspended MnO_2 particles and urea hydrogen peroxide as an oxygen source.

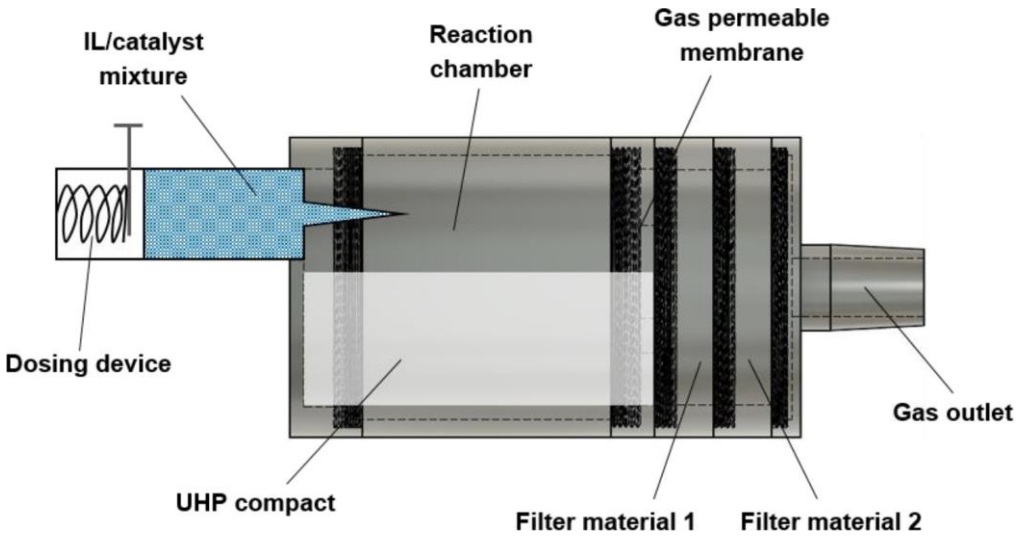

Figure 43: Concept from *Hinterberger* of a syringe-based injection mechanism.[36]

The main advantage of this system is the injection through a syringe, which allows for the use of high- and medium-viscous ionic liquids and a high reliability, that the reaction medium is making contact with the oxygen source independent of the spatial orientation of the generator. It is also possible to retain the mechanism previously used in conventional chlorate candles with a preloaded spring which is released by pulling a split pin.

An intrinsic disadvantage of syringe design is the high space requirement and spatial constraints. This is because space must be created for the reaction medium at two different locations. Once inside the syringe and once inside the reaction chamber.

4.8.1.2 Wall tearing mechanism

To avoid this space problem, the reaction medium should be kept right inside the reaction chamber. It can be separated from the oxygen source either by a partition or by packing the reaction medium in a kind of bag and opening it when required. The partition can be cut through either by a blade preloaded on a carriage along a rail or by a rotary closure familiar from the food packaging industry as shown in **Figure 44**.[42]

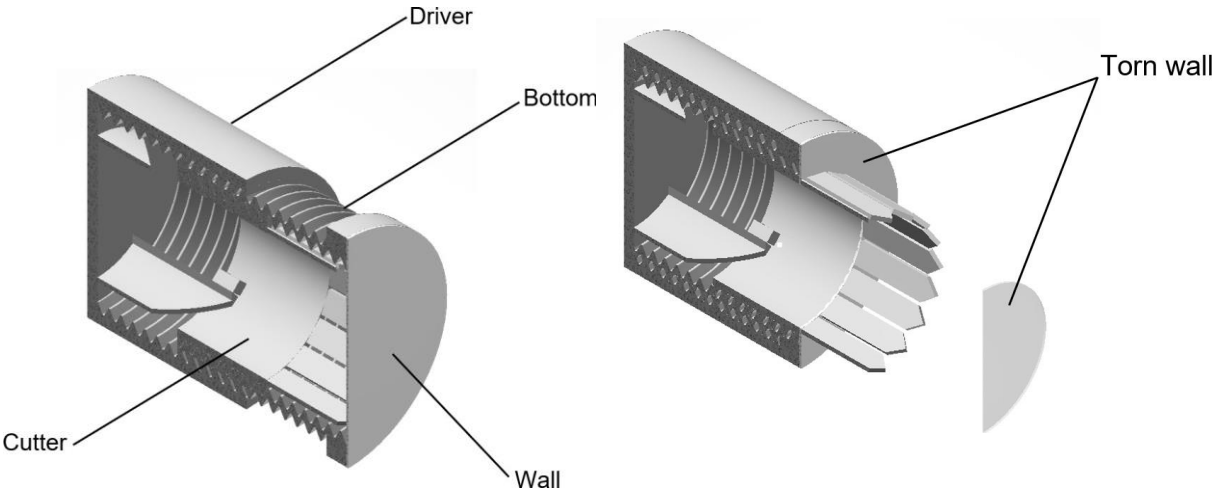

Figure 44: Initial (left) and final state (right) of the wall tearing mechanism.

Ideally, the wall should be made from a chemically stable material that also exhibits tearability under normal conditions. Torsion springs can be used to load the driver. Upon release, the torque will cause the driver to glide on the bottom, which is fixed. When the driver rotates, it will cause the cutter on the inside of the bottom to spin simultaneously with it and be pushed forward, cutting through the wall. Furthermore, as the driver pushes forward, the bag containing the reaction medium and catalyst becomes compressed, facilitating their delivery to the reaction chamber. As can be seen in **Figure 44** on the right, the opening mechanism has reached its final state.

The disadvantage of this opening mechanism described above is that, contrary to the syringe mechanism, the point at which the reaction solution comes into contact with the oxygen source cannot be determined precisely. The problem could be the spatial orientation and positioning of the generator.

4.8.2 Form of the oxygen source

According to **Figure 14** on page 17, a commercial chemical oxygen generator must meet a certain flow rate profile. In order to achieve this, the overall speed of the decomposition reaction has to be varied. From the nature of the decomposition reaction, it can be said that the overall reaction progress can be controlled by the surface area of the oxygen source, which can be manipulated by varying the geometry of the oxygen source. Assuming that the oxygen source is given in a cylindrical form such as tablets or compacts, the surface area and the volume of a cylinder as a function of height and diameter is given in **Figure 45**.

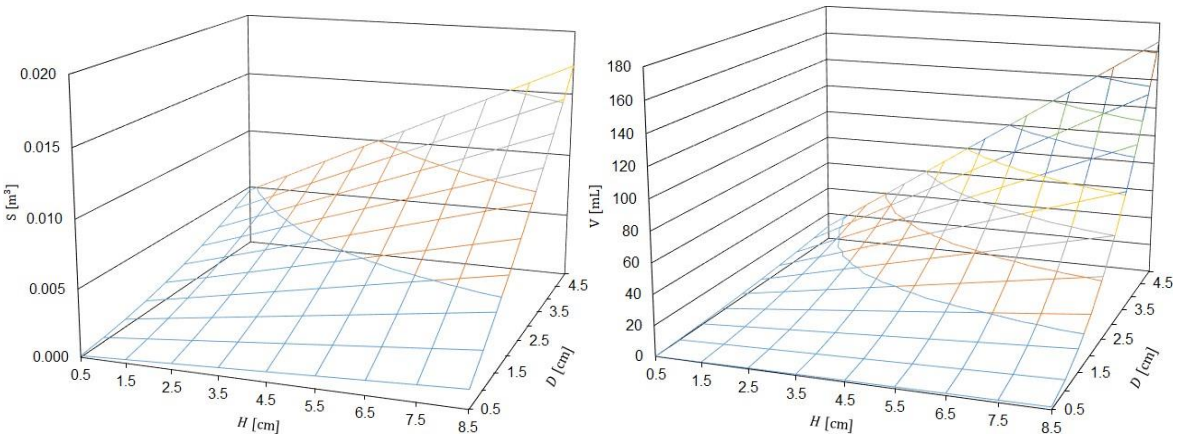

Figure 45: Dependence of the surface area (left) and volume (right) of a cylinder on height and diameter.

As can be seen, the larger the compact, the lower the specific area. It can be observed in both diagrams of **Figure 45** that the slope is unevenly distributed. The unevenness of the surface allows the equivalent amount of oxygen source to have a greater surface area, according to which it is possible to control reaction kinetics and so secondary parameters like gas flow rate and reaction temperature. As an example, if a certain amount of oxygen is compressed into a compact measuring 5 cm diameter and 7.5 cm height, the volume V and surface area S of the compact are calculated to be 147.26 mL and 0.016 m^2, respectively. The same volume would lead to more than 173 smaller tablets with a diameter of 1 cm and a height of 1.5 cm. Along with this, the surface area is increased by approximately seven times.

In **Figure 46** the same amount of oxygen source on the left is compacted into tablets forming a cylindrical packing as seen on the right. The packing can be stabilized by rids or similar supporting material. By varying the size of tablets used and increasing the overall density of the oxygen source packing, the stability of the oxygen source packing can still be assured under violent shaking or rotation.

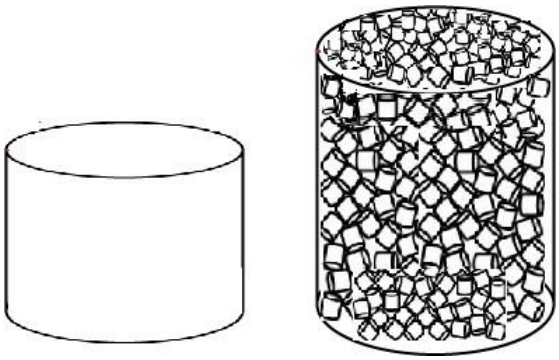

Figure 46: Oxygen source in form of a cylindrical compact and as packed bulk.[43]

The porosity of the packing can replace the free space of the reaction chamber seen in **Figure 43** allowing the oxygen to flow freely while the stability of the entire packing still can be assured. The overall surface area of the oxygen source can be tuned by varying the size of the tablets and the composition of the different tablet sizes.
Additional studies are still necessary in order to identify the optimal configuration of tablet size and tablet size composition that can satisfy the flow rate profile shown in **Figure 14** on page 17 and exhibit optimal reaction kinetics. To obtain more reliable and reproducible results, a pelleting machine so far not accessible should be used to get the oxygen source into shape.
In addition, compacting the oxygen source into a one large compact with abundant free space around, such as depicted in **Figure 43** on page 73, can pose the risk that the compact will fall apart if the aircraft shakes violently, resulting in extreme reaction kinetics that are hard to control and possible bear a safety risk.

4.8.3 Membrane

In order to meet the technical requirement that the generator must be fully functional orientated in all spatial directions, it is necessary to separate the reaction chamber with the highly reactive liquid from the gas outlet. Thermally and chemically very inert membranes supported by a grid structure are suitable for this purpose.

4.8.3.1 Membrane types

The membrane's influence on the flow rate profile and volume development will be investigated with the following experiments. Therefore, the decomposition setup is adapted with the aid of a membrane jig, shown in **Figure 47**.

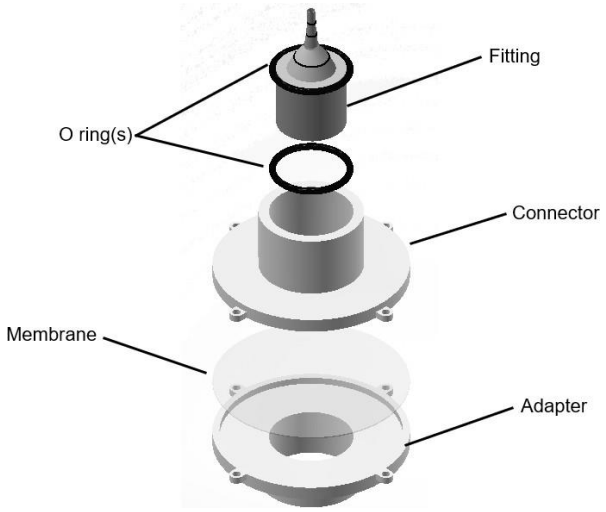

Figure 47: Exploded assembly drawing of the membrane jig within the membrane test setup.

The three following decomposition experiments with different amounts of oxygen source, as shown in **Table 28**, are performed to test the permeability of the membrane and its influence on the total volume measured as well as the flow rate profile.

Table 28: Considerations of the oxygen sources used and the associated substance quantities.

Oxygen Source	$n(Li_2O_2)$ [mol]	$n(Na_2O_2)$ [mol]	$n(O_2)$ [mol]	$V(O_2)$ [L]
5 g Li_2O_2	0.109	-	0.054	1.22
5 g Li_2O_2 + 5 g Na_2O_2	0.109	0.064	0.087	1.94
5 g Li_2O_2 + 10 g Na_2O_2	0.109	0.128	0.12	2.69

For this purpose, 5 g lithium peroxide in form of a fine powder are decomposed with 1 mol-% of $Mn(OAc)_2 \times 4\ H_2O$ in 100mL water in a modified reactor setup, as shown in chapter 7.4.3 on page 93. The corresponding evolved gas volumes and gas flow rates are shown in **Figure 48**.

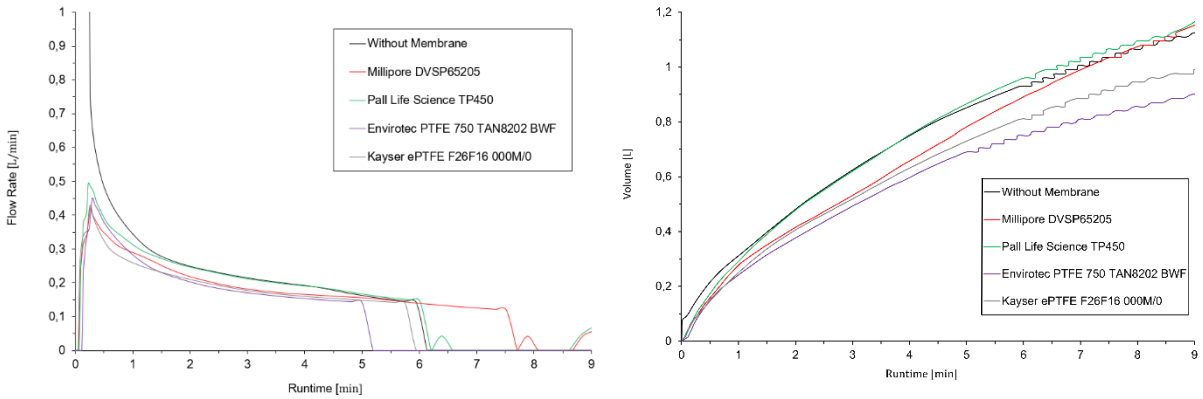

Figure 48: Flow rate and volume developments for the decomposition of 5 g lithium peroxide with 1 mol-% $Mn(OAc)_2 \times 4\ H_2O$ in 100 mL water with different membranes in between the reaction chamber and gas meter.

Regarding the flow rate plot, it is relatively similar for all membranes tested. For the experiment in which no membrane is installed, even though the flow rate initially starts high, its behavior is likely to that observed for other membranes over the course of the decomposition reactions. Clearly, all of the tested membrane types assure gas flow roughly equivalent to what would be expected in the absence of a membrane and the gas flow through the membrane is almost unaffected.

Increasing the amount of used peroxide to 5 g lithium peroxide and 5 g sodium peroxide the generated gas volume 1.6 g higher and the flow rate and volume profile plot can be observed to be vastly different by membrane type, as illustrated in **Figure 49**.

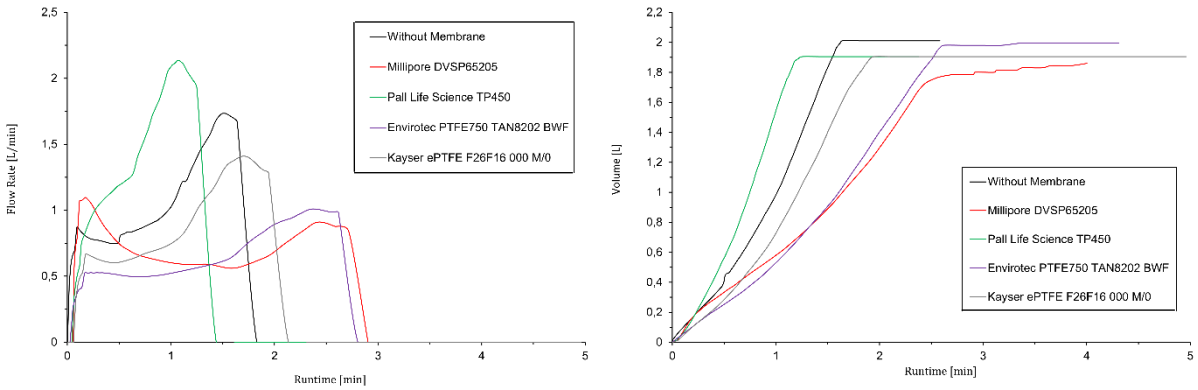

Figure 49: Flow rate and volume developments for the decomposition of 5 g lithium peroxide and 5 g sodium peroxide with 1 mol-% $Mn(OAc)_2 \times 4\ H_2O$ in 100 mL water with different membranes in between the reaction chamber and gas meter.

Nevertheless, all flow rate profiles follow the same trend. In the first minute of the decomposition reaction, the flow rate of the TP450 membrane is even greater than it would have been without the membrane, which may be due to inaccuracies and deviations within the oxygen sources used. The two membranes PTFE750 from *Envirotec* and ePTFE F26F16 from *Kayser* appeared to be particularly suitable, as they shape the flow rate profile beneficial. Since the volume flow per membrane area is still very low, however, care must be taken to ensure that insufficient permeability causes pressure build-up inside the reactor, which may be difficult to handle. The striking flow rate profile that slowly increases again after the formation of a plateau with a peak at the end can essentially be explained by two coherences. Firstly, the permeability increases due to the rising pressure inside the reaction chamber. Additionally, as the temperature of the reaction medium continues to rise and along with that temperature of the generated gas, it can be assumed that microscopic characteristics of the membrane chance too. According to Sharma *et al.*, increasing temperatures not only alter the pore sizes, but also other factors like tortuosity as well.[43] It is important to note that in this case, as the temperature increases, the membrane also reaches its critical temperature, at which point the overall pore size increases, resulting in an increase in flow rates.

4.8.4 Materials and additive manufacturing

Not only during its operation but also during its many years installed inside the aircraft, the generator housing is exposed to many forces and stress. For example, a temperature difference of 100 °C is nothing unusual considering -30 °C inside a non-tempered aircraft during night in Anchorage and +70 °C if stored at daytime in Qatar. In addition to the temperature load, the housing is also exposed to numerous vibrations in a wide range.

As can be seen from the temperature measurement experiments in chapter 4.3.3.3 on page 51, the temperature of the reaction mixture settles at around 110 °C during the decomposition. So that the housing does not deform due to the effects of heat treatment, plastics should withstand 110 °C permanently without sacrificing stability. Therefore, the maximum operating temperature of different and typical FDM-Filaments is compared in **Table 29**. Thereby, it is important to compare the corresponding data of the filaments from the supplier and do not confuse them with the data from the general synthetic material, as there are always additives subjoined to increase printability.

Table 29: Maximum operating temperature of different filaments.[48, 49, 50]

filament	max. operating temperature [°C]
PLA	52
PETG	73
PVA	75
$nylon_{6,6}$	90
ABS	98
PP	100
PC	121
PPS	200
PEEK	260

4.8.5 Prototype generator

Taking into consideration all of the compartments discussed above, a general concept is developed for a novel generator layout, as illustrated in **Figure 50**, **Figure 51** and **Figure 52**.

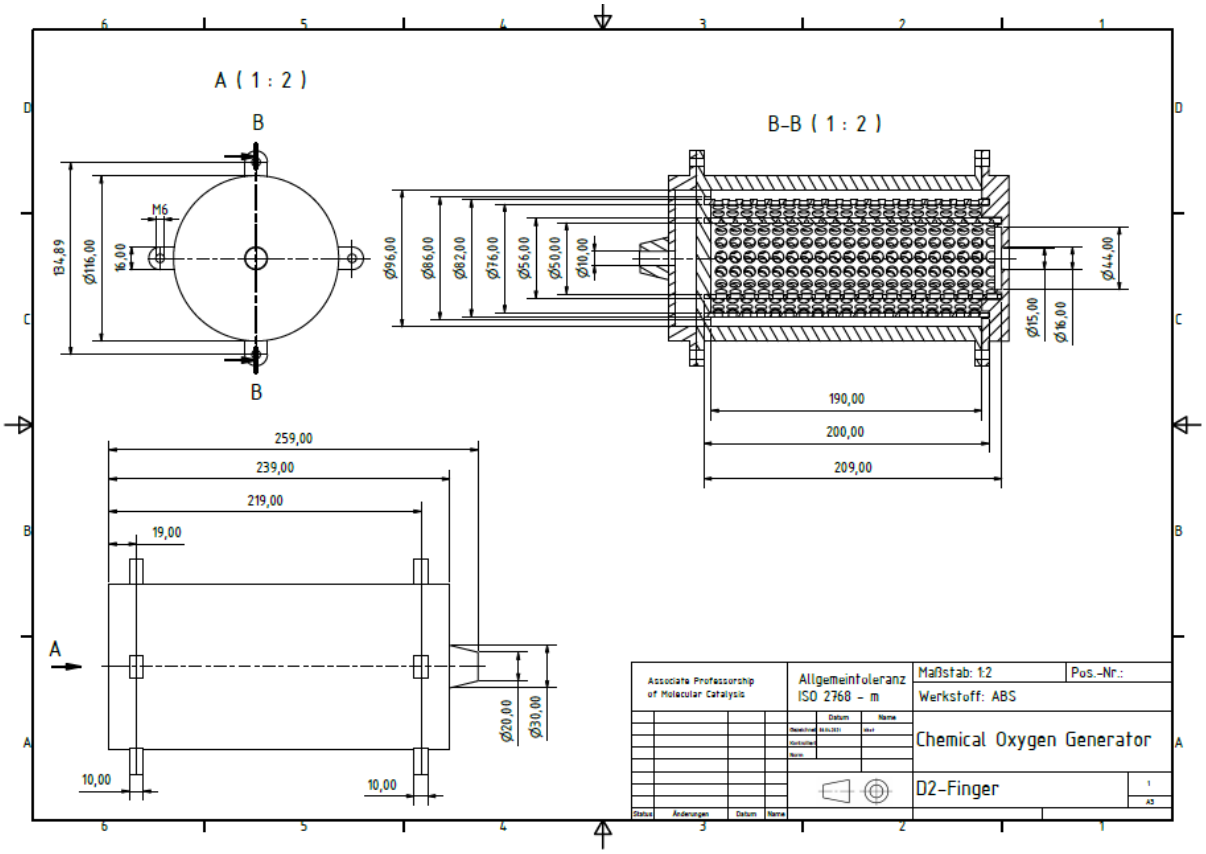

Figure 50: Technical drawing of the chemical oxygen generator prototype.

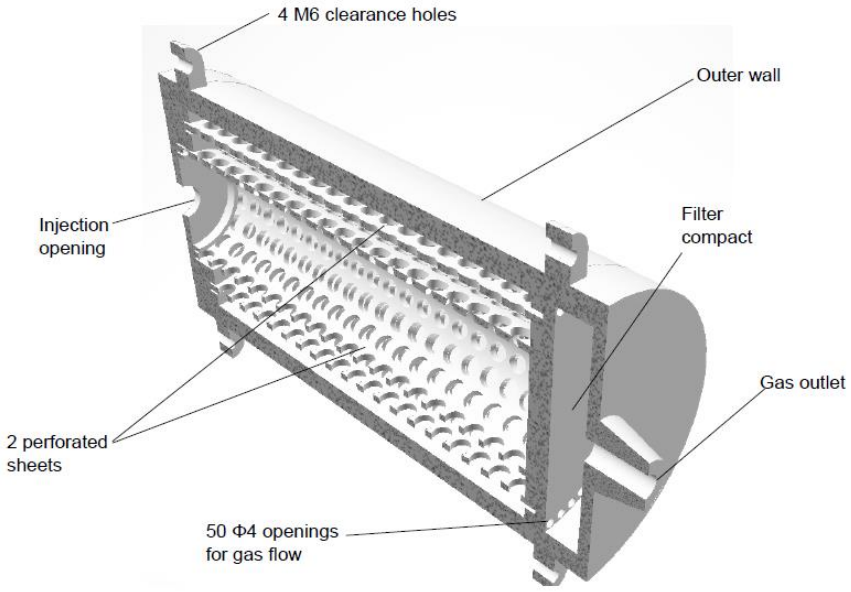

Figure 51: Sectional view of the chemical oxygen generator prototype.

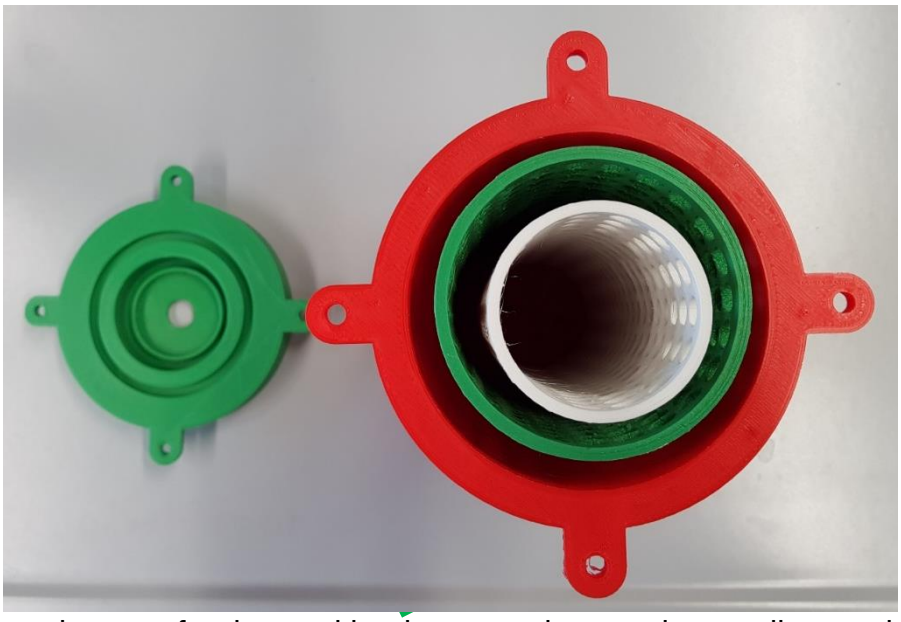

The shown generator housing is 3d-printed with polycarbonate PC and offers with placeholders the possibility to insert membranes, the pelletized oxygen source as well as a filter. There is no retainer yet for the partition between the reaction medium and the oxygen source as well as wall tearing mechanism. The cylinder is 116 mm broad and 239 mm long and weighs about 95 g.

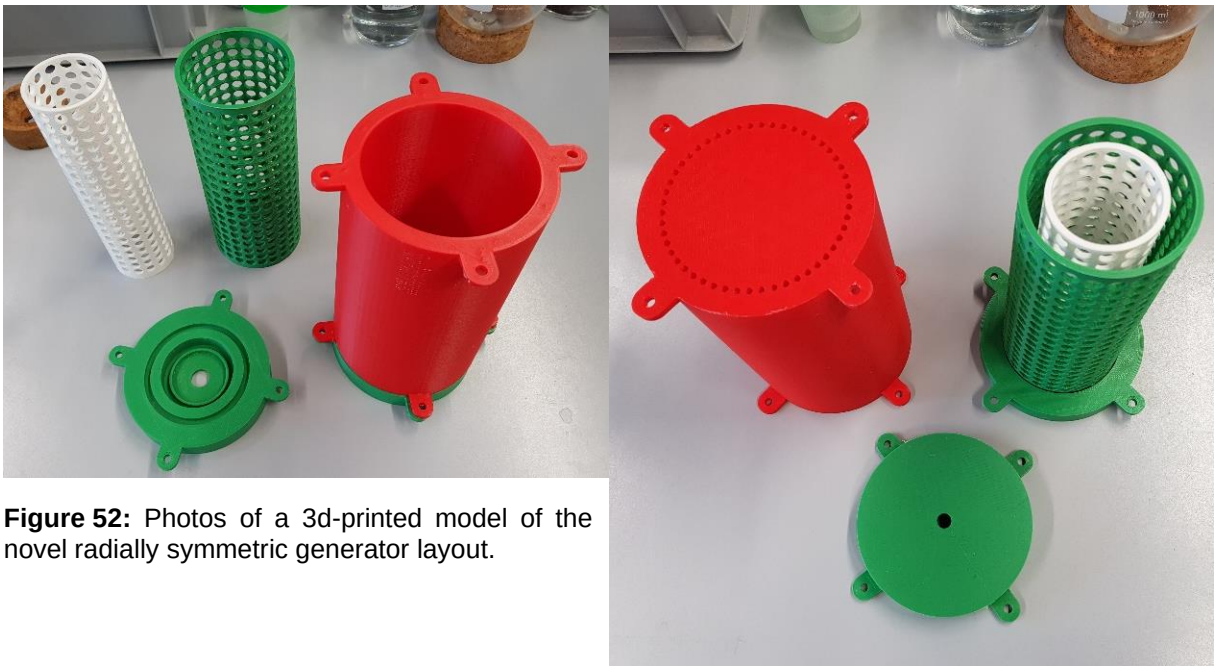

Figure 52: Photos of a 3d-printed model of the novel radially symmetric generator layout.

Thus, the housing could act as an exchange product for commercial and most prevalent chemical oxygen generators like the in chapter 3.5 on page 17 described one from *Avox*. Not only commercialization but also especially the installation as a retrofit kit for refurbished aircrafts is thus enormously simplified.

5 Summary

The pursuit of this thesis was to develop, design and build a low-temperature oxygen generator for civil aviation purposes. Different approaches have been taken in order to develop an oxygen evolution system based on inorganic peroxides like lithium peroxide, calcium peroxide and sodium peroxide as oxygen sources. Therefore, a variety of parameters and ingredients like solvent, ionic liquid, catalyst, catalyst loading and temperature were examined to develop a low-temperature light-weight chemical oxygen generator. A decomposition system based on the oxygen source lithium peroxide Li_2O_2, the aqueous solvent HCl (15%), the ionic liquid [EMIM][SO_4Me] and the homogeneous catalyst $Mn(OAc)_2 \times 4\ H_2O$ proved to be the most promising and applicable candidate.

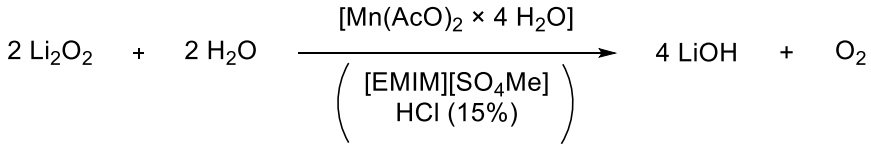

Scheme 9: Decomposition of lithium peroxide with one equivalent of water in a mixture of [EMIM][SO_4Me] and HCl (15%) with $Mn(OAc)_2 \times 4\ H_2O$.

With the main decomposition reaction components optimized, it was possible to run a decomposition reaction with 90 g lithium peroxide in a mixture of 270 mL HCl (15%) and 180 mL [EMIM][SO4Me] as well as 480 mg $Mn(OAc)_2 \times 4\ H_2O$ evolving 17 L gaseous oxygen corresponding to approximately 20% scale of the finale target size of a chemical oxygen generator. As the combination of these components is completely new, a patent application was filed for the composition and method of generating oxygen (EP 4 071 107 A1).

To gain a better understanding in the crucial compactability of the oxygen source, particle size distribution analysis was performed with samples of the utilized lithium peroxide and calcium peroxide. Based on our testing, it has been found that the particle size distribution of lithium peroxide is wider and, therefore, more favorable for the compaction towards stable cylindrical compacts than the particle size distribution of calcium peroxide.

The formation of disruptive foam occurring during the decomposition of inorganic peroxides was successfully suppressed by more detailed investigations and the addition of various antifoaming agents, resulting in an increased oxygen yield. As the use of antifoaming agents in the process of oxygen evolution is completely new, a patent application was filed (patent pending).

In addition to the chemistry inside such a generator, also a design and concept for the generator housing and the technical compartments had been developed. All key parts of a fully functional generator like housing, membrane, filter compartment, reaction chamber and starting mechanism were designed with CAD programs, additively manufactured, tested and discussed.

A PTFE Membrane with a pore size of 1.7 mm has been found to display suitable characteristics, including considerable membrane permeability and thermal stability which demonstrates its compatibility within chemical oxygen generators in the future. Furthermore, based on the standard flow rate requirements and technical necessities a new concept for the oxygen source has been developed. Thereby, the pulverulent oxygen source is pelletized and stored and as needed decomposed in a packing. Moreover, the wall tearing mechanism was introduced in order to optimize the space utilization efficiency.

6 Outlook

The results for the decomposition of inorganic peroxides in mixtures of acidic or basic aqueous solutions and ionic liquids provide a promising basis for the future development of an emergency oxygen generator for civil aircraft. A brief description of the next logical steps towards developing a functional prototype is presented below.

The effect of different ambient temperatures on the reaction is an important factor to consider. Based on initial research with a powder compact mixture, it was determined that sufficient oxygen flow rates could be achieved within the temperature range of -20 °C to room temperature. Furthermore, it is necessary to extend the temperature range to temperatures above room temperature as well. The reactivity must be consistent regardless of the ambient temperature within the range -20 °C to +60 °C.

During the studies on the decomposition of inorganic peroxides, their compaction has become an important tool to control the oxygen flow rate. So far, however, only cylindrical compacts with a maximum weight of 30 g lithium peroxide have been made due to technical limitations of the laboratory press and press dies. Acquisition of a large-scale press as well as a pelleting press would make great strides in the development of the oxygen generator on a technical level.

As a future development, an ionic liquid should be used, that bears multiple functions: a catalytically active transition metal, a Brønsted acidic functionality, foam inhibiting properties as well as a low viscosity and a melting point below -20 °C. This would simplify the system, since one component would incorporate various functions for the evolution of oxygen from inorganic peroxides.

The conceived generator concept should be tested for functionality and durability in future studies. Moreover, the enlisted and various different parameters such as the filter unit or starter unit need to be considered and further analyzed in order to achieve an optimal flow rate that complies with the legal requirements for a commercial chemical oxygen generator for aviation purposes.

Intensive research and innovative solutions are still necessary to get satisfactory solutions. Many of the questions require intensive scrutiny in order to achieve the design of a respective next generation oxygen generator. However, if a suitable concept can be derived a market disrupting technology might be on the verge.

7 Experimental

7.1 Abbreviations

ABS	acrylonitrile butadien styrene
AFA	anti-foaming agent
AOC	active oxygen content
BAIL	Brønsted acidic ionic liquid
CC	cylindrical compact
COG	chemical oxygen generator
CPO	calcium peroxide
DMSO	dimethyl sulfoxide
DSC	differential scanning calometry
et al.	et alii (and others)
FDM	filament deposition modeling
HT-pipe	high temperature pipe
LPO	lithium peroxide
OSU	oxygen supply unit
PC	polycarbonate
PEEK	polyether ether ketone
PETG	polyethylene terephthalate glycol
PLA	poly lactic acid
PVA	polyvinyl alcohol
PSU	passenger supply unit
PP	polypropylene
ppm	parts per million
PPS	polyphenylene sulfide
r.t.	room temperature
RTIL	room temperature ionic liquid
SILM	supported ionic liquid membrane
SPC	sodium percarbonate
SPO	sodium peroxide
UHP	urea hydrogen peroxide
wt.	weight

7.2 General

7.2.1 Chemicals

Unless otherwise mentioned, all chemicals were purchased from commercial suppliers and used without further purification. Reactions with air- and moisture-sensitive substances were carried out using standard Schlenk techniques under an atmosphere of argon.

Prior to application ionic liquids were dried and degassed under vigorous stirring *in vacuo* at 70 °C. Thereby the water content was reduced to values below 50 ppm.

7.2.2 Gas flow rate and gas volume measurements

Gas volume and gas flow rate measurements are conducted with the aid of a *TGA0.5/7* drum-type gas meter and recorded with the associated software *Rigamo* by *Ritter*.

7.2.3 Reaction temperature measurements

The temperature of the reaction mixture is measured simultaneously with a *SDL 200* electrical thermometer by *Extech instruments* equipped with a K-type thermocouple.

7.2.4 3D-Printing of prototype and test equipment

The prototype and test equipment designed and used in this study are created with the program *Autodesk Inventor Professional* and *Autodesk Fusion 360*. Prior to 3d-printing the slicer *Cura 4.7* from *Ultimaker* is used to set the printing parameters. Filaments and supplies used in this study are purchased from *conrad electronic SE*. The 3d-printer used is a FDM-type *Ultimaker 3 Extended*, with a build volume of 215 mm × 215 mm × 30 mm.

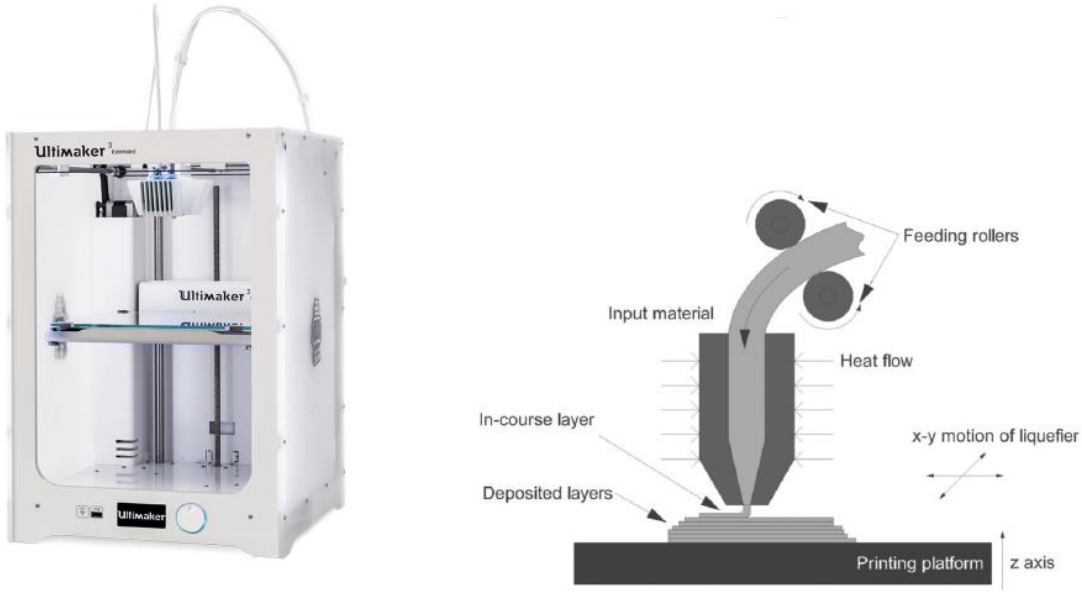

Figure 53: Photo of an Ultimaker 3 Extended 3d-printer (left) and ist functionality (rigth).[44, 45]

7.3 Chemical analysis

7.3.1 Nuclear magnetic resonance spectroscopy (NMR)

NMR spectra are recorded on a *Bruker AVIII HD 400US* instrument at 300 K. Chemical shifts are given in δ-values (ppm) and are calibrated to the residual ^{1}H- or ^{13}C-signal of the respective deuterated solvent.

Chloroform-d_1 ($CDCl_3$): ^{1}H-NMR: δ [ppm] = 7.26 (s); ^{13}C-NMR: δ [ppm] = 77.16 (t).

Dimethyl sulfoxide-d_6 (C_2D_6OS): ^{1}H-NMR: δ [ppm] = 2.50 (p); ^{13}C-NMR: δ [ppm] = 39.52 (hept).

Deuterium oxide-d_2 (D_2O): ^{1}H-NMR: δ [ppm] = 4.79 (s).

For the assignment of the signals and the signal multiplicity the following abbreviations are used: singlet (s), doublet (d), triplet (t), quartet (q), pentet (p), hextet (hex), heptet (hept), multiplet (m), broad singlet (br.s).

7.3.2 Electron spray ionization mass spectrometry (ESI-MS)

Mass spectra were measured using a *Thermo Scientific LCQ* Fleet from *Thermo Fisher Scientific* coupled with a time-of-flight (TOF) detector. Water was used as solvent for the ionic liquids. Mass numbers of the ion peaks are given as m/z values with the respective relative intensity in percent (%).

7.3.3 Particle size analysis via optical microscopy

Measurements of the particle size distribution and analyses of the particle shape are conducted with a *Morphologi G3SE-ID* from *Malvern Pananalytical*. Data analysis is performed with the aid of the software *Morphologi* from the company *Malvern Pananalytical*.

For the particle analysis of inorganic peroxide powders, 13 mm2 of the powder are dispersed on a microscope slide with an injection pressure of 5.0 bar, an injection time of 20 ms and a settling time of 180 s. A measuring range from 0.54 µm to 1000 µm is obtained by utilizing objectives with magnification factors of 2.5, 5, 10 and 20.

7.3.4 Determination of water content

Water contents were determined by coulometric Karl-Fischer titration with the aid of a *DL 39* from *Mettler Toledo*. Prior to measurement, about 0.6 g to 0.8 g of the corresponding ionic liquid was injected with a syringe and stirred for 30 s.

7.4 Procedure for the catalytic decomposition of inorganic peroxides

7.4.1 Room temperature decomposition experiments

In a typical experiment, the oxygen source is placed in a reaction vessel, which can vary in size, diameter and material. Small-scale experiments are conducted in a 1 L Schlenk flask with a diameter of 5 cm, while for larger scale experiments HT pipes DN 75 with an outer diameter of 7.5 cm are utilized. The oxygen source is applied in the form of either powder, cylindrical compacts with different sizes or mixtures of powder and cylindrical compacts or differently sized cylindrical compacts. Compacts are prepared by using a laboratory press and press dies of different diameters. Also, the additional reactants are prepared in advance. For small-scale experiments, solvent and ionic liquid are drawn up in a syringe, and the catalyst is prepared by either dissolving or suspending it in a small fraction of the utilized aqueous medium. To start the reaction, all reactants are added to the peroxide compound as fast as possible. The reaction vessel is then closed, and the flow rate and volume developments of the evolving gas are measured with a drum-type gas meter. To measure the reaction temperature, in some experiments an electrical thermometer is attached to the reaction setup. **Figure 54** portrays a schematic drawing of the utilized experimental setup.

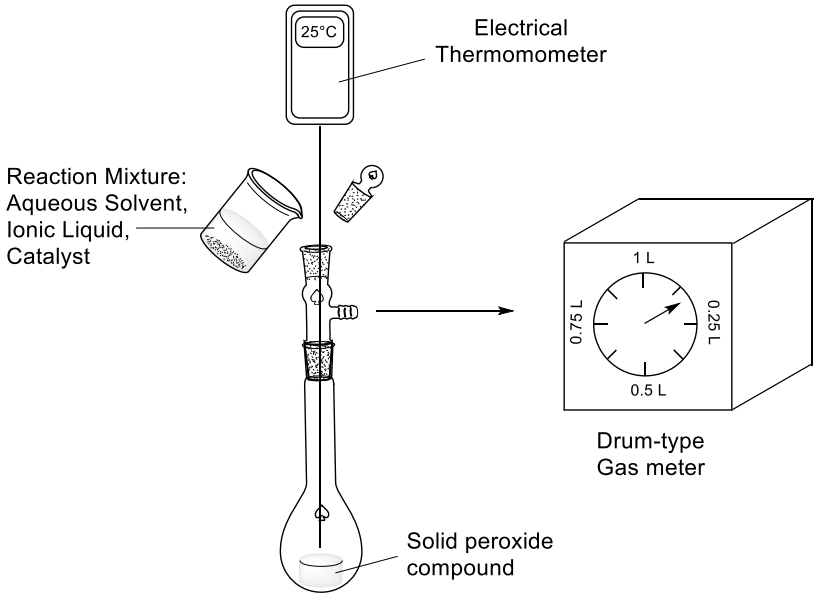

Figure 54: Schematic drawing of the experimental setup for the decomposition of inorganic peroxides.[11]

7.4.2 Decomposition experiments at -20 °C

To conduct experiments at -20 °C, the described experimental setup is used in a so-called climate chamber. The climate chamber contains a compartment that can hold a constant temperature over a long period of time. To ensure that the utilized reaction compounds are sufficiently cooled, all reactants are cooled at least overnight. For this purpose, the reaction mixture including aqueous solvent, ionic liquid and catalyst is prepared beforehand and stored in a glass vessel with screw cap.

Analogous to the decomposition experiments at room temperature, the reaction vessel is equipped with the pre-cooled solid peroxide compound and placed in the cold compartment. The reaction vessel is then connected with the drum-type gas meter, which is located outside of the climate chamber. Since opening the chamber leads to a temperature increase within the compartment, it is waited until it reaches the desired reaction temperature of -20 °C again. To start the reaction, the pre-cooled reaction mixture is added to the solid peroxide compound, and the reaction vessel and the climate chamber are closed as fast as possible.

7.4.3 Membrane permeability experiments

An HT pipe measuring 75 mm in diameter and 115 mm in length is used as a reaction vessel in these decomposition experiments as illustrated in **Figure 55** on the right. There is a cap on the bottom side of the pipe that seals it completely. On the other side, the pipe is connected to a HT junction box measuring 75 mm x 75 mm x 67 °. On the left branch, another HT junction box of 75 mm x 75 mm x 87 ° is connected with its top sealed. An additional opening can be opened and closed with a screw cap. A mechanism of membrane fixing is installed on the top branch, which is manufactured additively using the FDM method with tough PLA as building material. Four bolts and nuts of ISO 1502 size M6 are used to secure the membrane between adapter and connector as shown in **Figure 55** on the left below.

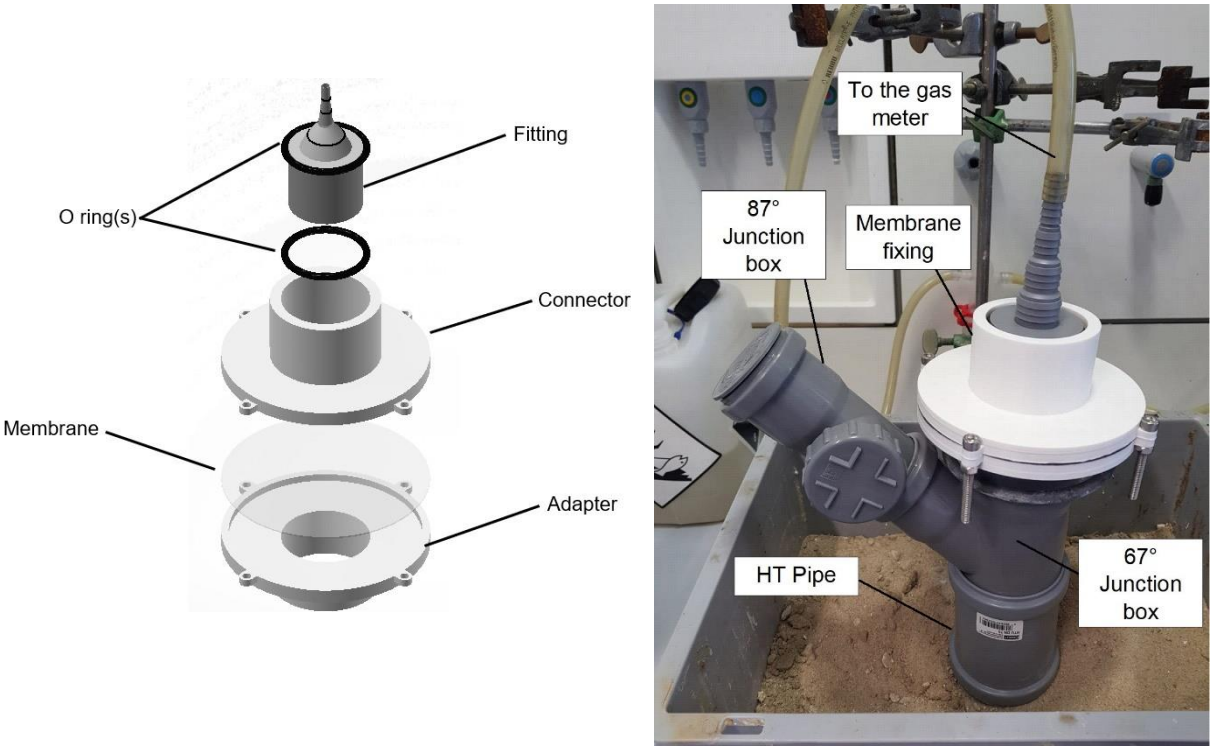

Figure 55: Exploded assembly drawing (left) and photo (right) of the membrane test setup.

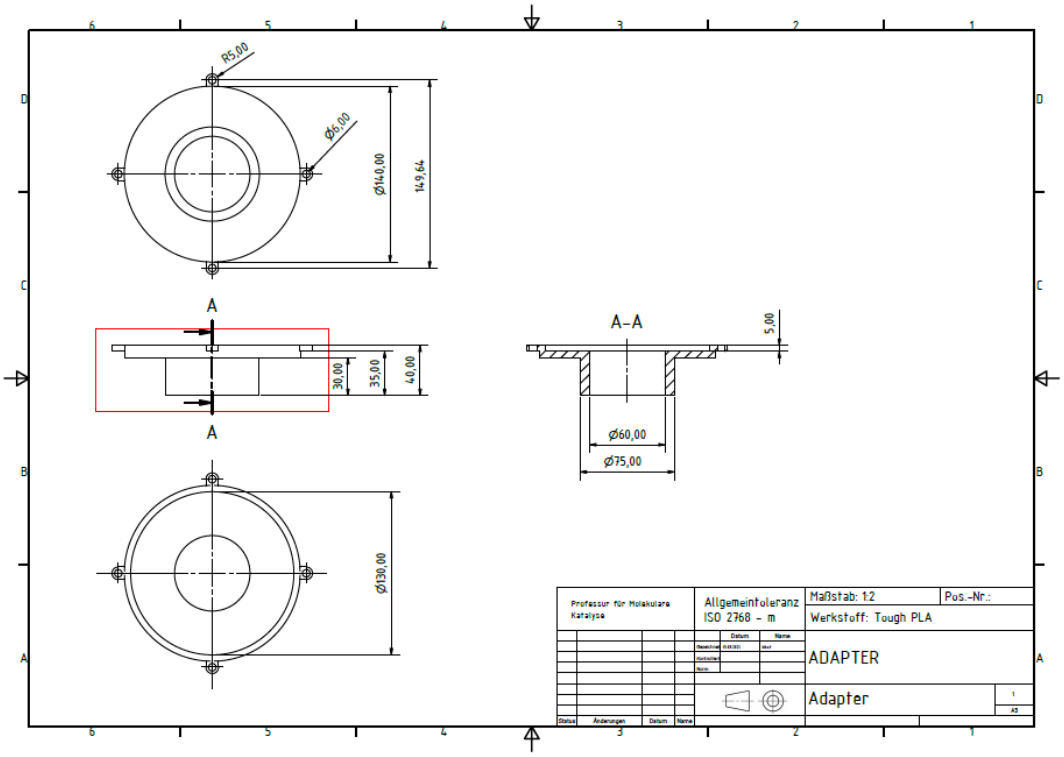

Figure 56: Technical drawing of the adapter of the membrane test setup.

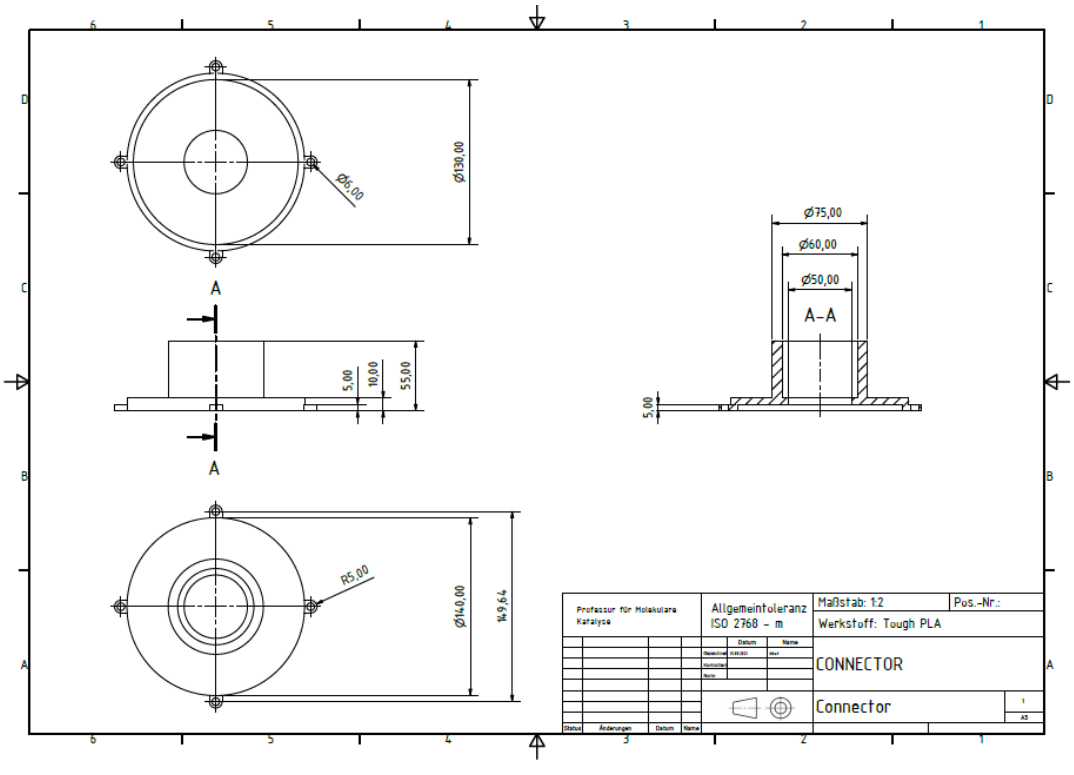

Figure 57: Technical drawing of the Connector of the membrane test setup.

7.5 Synthesis procedures

1-Ethyl-3-methylimidazolium methyl sulfate

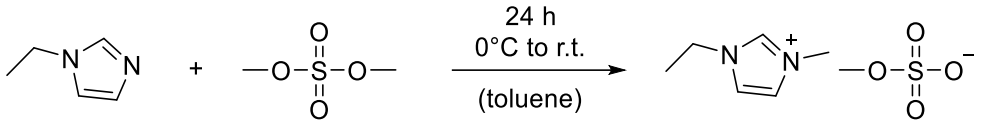

197.81 g 1-Ethylimidazole (2.06 mol, 1.00 eq) is dissolved in 350 ml toluene. Afterwards, 259.53 g dimethylsulfate (2.06 mol, 1.00 eq.) is added dropwise under vigorous stirring and cooling in an ice bath. The reaction is stirred overnight at room temperature, leading to a phase separation of toluene and the product. Subsequently, the organic phase is decanted. The product is washed with toluene (3 x 200 ml) and dried *in vacuo* at 70 °C for 24 h to yield 449.70 g (98%) as a yellow viscous liquid.

^{1}H NMR (400 MHz, $CDCl_3$, 300 K): δ [ppm] = 1.52 (t, 3 H, ^{3}J = 7.34 Hz, CH_2CH_3), 3.67 (s, 3 H, OCH_3), 3.97 (s, 3 H, NCH_3), 4.27 (q, 2 H, ^{3}J = 7.34 Hz, NCH_2), 7.48 (s, 2 H, C_4HC_5H), 9.37 (s, 1 H, C_2H).

^{13}C NMR (101 MHz, $CDCl_3$): δ [ppm] = 15.5 (CH_2CH_3), 36.4 (NCH_3), 45.2 (NCH_2), 54.5 (OCH_3), 122.0 (C_5), 123.8 (C_4), 137.1 (NCHN).

MS (ESI (+), 70 eV): m/z (%) = 82.85 (40, $[HMIM]^+$), 110.88 (100, $[EMIM]^+$).

MS (ESI (-), 70 eV): m/z (%) = 110.83 (100, $[SO_4Me]^-$), 332.60 (16, $[EMIM][SO_4Me]_2^-$), 554.49 (48, $[EMIM]_2[SO_4Me]_3^-$), 776.20 (16, $[EMIM]_3[SO_4Me]_4^-$).

1-Ethyl-3-methylimidazolium ethyl sulfate

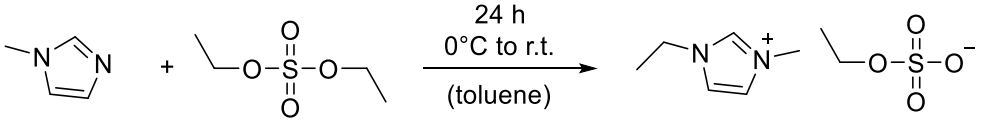

308.36 g of diethyl sulfate (2.00 mol, 1.00 eq.) is added dropwise to an ice-cooled solution of 164.21 g of 1-methyl imidazole (2.00 mol, 1.00 eq.) in 250 ml toluene under an atmosphere of argon. After complete addition of diethyl sulfate, the reaction mixture is stirred overnight at room temperature. The organic phase is decanted, and the product is washed with toluene (3 x 200 ml). Remaining solvent is evaporated *in vacuo* at 70 °C to yield 460.89 g (98%) of a slightly yellow liquid.

^{1}H NMR (400 MHz, $CDCl_3$, 300 K): δ [ppm] = 1.22 (t, ^{3}J = 7.1 Hz, 3 H, NCH_2CH_3), 1.51 (t, ^{3}J = 7.3 Hz, 3 H, OCH_2CH_3), 3.96 (s, 3 H, NCH_3), 4.04 (q, ^{3}J = 7.1 Hz, 2 H, OCH_2CH_3), 4.27 (q, ^{3}J = 7.3 Hz, 2 H, NCH_2CH_3), 7.45-7.51 (m, 2 H, NCHCHN), 9.44 (s, 1 H, NCHN).

^{13}C NMR (101 MHz, $CDCl_3$): δ [ppm] = 15.22 (NCH_2CH_3), 15.50 (OCH_2CH_3), 36.30 (NCH_3), 45.08 (NCH_2CH_3), 63.28 (OCH_2CH_3), 122.06 (NCHCHN), 123.82 (NCHCHN), 136.99 (NCHN).

MS (ESI (+), 70 eV): m/z (%) = 347 (100, $[EMIM]_2[SO_4Et]^+$).

Butylammonium nitrate

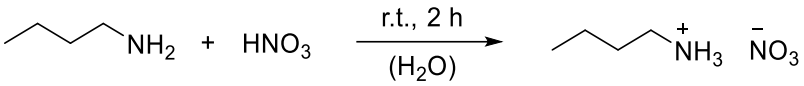

94.77 g nitric acid (65 wt. % in water, 977.6 mmol, 1.00 eq.) is added dropwise to a solution of 71.50 g butylamine (683.6 mmol, 1.00 eq.) in 23.88 g water while cooling in an ice bath. Afterwards, the water is removed *in vacuo* at 60 °C to yield a 131.81 g (99%) of a slightly yellow viscous liquid.

^{1}H NMR (400 MHz, D_2O): δ [ppm] = 0.82 (t, ^{3}J = 7.4 Hz, 3 H, $H_3CCH_2CH_2CH_2NH_3^+$), 1.21-1.35 (m, 2 H, $H_3CCH_2CH_2CH_2NH_3^+$), 1.47-1.59 (m, 2 H, $H_3CCH_2CH_2CH_2NH_3^+$), 2.89 (t, 2 H, $H_3CCH_2CH_2CH_2NH_3^+$).

^{13}C NMR (400 MHz, D_2O): δ [ppm] = 12.65 ($H_3CCH_2CH_2CH_2NH_3^+$), 18.93 ($H_3CCH_2CH_2CH_2NH_3^+$), 28.69 ($H_3CCH_2CH_2CH_2NH_3^+$), 39.21 ($H_3CCH_2CH_2CH_2NH_3^+$).

MS (ESI (+), 70 eV): m/z (%) = 73.79 (100, $[BNH_3]^+$), 209.76 (26, $[BNH_3]_2[NO_3]^+$), 345.79 (64, $[BNH_3]_3[NO_3]_2^+$), 481.75 (38, $[BNH_3]_4[NO_3]_3^+$), 617.60 (32, $[BNH_3]_5[NO_3]_4^+$), 753.54 (50, $[BNH_3]_6[NO_3]_5^+$), 889.34 (24, $[BNH_3]_7[NO_3]_6^+$).

MS (ESI (-), 70 eV): m/z (%) = 61.72 (100, $[NO_3]^-$), 195,86 (40, $[BNH_3][NO_3]_2^-$).

1-(4-sulfonic acid)butyl-3-methylimidazolium Zwitterion

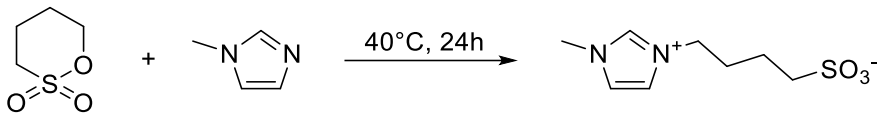

50.28 g of 1,4-butane sultone (369.3 mmol, 1.00 eq.) and 30.32 g of 1-methylimidazole (369.3 mmol, 1.00 eq.) are placed in a Schlenk flask under an atmosphere of argon. The mixture is heated to 40 °C for 24 h. Afterwards, the product is dissolved in 300 ml of water and washed with diethylether (3 x 200 ml). The product is dried *in vacuo* to yield 73.80 g (91%) as a white solid.

^{1}H NMR (400 MHz, D_2O): δ [ppm] = 1.66-1.79 (m, 2 H, NCH_2CH_2), 1.95-2.07 (m, 2 H, $NCH_2CH_2CH_2CH_2SO_3^-$), 2.93 (t, 2 H, $NCH_2CH_2CH_2CH_2SO_3^-$), 3.87 (s, 3 H, NCH_3), 4.23 (t, ^{3}J = 7.0 Hz, 2 H, $NCH_2CH_2CH_2CH_2SO_3^-$), 7.42 (s, 1 H, NCHCHN), 7.48 (s, 1 H, NCHCHN), 8.73 (s, 1 H, NCHN).

^{13}C NMR (400 MHz, D_2O): 20.82 ($NCH_2CH_2CH_2CH_2SO_3^-$), 28.00 ($NCH_2CH_2CH_2CH_2SO_3^-$), 35.52 (NCH_3), 48.80 ($NCH_2CH_2CH_2CH_2SO_3^-$), 49.93 ($NCH_2CH_2CH_2CH_2SO_3^-$), 122.03 (NCHCHN), 123.51 (NCHCHN).

MS (ESI (+), 70 eV): m/z (%) = 219.17 (30, $[MIMBS+H]^+$), 437.15 (44, $[MIMBS][MIMBS+H]^+$), 459 (26, $[(2\ MIMBS)+Na]^+$, 676.95 (66, $[(3\ MIMBS]+Na]^+$), 894.83 (100, $[(4\ MIMBS)+Na]^+$).

1-(4-sulfonic acid)butyl-3-methylimidazolium hydrogen sulphate

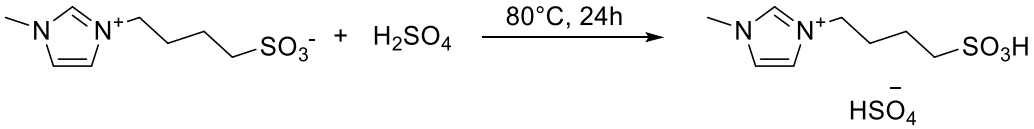

A Schlenk flask is equipped with 73.74 g of the zwitterionic species (336.6 mmol, 1.00 eq.). 34.39 g of H_2SO_4 (96%, 336.6 mmol, 1.00 eq.) are added dropwise and the reaction mixture is stirred for 24 h at 80 °C. The product is dried at 70 °C *in vacuo* to yield 100.03 g (94%) as a colorless viscous liquid.

^{1}H NMR (400 MHz, DMSO-d_6): δ [ppm] = 1.49-1.61 (m, 2 H, $NCH_2CH_2CH_2CH_2SO_3H$), 1.88 (p, ^{3}J = 7.2 Hz, 2 H, $NCH_2CH_2CH_2CH_2SO_3H$), 2.50-2.57 (m, 2 H, $NCH_2CH_2CH_2CH_2SO_3H$), 3.86 (s, 3 H, NCH_3), 4.19 (t, ^{3}J = 7.0 Hz, 2 H, NCH_2), 7.72 (t, ^{3}J = 1.8 Hz, 1 H, NCHCHN), 7.78 (t, ^{3}J = 1.8 Hz, 1 H, NCHCHN), 9.16 (s, 1 H, NCHN).

^{13}C NMR (101 MHz, DMSO-d_6): δ [ppm] = 20.82 ($NCH_2CH_2CH_2\mathit{C}H_2SO_3H$), 28.00 ($NCH_2\mathit{C}H_2CH_2CH_2SO_3H$), 35.52 ($NCH_2CH_2\mathit{C}H_2CH_2SO_3H$), 48.80 ($N\mathit{C}H_3$), 49.94 ($N\mathit{C}H_2$), 122.03 (NCH*C*HN), 123.51 (N*C*HN).

MS (ESI (+), 70 eV): m/z (%) = 219 (30, $[MIMBS]^+$), 241 (10, $[MIMBS+Na]^+$), 459 (100, $[(2\ MIMBS)+Na]^+$), 677 (60, $[(3\ MIMBS)+Na]^+$), 895 (20, $[(4\ MIMBS)+Na]^+$).

1-(4-sulfonic acid)butyl-3-methylimidazolium nitrate

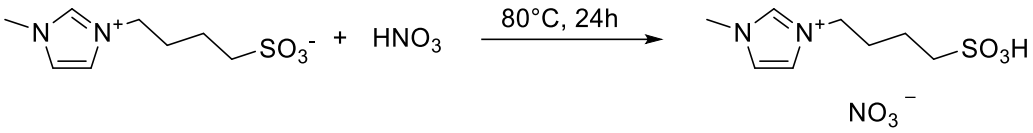

59.55 g of the zwitterionic species (272.83 mmol, 1.00 eq.) are placed in a Schlenk flask. 26.45 g HNO_3 (65%, 272.83 mmol, 1.00 eq.) are added dropwise and the reaction is stirred at 80 °C for 24 h. The ionic liquid is dried *in vacuo* to yield 73.82 g (96%) as a colorless viscous liquid.

^{1}H NMR (400 MHz, D_2O): δ [ppm] = 1.45-1.55 (m, 2 H, $NCH_2CH_2CH_2C\mathit{H}_2SO_3H$), 1.73-1.82 (m, 2 H, $NCH_2C\mathit{H}_2CH_2CH_2SO_3H$), 2.67-2.73 (m, 2 H, $NCH_2CH_2C\mathit{H}_2CH_2SO_3H$), 3.65 (s, 3 H, $NC\mathit{H}_3$), 4.00 (t, ^3J = 7.1 Hz, 2 H, $NC\mathit{H}_2$), 7.19 (t, ^3J = 1.8 Hz, 1 H, NCHC*H*N), 7.25 (t, ^3J = 1.9 Hz, 1 H, NC*H*CHN), 8.49 (s, 1 H, NC*H*N).

^{13}C NMR (101 MHz, D_2O): δ [ppm] = 20.77 ($NCH_2CH_2CH_2\mathit{C}H_2SO_3H$), 27.96 ($NCH_2\mathit{C}H_2CH_2CH_2SO_3H$), 35.40 ($NCH_2CH_2\mathit{C}H_2CH_2SO_3H$), 48.73 ($N\mathit{C}H_3$), 49.91 ($N\mathit{C}H_2$), 121.96 (NCH*C*HN), 123.47 (N*C*HN).

MS (ESI (+), 70 eV): m/z (%) = 219 (40, $[MIMBS+H]^+$), 459 (100, $[(2\ MIMBS)+Na]^+$), 677 (40, $[(3\ MIMBS)+Na]^+$).

2-Hydroxy ethylammonium formate

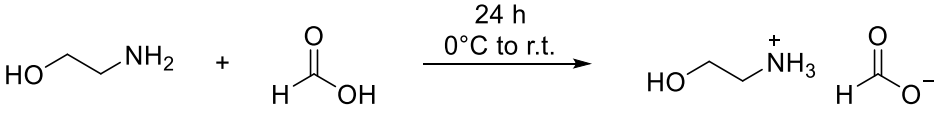

104.00 g of 2-amino ethanol (1.69 mol, 1.00 eq.) are cooled to 0 °C in a Schlenk flask under an atmosphere of argon. 82.07 g of formic acid (1.69 mol, 1.00 eq.) are added dropwise over a period of 3 h. The reaction mixture is stirred overnight to yield 178.6 g (98%) of a slightly yellow liquid.

^{1}H NMR (400 MHz, DMSO-d_6): δ [ppm] = 2.81 (t, 2 H, ^3J = 5.44 Hz, $OC\mathit{H}_2$), 3.55 (t, 2 H, ^3J = 5.44 Hz, $C\mathit{H}_2$), 6.81 (s, 4 H, $N\mathit{H}_3$ + O*H*), 8.39 (s, 1 H, *H*COO^-).

^{13}C NMR (101 MHz, DMSO-d_6): δ [ppm] = 40.58 (O*C*H_2), 58.11 (N*C*H_2), 161.89 (H*C*OO^-).

MS (ESI (+), 70 eV): m/z (%) = 61.73 (100, $[HOEtNH_3]^+$).

Triethylammonium hydrogen sulphate

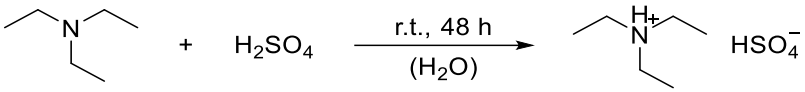

A Schlenk flask is equipped with 50.00 g of triethyl amine (494 mmol, 1.00 eq.) and 70 ml water. A mixture of 50.48 g of sulphuric acid (96%, 494 mmol, 1.00 eq.) in 90 ml water is added dropwise. The reaction is stirred for two days at room temperature. After removal of water *in vacuo* at 80 °C 95.3 g (97%) of triethylammonium hydrogen sulphate is obtained as a colorless solid.

^{1}H NMR (400 MHz, DMSO-d_6): δ [ppm] = 1.18 (t, 9 H, ^3J = 7.3 Hz, NCH_2CH_3), 3.08 (q, 6 H, ^3J = 7.3 Hz, NCH_2CH_3).

^{13}C NMR (101 MHz, DMSO-d_6): δ [ppm] = 9.02 (NCH_2CH_3), 46.2 (NCH_2CH_3).

MS (ESI (+), 70 eV): m/z (%) = 301 (100, $[Et_3NH]_2[HSO_4]^+$).

Diethylammonium hydrogen sulphate

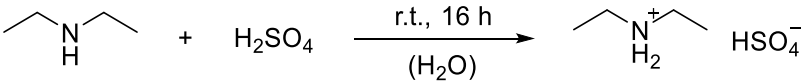

A solution of 48.89 g of sulfuric acid (96%, 479 mmol, 1.00 eq.) in 90 ml water is added dropwise to a solution of 35.00 g of diethyl amine (479 mmol, 1.00 eq.) in 50 ml water. The reaction is stirred at room temperature overnight. Afterwards, water is removed *in vacuo* at 80 °C to yield 80.67 g (98%) of diethylammonium hydrogen sulphate as a brown viscous liquid.

^{1}H NMR (400 MHz, DMSO-d_6): δ [ppm] = 1.14-1.20 (t, 6 H, ^3J = 7.3 Hz, CH_3), 2.88-2.96 (q, 4 H, CH_2CH_3), 8.34 (br.s, 2 H, NH_2^+).

^{13}C NMR (101 MHz, DMSO-d_6): δ [ppm] = 11.47 (NCH_2CH_3), 41.91 (NCH_2CH_3).

MS (ESI (+), 70 eV): m/z (%) = 364 (70, $[(2\ Et_2NH_2)+Na]^+$.

8 List of figures

9 List of schemes

10 List of tables

11 Bibliography

[1] https://www.sueddeutsche.de/wissen/klima-fliegen-co2-grafik-1.4534651

[2] https://www.dlr.de/content/de/artikel/news/2021/03/20210722_eiswolken-waermen-die-arktis.html

[3] A. Imhof, Chemical Oxygen Generation from Urea Hydrogen Peroxide by Catalytic Decomposition in Ionic Liquids, **2019**.

[4] M. Mahnken, Integration von Kabinensystemen in BWB-Flugzeugkonfigurationen, **2006**.

[5] https://www.aircraftsystemstech.com/2017/05/aircraft-oxygen-systems.html

[6] http://sfs.sabic.eu/news/sabic-features-space-age-material-technologies-meet-aircraftweight-out-safety-eco-challenges-aircraft-interiors-expo-2011/

[7] P. Walden, *Bull. Acad. Imper. Sci*. St. Petersbourg, **1914**, *8*, 405.

[8] F. Hurley, T. Wier; *Electrochem. Soc*., **1951**, *98*, 207.

[9] T. Schefler, C. Hussey, K. Seddon, C. Kear, P. Armitage, *Inorg. Chem.*, **1983**, *22*, 2099.

[10] N. Plechkova, K. Seddon; *Chem. Soc. Rev*., **2008**, *37*, 123.

[11] J. Keller, Studies on the Catalytic Decomposition of Inorganic Peroxides for Chemical Oxygen Generation, **2020**.

[12] J. Stoimenovski, P. Dean, E. Izgorodina, D. MacFarlane, *Faraday Discuss*; **2012**, *154*, 335.

[13] S. Singh, A. Savoy; *J. Mol. Liq*.; **2020**, *297*, 112038.

[14] C. Schmid, C. Beck, J. Cronin, M. Staszak*, Org. Process Res. Dev*.; **2004**, *8*, 670.

[15] A. Cole, J. Jensen, I. Ntai, K. Tran, K Weaver, D Forbes, J. Davis, *J. Am. Chem. Soc*.; **2002**, *124*, 5962.

[16] R. Kalkhambkar, S. Waters, K. Laali, *Tetrahedron Lett*.; **2011**, *52*, 867.

[17] M. Yoshizawa, W. Xu, C. Angell; *J. Am. Chem. Soc*.; **2003**, *125*, 15411.

[18] https://iolitec.de/en/node/675

[19] S. Schneider, T. Hawkins, M. Rosander, G. Vaghjiani, S. Chambreau and G. Dranke; *Energy Fuels*, **2008**, *22*, 2871.

[20] H. Gao, J. Shreeve; *J. Mater. Chem*., **2012**, *22*, 11022.

[21] Z. Xiangping; Z. Xiaochun; D. Haifeng; Z. Zhijun, *Energy Environ. Sci.*, **2012**, *5*, 6668.

[22] https://iolitec.de/node/658

[23] A. Imhof, Influence of the aqueous phase on macroscopic amino functionalized silica spheres, **2016**.

[24] X. Fan, L. Wang; *ACS Appl. Mater. Inter.* **2014**, *6*, 14660.

[25] H. Qi, Y. Ren, S. Guo, Y. Wang, S. Li, Y. Hu, F. Yan, *ACS Appl. Mater. Interfaces,* **2020**, *12*, 591.

[26] H. Lu, Y. Zhu, B. Zheng, H. Du, X. Zheng, C. Liu, Y. Yuan, J. Fang and K. Zhang; *New J. Chem.*, **2020**, *44*, 361.

[27] J. Zhu, L. Bai, B. Chen, W. Fei; *Chem. Eng. J.*, **2009**, *147*, 58.

[28] https://shop.boeing.com/medias/1529.pdf?context=bWFzdGVyfHBkZnwxMDQzODc2fGFwcGxpY2F0aW9uL3BkZnwzGYvaGVlL2g2MC84ODE0MTUzMzM0ODE0LnBkZnw3ZGVkYzg2MmY0MWJjMjZmZDVmMmU5NTA0NGJkNjUyZDU3MTI5NWM1NzY0NDY3MWM4YjFkYjQ3NDBiMGU1ODUz&attachment=true

[29] SAE AS8010, SAE Aerospace, **1997**.

[30] D. Cassidy, R. Irvine, *J. Hazard. Mater.*, **1999**, *69*, 25.

[31] SAE International, ARP1398A. Testing of Oxygen Equipment.

[32] Ullmann's encyclopedia of industrial chemistry, Wiley, Chichester, **2010**

[33] R. Watts, J. Sarasa, F. Loge, A. Teel, *J. Environ. Eng.* **2005**, *131*, 158.

[34] D. Clark, *Peroxides and Peroxide-forming Compounds*, Texas A&M University, College Station, **2000**.

[35] J. Hem, C. Lind, *Geochim. Cosmochim., Acta,* **1983**, *47*, 2037.

[36] A. Hinterberger, Peroxide-Based Oxygen Generator for Aircraft Use, **2019**.

[37] F. Groche, Chemical Oxygen Generation from Peroxo-Compounds For Aviation Purposes, **2017**.

[38] J. Graf, Oxygen Candle Background for Submarines and Space, *NASA-JSC*, **2017**.

[39] A. Hazen, *Massachusetts State Board of Health - 24th Annual Report,* **1892**, 539.

[40] T. Brunn, *Chemical Oxygen Generators: Deeper Insights into Particle Size Distributions and Particle Shape*, **2020**.

[41] N. Chew, H. Chan, *Pharm. Res.,* **2001**, *18*, 1570.

[42] https://www.youtube.com/watch?v=sEOGUsQm64c.

[43] R. Sharma, S. Chellam, *Environ. Sci. Technol.*, **2005**, *39*, 5022.

All websites were visited on 31th of December in 2022.

"So eine Arbeit wird eigentlich nie fertig, man muß sie für fertig erklären, wenn man nach Zeit und Umständen das Möglichste getan hat."

Johann Wolfgang von Goethe